Freiberg On-line
Geoscience Vol. V

FOG is an electronic journal registered under ISSN 1434-7512.

Groundwater study for the Wadi Zerqa catchment area.

Diplomarbeit

Stefan Martens

Institute for Geology, University of Mining and Technology Freiberg

Table of contents

Table of figures

Table of tables

1 Acknowledgement

The author is highly indebted to Prof. Dr. B. Merkel for his supervision, sincere criticism, advice, help and general support during the progress of this work.

The author is equally grateful to Prof. Dr. O. Rimawi for his supervision, help, advice discussion and assistance during his fieldwork in Jordan.

The author also thanks Prof. Dr. E. Salameh, Dr. M. Al Qusis for their help and comments, Prof. Dr. Seiler at the Forschungszentrum für Umwelt und Gesundheit (GSF), Inst. for Hydrology and Prof. D. Hebert at the TU-Bergakademie for the isotope analysis.

Sincere thanks are also extended to the staff members and employees of the Department of Geology & Mineralogy at the University of Jordan and the TU Bergakademie Freiberg, for their help in analysing water samples and for the technical equipment made available for the laboratory and field analyses.

2 Introduction and objectives

With the increase of the water demand in Jordan, new sources of drinking and industrial water have to be explored and a better water management should be adopted to the existing ones to satisfy these demands. Therefore several investigations and efforts had been made in the past, most of them concerning the upper aquifer system. During the last years, the deeper aquifer system has been taken into consideration, too. Jet, there is not much information about the water quality and quantity for this aquifer system in the northern part of Jordan.

This work tries to collect existing data as well as it provides new data concerning hydrochemistry and hydrogeology of all aquifer systems in the Wadi Zerqa catchment area.

The main objectives of this work are:

Mapping:

- Present a geological map scale 1:20,000 (paper copy) generated with TNT-Mips of the western Wadi Zerqa area near the town of Deir Alla.
- Describe the stratigraphic sequence, geological formations and structural elements of the mapped area.

Master thesis:

- Taking water samples (wells and springs) for AAS and ICP-MS analysis as well as $\delta^{18}O$ and Tritium.
- Interpretation of chemical data by PHREEQC.
- Collect and check available data concerning hydrogeology and hydrochemistry.
- Use remote sensing tools to get information of the area with reference to the model.
- Using the USGS 30minutes DEM and generate a more detailed grid in the mapping area.
- Create a box model for a better estimation of the groundwater recharge for the area.
- Create a 3d hydrogeological model using the collected data.
- Design and calibrate (steady state) a 3d ground water flow model using the collected data with FEMWATER in combination with the graphical interface GMS.

3 Background

The Hashemite Kingdom of Jordan is a country of about 96500 km² in the northern part of the Arabian Peninsula. It is located between 29,5° N and 33°N and between 35° E and 39,5°E (Fig. 1). It borders on Syria in the north, Iraq in the north-east, Saudi Arabia in the east and south and Israel in the west.

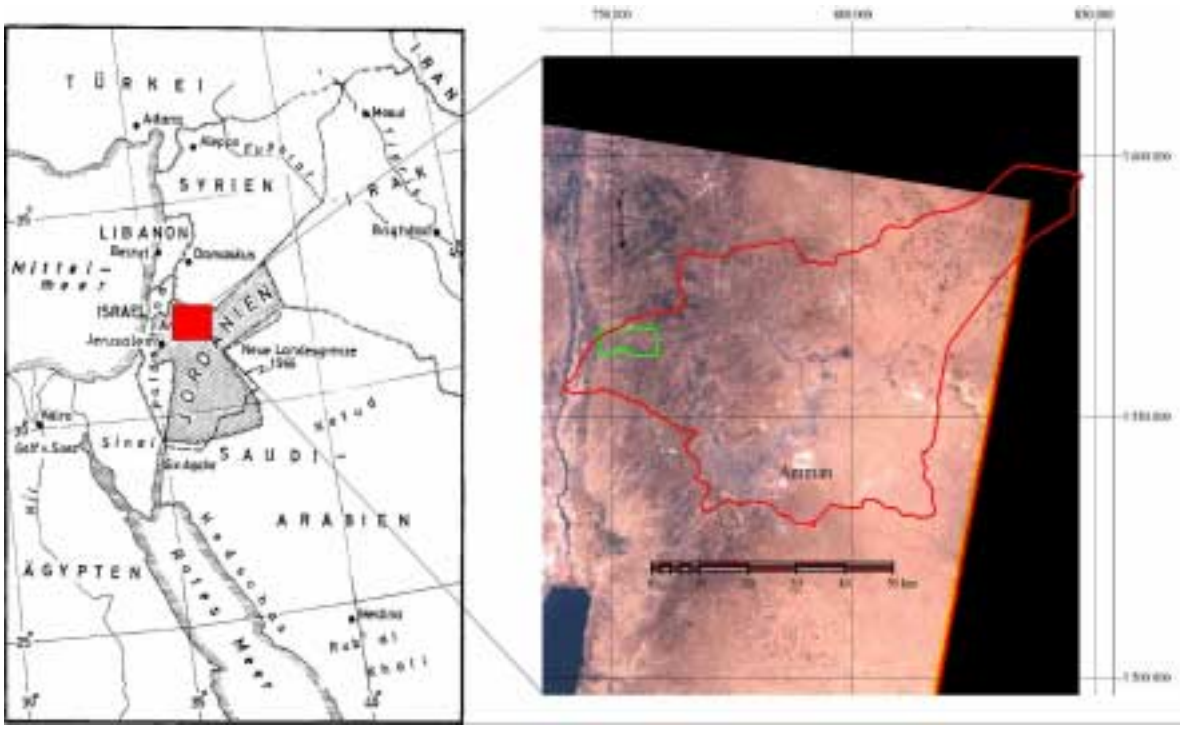

• Fig. 1 Situation map of the study area (red line = model area, green line = mapping area).

About 80% of the total area of Jordan is classified to have semi-arid to arid climate with less than 200 mm/a of rainfall and a high potential evaporation rate exceeding 2000 mm/a. In the high rainfall area - the Western Highlands - the climate is of Mediterranean type with rainfall reaching 650 mm/a. Rain in Jordan mostly falls during winter (October - May). The basement complex (outcrops in the south) is unconformably overlain by variable thicknesses of sandstones and shale of Cambrian, Ordovician and Silurian ages, of continental and marine origin. The rock units generally are dipping to the north and north-east and are overlain by a succession of younger marine sediments which are mostly aged Upper Cretaceous to Eocene.

3.1 Geomorphology

Jordan can be divided into seven physicogeographic provinces which are about the shape of the geological provinces (Fig. 2).

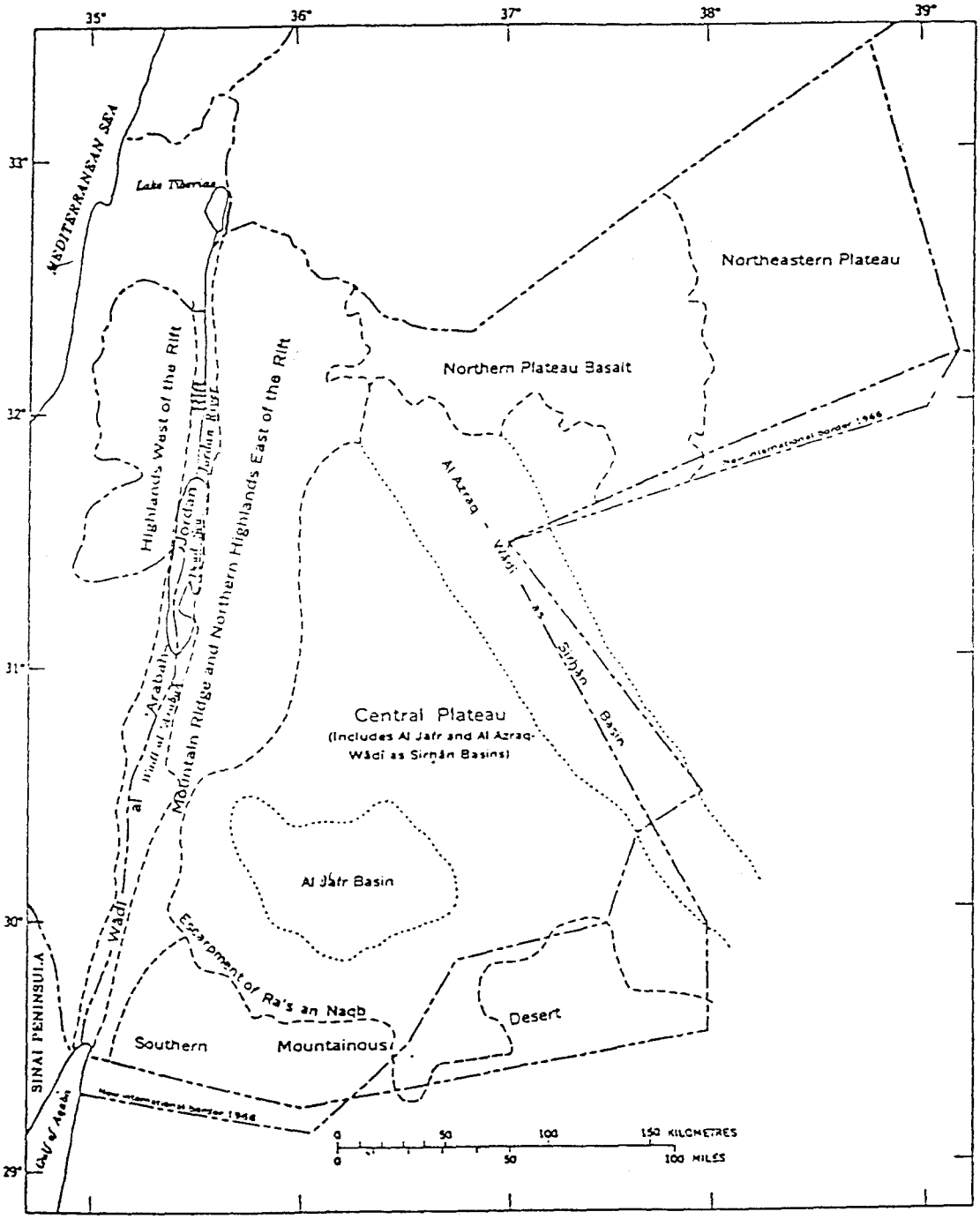

• Fig. 2 Geological provinces, major morphological units (modified after BENDER, 1974).

The study area of this work crosses three of them, the remaining four will only be mentioned:

1. Wadi Araba-Jordan Rift
   The Rift Province is a narrow depression which reaches from the Gulf of Aqaba to the Lake Tiberias. It represents a small part of the East African-Asian Minor Rift

System. The floor rises from the Gulf of Aqaba to about 250m above sea level in the Central Wadi Araba and then falls gently to the Dead Sea to about 392m below sea level. To the North of the Dead Sea, it rises again to 212m below sea level at the Lake Tiberias.

2. Highland to the east of the rift
   The Mountain Ridge Province stretches north-northeast to north and is situated to the east of the rift valley. Reaching a height of about 1850m, these are the highest peaks of the country. In general it slopes gently to the east, whereas it slopes very steeply towards the Rift Province in the west.

3. Northern Plateau Basalt
   The Plateau Basalt forms a shield of almost inaccessible flows, fissure effusions and isolated volcanoes. It falls from about 1100m at the border to Syria to approximately 550m in the south close to Wadi Sirhan Basin.

4. Highland to the west of the Rift
5. Southern Mountain Desert
6. The Central Plateau
7. The Northeastern Plateau

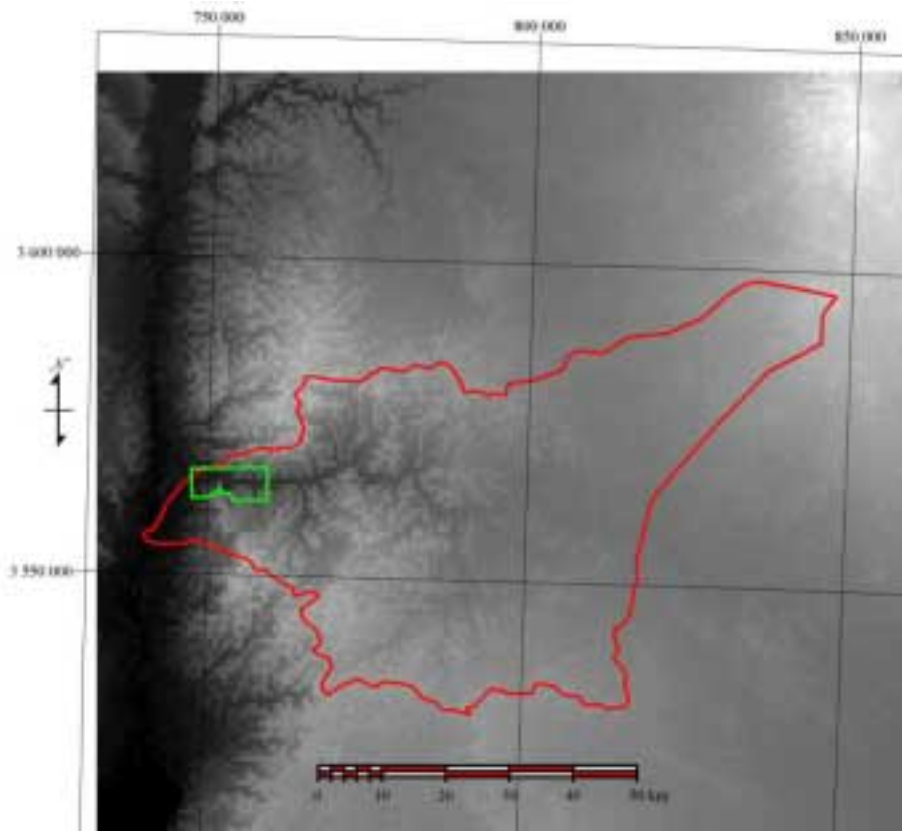

• Fig. 3 DEM computed by the USGS (red line = model area, green line = mapping area; black = low, white = high).

For the investigations, a corrected Digital Elevation Model (DEM) computed by the USGS was used (http://edcwww.usgs.gov/landdaac/gtopo30/hydro/index.html). It has a resolution of 1km. In this DEM, the three physicogeographic provinces of the study area can already be estimated (Fig. 3).

3.2 Climate

Jordan lies within a semi-arid to arid climate type with the essential features of dry, hot summers and moderate winters. The climate is influenced by two major atmospheric circulation patterns. During the winter, the temperature latitude climatic belt prevails and moist cool air is delivered from the Mediterranean area lying in the west. The subtropical high pressure belt of dry air causes high temperature and a lack of rainfall during the summer. The climate of the mountainous parts of the study area is Mediterranean but, moving eastward, there is a change to semi-arid and arid types. The influence of the Mediterranean Sea decreases. The land mass to the west minimizes the amount of rainfall and causes increasement in the range of temperature (Fig. 4-Fig. 7, (locations shown in Fig. 41)).

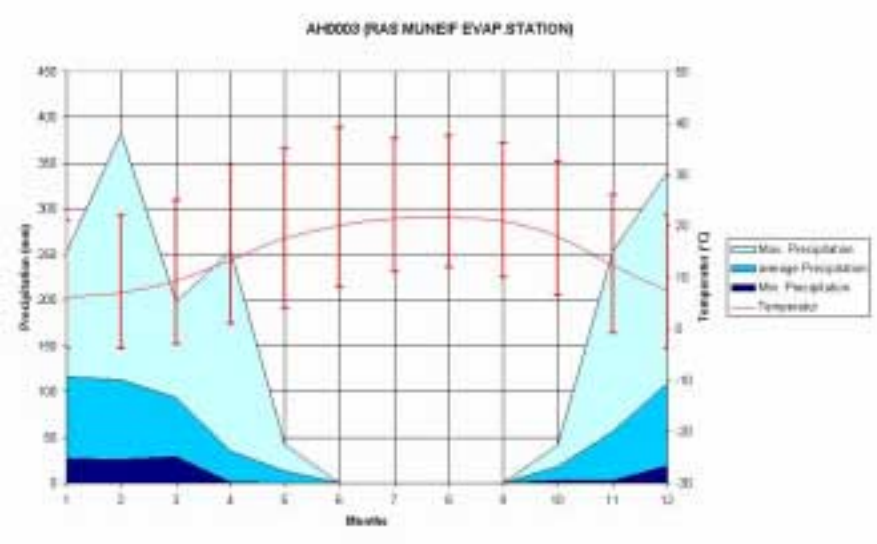

• Fig. 4 Climate courses of Ras Muneif Evap. Station (AH0003), situated in the NW of the study area.

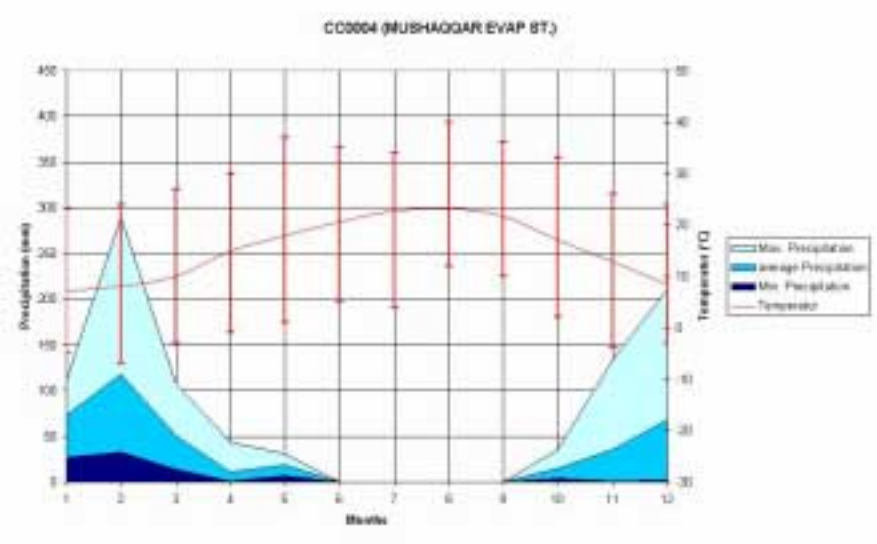

• Fig. 5 Climate courses of Mushaqqar Evap. Station (CC0004), situated in the SW of the study area.

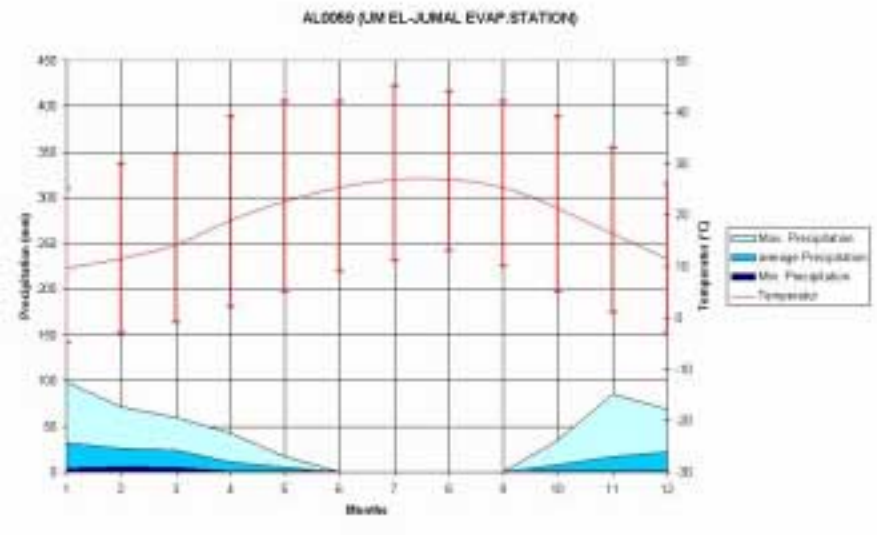

• Fig. 6 Climate courses of Um El-Jumal Evap. Station (AL0059), situated in the NE of the study area.

The cold and wet periods in winter generally are restricted from October to the end of April reaching their maximum in December to March. The rainfall distribution results from the topographic features. Thus the areas with a high amount of precipitation are around the mountains at the shoulders of the Jordan Valley, followed by a rain shadow in the lee. So the rain amount decreases gradually from north to south and rapidly from west to east.

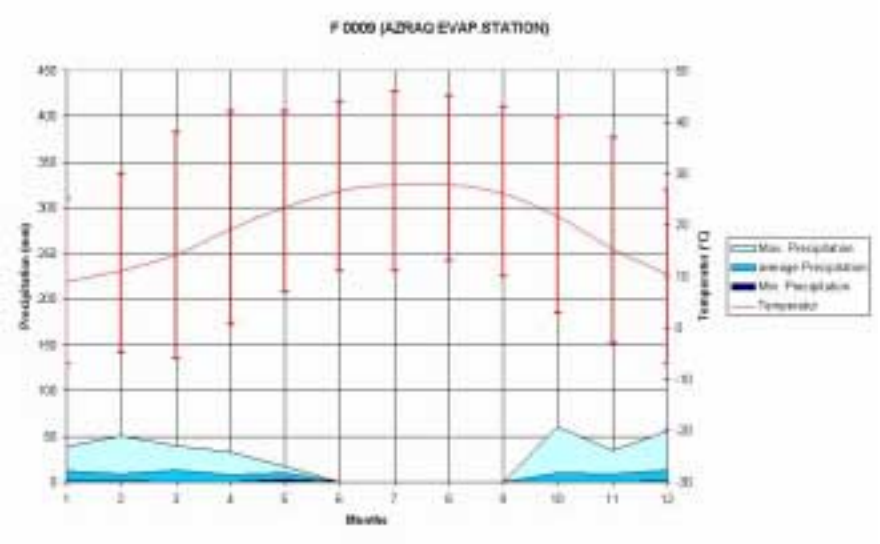

• Fig. 7 Climate courses of Azraq Evap. Station (F 0009), situated in the SE of the study area.

The average wind velocity also correlates with the elevation (~4.2m/s in the higher parts and ~2m/s in the lower parts excluding sandstorms in the dry period). The sunny hours per day ranges from 7 to 10 hours in the summer and from 4 to 6 hours in the winter.

3.3 Hydrogeology

The classification of hydrogeological rock units is shown in Tab. 1. The sequence can be divided into two main complexes.

1. The upper Aquifer Complex: It has a total thickness of about 600 to 700 m consisting of the limestone and marl complex of the upper Cretaceous. It can be subdivided into several smaller aquifers and aquicludes. The groundwater in the upper complex generally moves towards the east (Fig. 8).

2. The lower Aquifer Complex: The thickness of this unit increases from south to north. It consists mainly of sandstone interrupted by thin layers of marl and limestone from the lower Cretaceous. According to SALAMEH & UDLUFT (1985), the thickness is assumed to be about 600m with a general groundwater movement towards the west (Fig. 8).

• Tab. 1 Simplified hydrogeological classification of rock units in the study area (JICA, 1995).

geological formation or group	regional hydrogeological classification		hydrogeological classification	lithology	saturated thicknesses (m)	permeability (m/s)
Mio-Plio-Quaternary	Jordan Valley Aquifer		aquifer / aquiclude	sand, limestone, clays, conglomerates	100-400	$6.6*10^{-3}$
Rijam (B4)	Upper Aquifer Complex	Upper Cretaceous Aquifer	aquifer	limestone / chert	15 ->100	
Muwaqqar (B3)			aquiclude	marl	50-400	
Amman-Wadi Sir (B2/A7)			aquifer	limestone / chert	50- >350	$10^{-5} – 3*10^{-4}$
Hummar (A4)			aquifer	dolomitic limestone	40-45	$7.58 *10^{-4}$
Ajlun (A1-A6)			aquifer	limestone / shale / marl	200-600	$5.3*10^{-7}$
Kurnub (K)	Lower Aquifer Complex		aquifer	sandstone / siltstone	50-300	$4.48*10^{-5}$
Zerqa (Z)			aquifer	limestone / marl dolometic limestone sandstone	50-600	

The hydrodynamic pattern according to SALAMEH & UDLUFT (1985) is shown in Fig. 8. The local recharge area is situated in highlands within the outcrops of the upper aquifer system. The groundwater flowing towards the west in the upper aquifer system discharges along the slope of the Jordan Valley in cold water springs. Groundwater recharged more to the east, flows towards the Azraq basin and infiltrates through the aquitards downward to the underlying lower aquifer system. The Dead Sea is forming the general base level of the area. This is why the groundwater in the lower aquifer system changes its flow direction to the west.

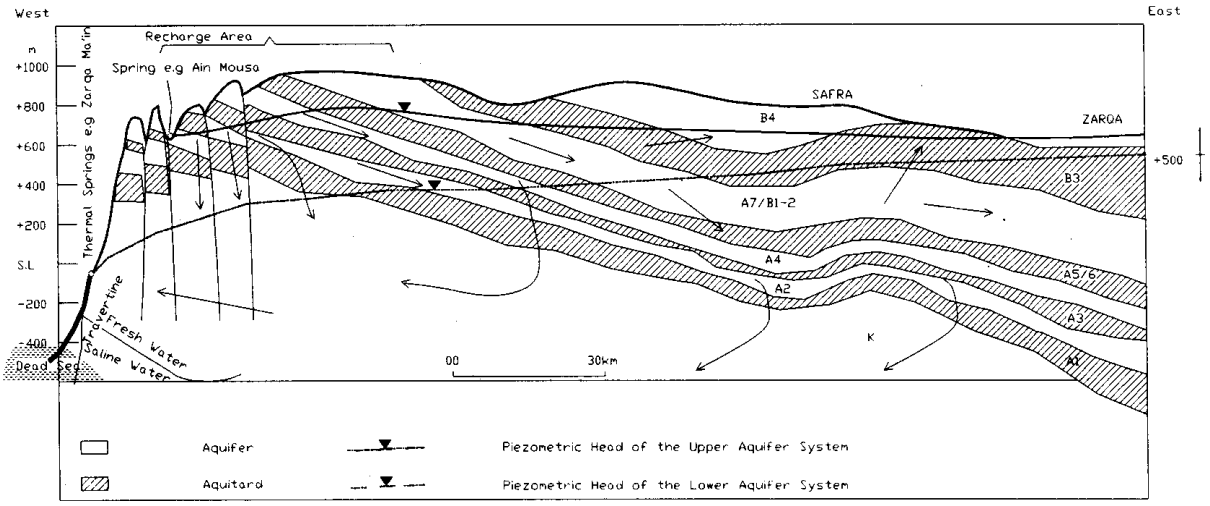

• Fig. 8 Hydrodynamic pattern of the central part of Jordan (after SALAMEH & UDLUFT, 1985).

A more detailed profile, explaining the leakage distribution of the deeper aquifer near the Jordan Valley Slope, is shown in Fig. 9. Due to the relief of the potential of the Kurnub sandstone, there is not only a downward leakage from the Kurnub sandstone to the Zerqa Ma'in group. According to JICA (1995) there might be an upward leakage from the Zerqa Ma'in group to the Kurnub sandstone.

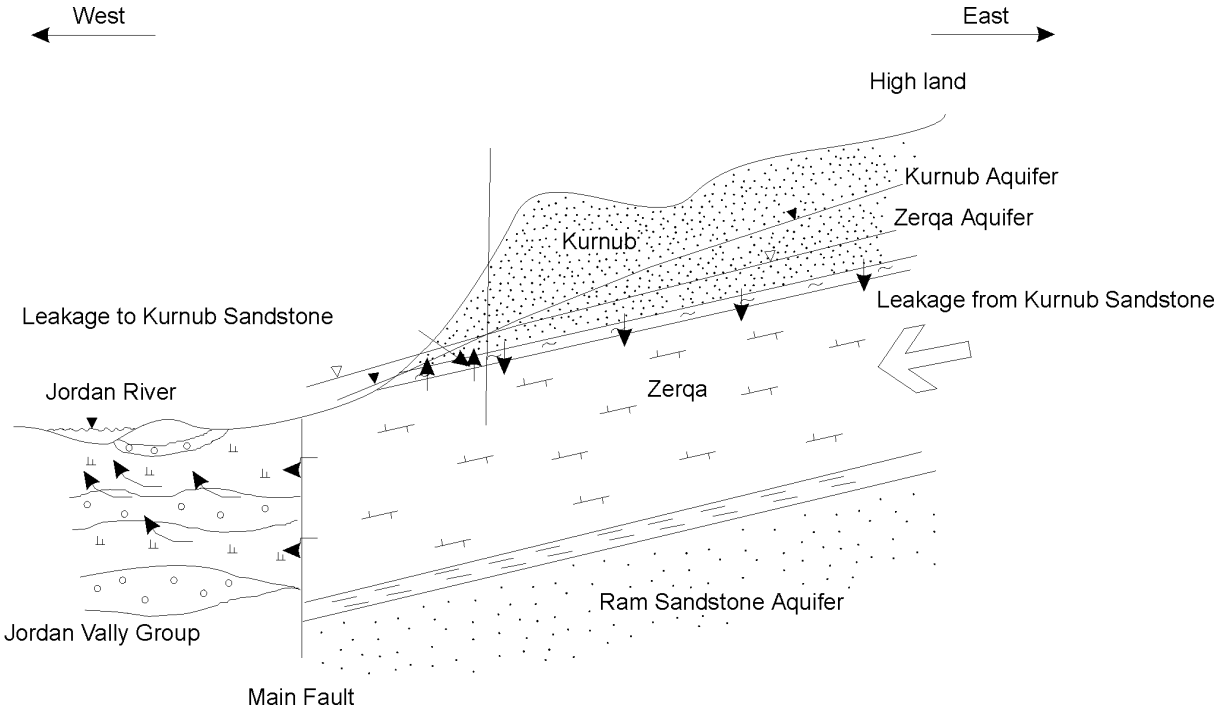

• Fig. 9 Schematic hydrogeological profile of the deeper aquifers in the study area. (modified after JICA, 1995).

3.4 Agriculture & Vegetation

Due to its climate, only 6% of Jordan is used for agriculture purposes (Fig. 10). Extensive agriculture can only be developed in regions with higher precipitation. Farm projects can be found along perennial rivers and wadis. Farmers use surface water for irrigation. Where the depth to the water table is not too large, the farmers withdraw groundwater from the upper aquifers for irrigation. Older wells are mostly dug by hand.

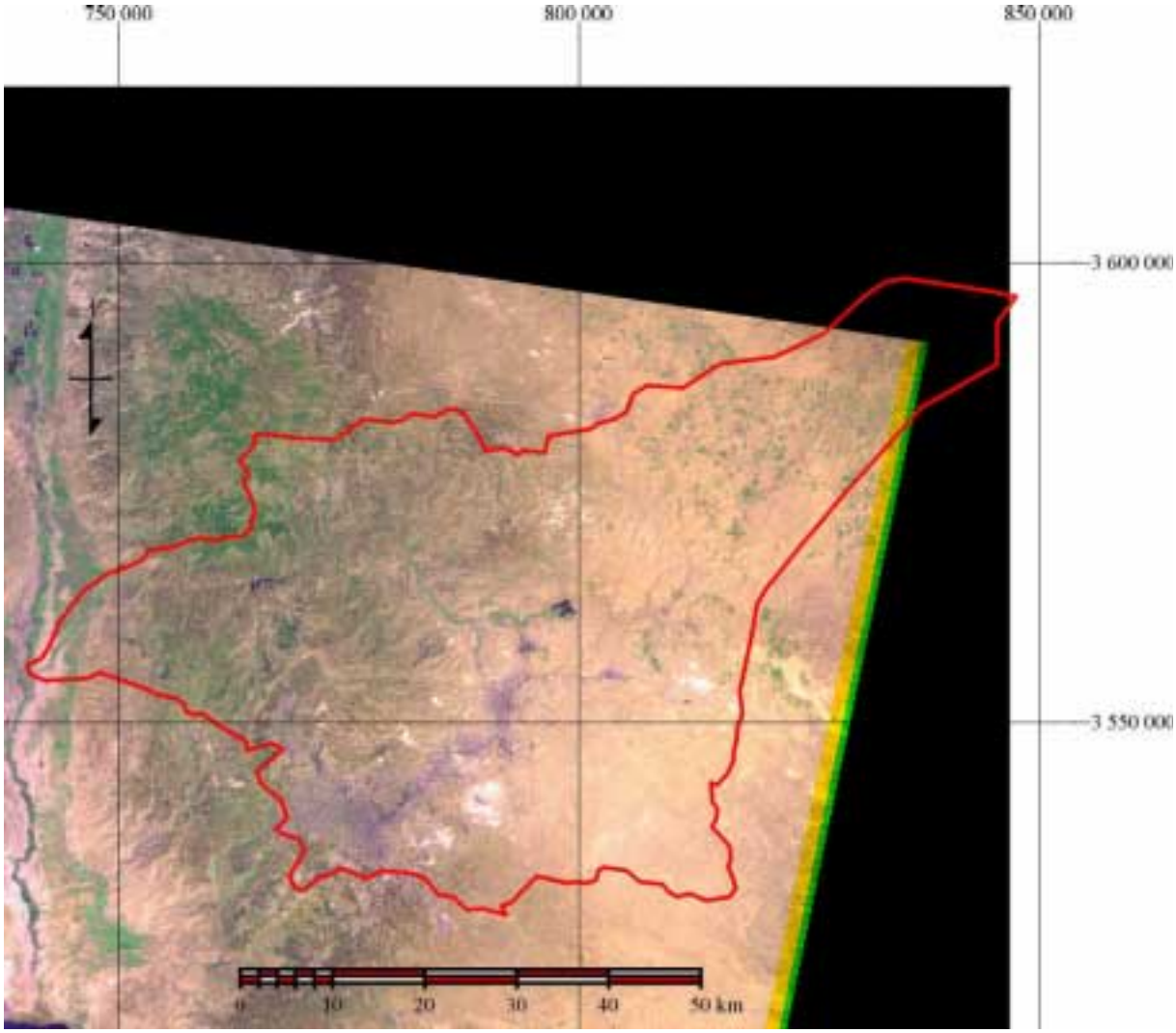

• Fig. 10 Satelliteimage view (RGB: 341), red line is the boarder of the model area; green colour indicates vegetation.

According to BENDER (1968), the original fauna was a forest of *Quercus aegilops* and *Pinus halepensis* which was cut down in the early history (since about 6000 BC) for copper smelting. Remains of this kind of forest can be found in the Ajlun-district. The main crop products are wheat, citrus fruits, tomatoes, cucumbers, olives and aubergines. A shift to plants with a higher water demand and even flowers can be observed nowadays.

4 Geological Mapping

The mapping area is situated to the east of the town of Deir Alla (Fig. 11), which liess in the Jordan Valley about 50km to the north of the Dead Sea. The field work was done during the first visit of Jordan. The western border of the area has been positioned at the mouth of the Wadi Zerqa, whereas the eastern border has been set to the large landslips about 10km from the mouth. The latest landslips occurred in 1996, when the river was dammed up for a certain time. The northern and southern border has been either set within the Kurnub sandstone or at the top of it, so that the north-south extension is about 5km.

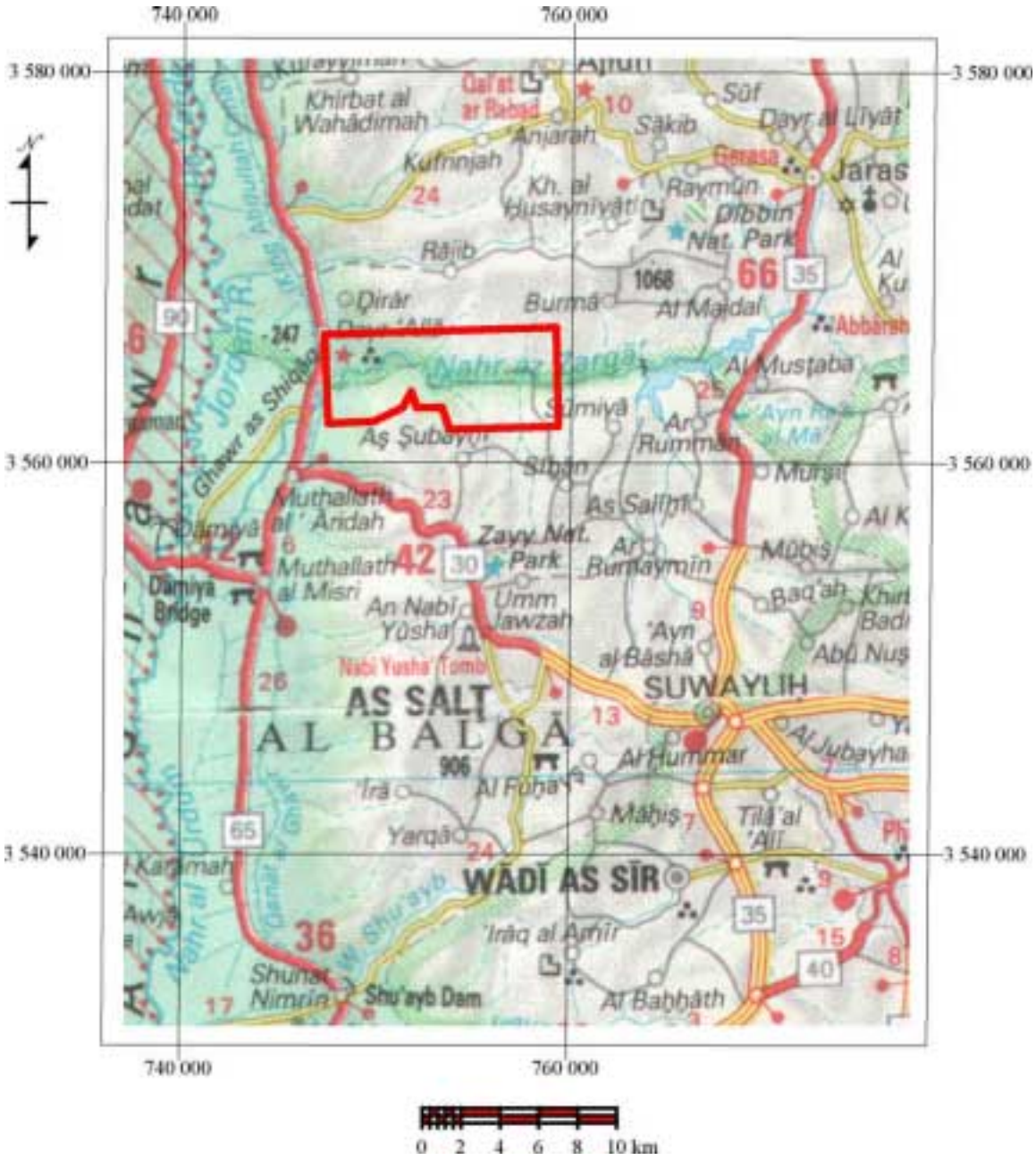

• Fig. 11 Location map of the mapping area (surrounded by red lines).

The stratigraphic sequence of the mapping area starts with the Zerqa Ma'in Group (Triassic) at the bottom and reaches up to the Kurnub sandstone (lower Cretaceous) (Tab. 2). Cenozoic sediments were deposited in the Wadi. The sequence has a total thickness of about 460m (Fig. 12).

• Tab. 2 Different nomenclatures of Jurassic rock Sequence in Jordan.

Quennell 1951	Wetzel and Morton 1959	Van den Boom & Lahluob 1962	Parker 1970	Basha 1980	Bandel 1981	This work	
Kurnub							Lower Cretaceous
Zerqa Group	Raman Group	Huni Form.	Limestone - Dolomite	Zerqa Group	Azab Formation (Z2)	Huni Marl Formation	Muaddi Formation	Mughanniyya Formation: Tahuna Clay Member	Azab Group	Jurassic
						Huni Dolomite-Limestone Formation	Arda Formation	Mughanniyya Formation: Shaban Limestone Member; Hamam Limest.-Sandst. Formation		
			Spotted Sandstone			Huni Dolomite Formation	Umm Maghara Formation	Ramia Sandstone Formation		
			Blocky Limestone			Huni Limestone Formation	Dhahab Limestone Formation	Dhahab Limestone Formation		
		Plant- Bearing Subeihi Sandst. Form.	Brown Sandstone			Huni Sandstone Formation	Zerqa Formation	Silal Sandstone Formation		
		Zerqa Gypsum Form.	Red Spotted Gray Limestone				Deir Alla Formation: Nimr Member	Nimr Limestone Formation		
							Deir Alla Formation: Huni Member	Hihi Claystone Formation		
					Ma'in Form.		Abu Ruweis Formation	Abu Ruweis Gypsum Formation		Triassic

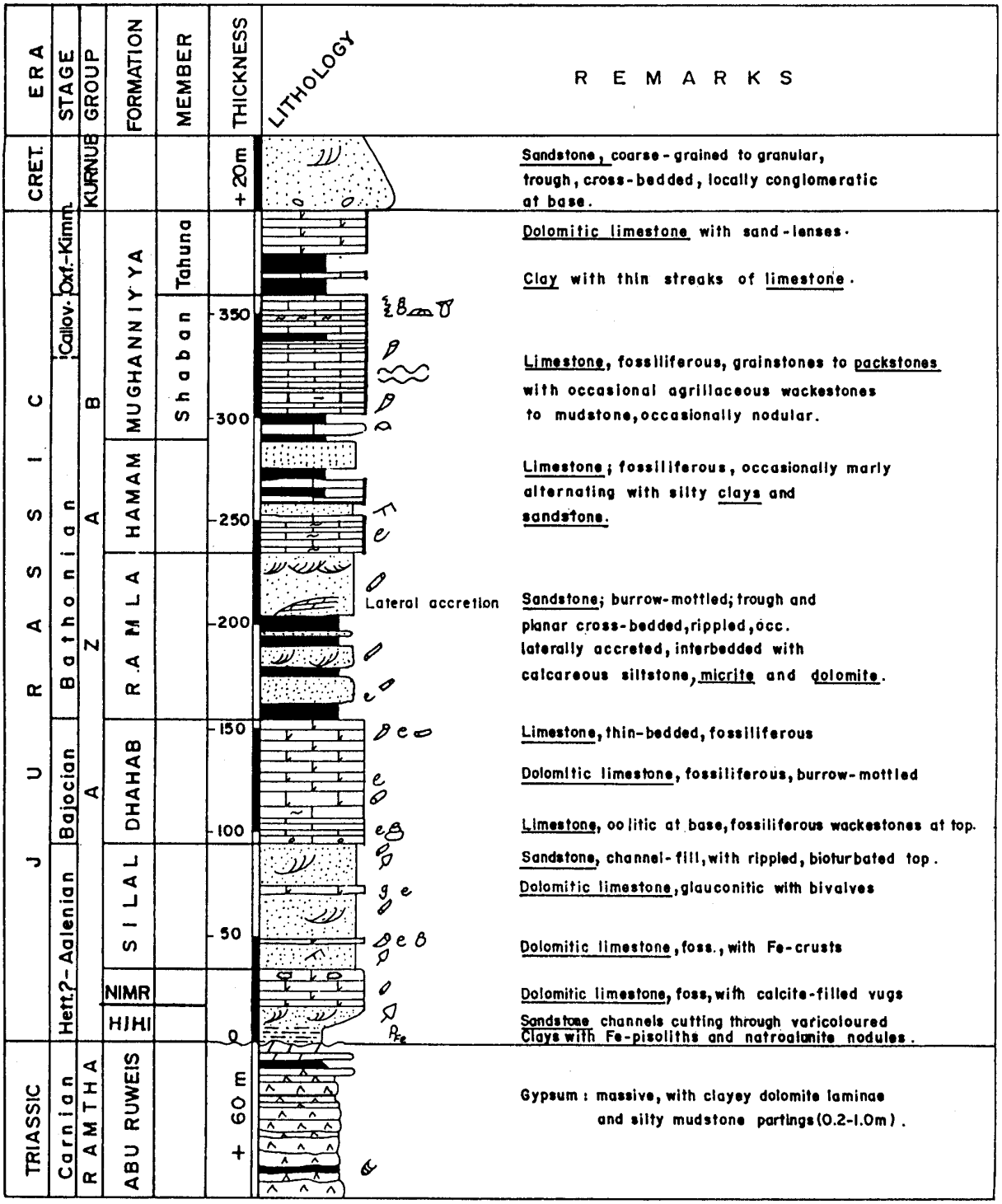

• Fig. 12 A generalised columnar section from the Jurassic sequence near the Zerqa river (KHALIL, 1992).

4.1 General geological settings

There are many different names for groups and formations mentioned in earlier works over Triassic, Jurassic and Cretaceous rocks in Jordan and Israel (Tab. 3). This works follows the recommendations on stratigraphical nomenclature outlined in Hedberg (1976), Holland et al. (1978) and particularly the North American Commission on Stratigraphic Nomenclature (NACSN, 1983) as closely as possible.

During the Mesozoic and Early Cenozoic, sedimentation was controlled by oscillating movements of the Tethys Ocean which was in the north and northwest of Jordan and the eustatic movement of the Arabian-Nubian Shield in the south. The Arabian-Nubian Shield was covered with Palaeozoic rocks.

Earlier authors observed a flattening of the Permo-Triassic sequence that thins southward below the unconformably overlaying Cretaceous Kurnub Sandstone. The sequence has also been intruded by basic dykes and sills. Generally the Permo-Triassic, Triassic and Jurassic sequences become more complete when traced northward. Bandel (1981) suggested that the relative completeness of the early Mesozoic sequence in the north of Jordan, as compared to the Dead Sea area, was due to the step-like northerly downfaulting of the sequence in pre-Cretaceous times rather than a result of north warding tilting and subsequent erosion of the sequence prior to deposition of the Kurnub sandstone.

- Tab. 3 Regional Time-Stratigraphic Correlation Chart of the different geological relevant units and formations recognised by various authors.

Geological time scale			Quennel (1951)			Masri (1963)[1]	German Geological mission (1966)[2]	UNDP / FAO (1970)[1]
Era	Period	Epoch	Group	Symbol				
Cenozoic	Quarter.	Holocene	Balqa Group				Basalt Flows	
		Pleisto.		Ba				
	Tertia.	Oligo.						
		Eocene		B5	Balqa Series		Chert Limestone	Shallala
		Paleo.		B4				Rijam
Mesozoic	Cretaceous	Maastr.		B3		Muwaqqar	Chalk-Marl	Muwaqqar
		Campan.		B2		Amman	Phosphor L.S.	Amman
							Silisified L.S.	
		Santon.		B1			Massive L.S.	W.Ghudran
		Turonian	Ajlun Group	A7	Ajlun Series	W. ES-Sir		W. Es-Sir
		Cenomanian		A6		Shueib	Echinoidal L.S.	Shueib
				A5				
				A4		Hummar		Hummar
				A3		Fuheis	Nodular L.S.	Fuheis
				A2		Na'ur		Na'ur
				A1				
		Albian	Kurnub Group	K2	Kurnub Sandstone	Subeihi	Kurnub S.S.	
		Aptian		K1		Ard'a		
	Jurass.		Zerqa Group	Z2	Zerqa Group	Azab	Zerqa S.S.	
	Tiass.			Z1		Ma'in		
Major unconformaity								

[1] Formation ; [2] Units

NB: the shaded area indecates the main water bearing formation in the carbonate aquifer system.

4.2 Zerqa Ma'in Group

The Zerqa Ma'in group is the lowest part of stratigraphy in the mapping area that rocks crop out of. The group belongs to the Triassic.

4.2.1 Abu Ruweis Gypsum Formation

The outcrop of the evaporitic formation has a length of about 3km and borders on large landslips so that its whole extension only can be estimated. The gypsum deposits are at present being quarried for the cement industry in two locations. The Abu Ruweis Gypsum formation was penetrated at the wells AJ-1, ER-1A, NH-2 and S90. The unit reaches a maximum thickness of 392 to 505m in the Al-Harra and western Risha areas. In the well AJ-1 (N32°1722, E35°4608) which is located about 5km to the northeast, the whole formation shows a thickness of 230m, the upper most 60m crop out in the mapping area. They consist of interbedded layers of massive gray gypsum, thin beds of dolomite, predominate red clay and bituminous silty mudstones which are slightly folded. Particularly the clay may thicken laterally. The content of $CaSO_4$ is inconsistent. According to AMIREH (1987), the upper boundary with the unconformably overlaying Hihi formation of the Azab Group is characterised by the presence of a paleosol horizon which is laterally variable in thickness between 0 to 8m. This horizon consists of claystone with one or more of the following: colour mottling, desiccation cracks, ferruginous glaebules and natroalunite patches. The claystone usually is capped by irregular iron crusts. Due to the landslips, this boundary was not clearly recognised in the mapping area. The deposition of the Abu Ruweis formation took place during a regressive phase in north Jordan. Due to the presence of anhydrite and dolomite, many authors consider the formation to be deposited within a marginal sabkah environment. The occurrence of halite in many wells indicates a salt pan development in the northeast.

The occurrence of gypsum and the slope of the wadi sides are estimated to be the reasons for the landslips.

There are two stone pits in the mapping area where the Abu Ruweis Gypsum formation is mined for cement industry. The southern one is at N 35643260 E 36756190, the northern one on the other wadi side at N 3564405 E 36758230 (Fig. 13). In both outcrops the bottom is built by a massive, slightly folded gypsum layer followed by thin beds of dolomite, predominate red clay and bituminous silty mudstones.

←W E→

• Fig. 13 Foto of the Stratigraphy of the Abu Ruweis Gypsum formation in the outcrops (N 3564405, E 36758230).

As shown in Fig. 14, there are one major (NW-SE) and two minor directions (ENE-WSW, NNW-SSE) of the cleavage. The bedding dips with about 15° and strikes with about 342° in the southern part. A measuring in the northern outcrop could not be done because of the current mining work.

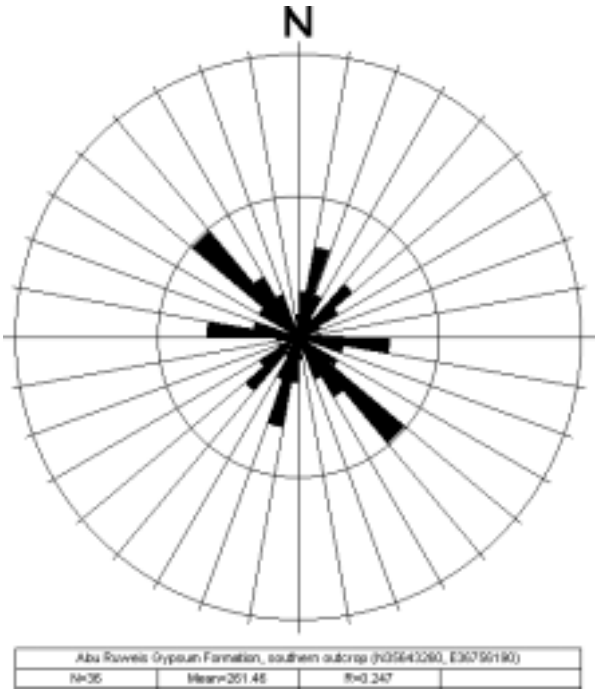

• Fig. 14 Rose diagram of the cleavage for the Abu Ruweis Gypsum formation in the southern outcrops.

4.3 Azab Group

The Azab Group incorporates the following seven formations (from bottom to top): the Hihi Claystone formation, the Nimr Limestone formation, the Silal Sandstone formation, the Dhahab Limestone formation, the Hamam Sandstone-Limestone formation and the Mughanniyya Limestone formation. The group forms a coherent unit of predominantly coastal carbonates and siliclastics. During the fieldwork it was recognised that units belonging to this group mainly form rugged, steep-faced cliffs of carbonate and sandstone and more gentle topographies underlain by clay-marl lithologies. The group is incised by deep wadis draining into the Jordan Valley, which is the general drainage in this area. The Azab Group is also known as the Z2 - Aquifer. It builds the main part of the stratigraphy of the mapping area.

4.3.1 Hihi Claystone Formation

The Hihi Claystone formation forms the lowest part of the Azab Group. Above the generally massive gypsum of the Abu Ruweis formation it starts with a varicoloured, soft weathering morphology and is overlain by a brown-yellow sandy horizon of the Nimr Limestone formation. It consists mainly of yellow and red silty mudstone commonly separated by thin layers of limestone. These mudstone facies is cutted by Sandstone channels.

As mentioned above, the Hihi formation starts with a gray, yellow and red silty mudstone with natroalunite nodules and iron pisoliths. This paleosol facies varies in thickness from 0 to 8m within a short distance. These thickness changes may indicate freshwater solution with extensive solution cavities and karstic surfaces. Due to the occurrence of Natroalunite, desiccation cracks and plant roots there should be seasonal, continental conditions including short dry periods during sedimentation. The paleosol is followed by bituminous siltstone often containing pebbly intraclasts. This facies is overlain by a fossiliferous thin-bedded limestone intercalated by shale. According to BANDEL (1981), the limestone has a fauna reflecting full marine conditions. The limestone-shale succession is overlain by a yellow-brown, iron-cemented, continuously cross-bedded and bioturbated sandstone with quartz granules. This sandstone fills channels which are up to 5m deep. The top is set at the first appearance of continuous carbonates of the overlaying Nimr formation (Fig. 15).

The total thickness of this formation in the mapping area is about 20m whereas 51m were recorded in the well AJ 1 (N32°1722, E35°4608). Due to the badland morphology, sliding in the evaporites, poor exposure and rapid lateral thickness changes it is impossible to get the whole thickness in one outcrop.

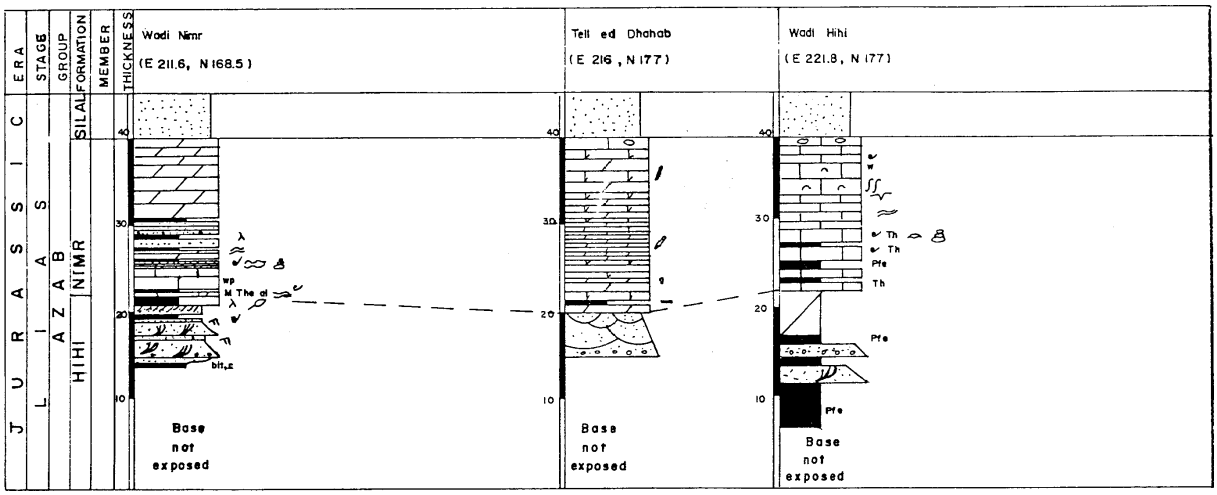

• Fig. 15 Profiles of the Hihi and Nimr formation in the Zerqa river (Tell ed Dhahab and Wadi Hihi) and Wadi Nimr (KHALIL, 1992).

4.3.2 Nimr Limestone Formation

This formation is characterised by its step-like, well-bedded, light gray carbonate ledges. They represent the first massive marine transgression of the Jurassic in Jordan. It forms a cliff above the soft weathering facies of the Hihi formation. In the Zerqa river area, the Nimr Limestone formation appears as a continuous outcrop from Wadi Hihi in the east to eastern Tell Ed Dhahab in the west.

The basal part of the Nimr Limestone formation is a gray, micritic limestone with a thickness of about 40 cm. It is followed by a reddish siltstone with iron pisoliths with an estimated thickness of 20 cm. This siltstone is followed by ~40cm thick, yellow-gray, fossiliferous limestone overlain by about 1m of yellow-gray clay. Similar shallowing-upward sequences of a total thickness of about 6m change upwards either to thin, very fine-grained sandstone, siltstone and shale or to finer carbonate. They are overlain by a fossiliferous limestone of about 2.5m thickness. The topmost 7m represent a massive, light limestone that is shallowing-upward. The base is formed by a packstone to grainstone, whereas the top consists of wackestone to mudstone. Load casts were developed between this unit and the underlying one.

The total thickness of this unit in the mapping area is 17 to 20m, whereas in the Ajlun Well (AJ 1 N32°1722, E35°4608) it reaches a thickness of 26m.

The Nimr formation records a transgression of the sea. The shoreline was south of the Wadi Nimr. In the higher parts of this formation, carbonate-dominated platforms with peritidal and lagoonal conditions were developed. Clastic source areas were no longer important. The shallowing-upward sequences, ripple cross-lamination (wavy bedding), algal lamination, wispy lamination and dolomitisation are the evidence for the interpretation as peritidal sedimentation. The grainstone-packstones of lagoonal or subtidal origin near the base of the shallowing-upward cycle is usually overlain by wackstone-mudstones with a wavy bedding, algal and wispy lamination that indicates an intertidal environment. The mudstone at the top should be built under supratidal conditions.

4.3.3 Silal Sandstone Formation

The Silal Sandstone formation mainly consists of siliclastic rocks. The friable sandstones and silty claystones have a gentle topography. Due to the thin layers of dolomitic limestone and ferruginous cemented Sandstone, it has a step-like morphology.

The Silal Sandstone formation is built of thick units of cross-bedded and channelled sandstone (Fig. 16). Laterally and to the top of the unit, they pass over a thin-bedded, sometimes rippled sandstone into a very fine-grained, often flaser-bedded, slightly burrowed sandstone or siltstone. Sometimes, the tops of these cycles contain carbonates, often glauconitic. Iron appears in the form of nodules, bands, ooliths and cement. Within the mapping area, about 8 of the fining-upward sequences were found. They have thicknesses of 1.6 to 8m. The base of a cycle usually is erosional.

The base is marked by the change from the massive, light limestone of the Nimr formation to the brown, ripple marked and cross bedded sandstone. The top has been placed where a yellow-brown sandstone is overlain by a medium-bedded white wackestone.

In the vicinity of the Zerqa river, the formation reaches a thickness of 35 to 45m and increases towards the south. BANDEL (1981) reports a thickness of 59 to 75m for the Wadi Umm Butma area.

During the sedimentation process of the lower units of this formation, the shoreline was in the south of the mapping area. Due to the characteristics of shallow water sediments (flaser-bedding, channels), the shoreline should not be too far away from the Zerqa river. The supply of sand varied in grain size from fine sand to gravel. During the deposition of the upper member of the formation, the shore retreated northward and oscillated at a line close to the current Zerqa river. The presence of limestone proves a transgression at the Wadi Zerqa area.

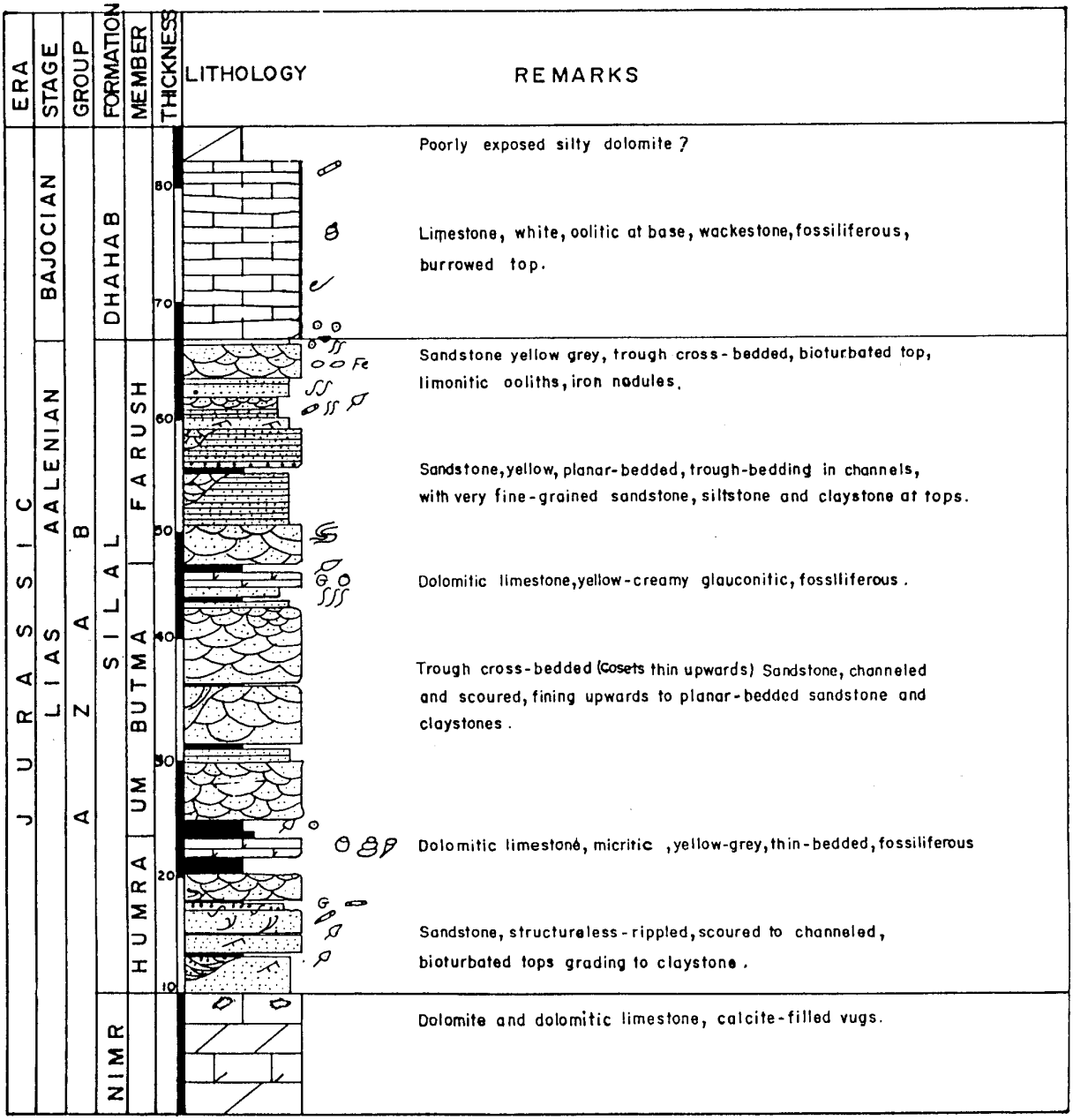

• Fig. 16 Lithological section in the Silal Sandstone formation, from the eastern Tell ed Dhahab area (E 215.5, N 177.3), Zerqa river (KHALIL, 1992).

4.3.4 Dhahab Limestone Formation

This carbonate formation builds distinctive steep rock walls and cliffs (Fig. 17). BANDEL (1981) subdivided the formation at Wadi Umm Butma into four subunits. These subunits can also be found in the mapping area (Fig. 18):

1. The thickness of the lowest subunit is about 10m. It consists of white, medium-bedded, slightly wavy-bedded biomicrite (wackestone) with bivalves and gastropods in it. The top of this subunit is a more massive-bedded and dolomitic limestone which contains less fossils.

2. The thickness of the second subunit is about 8m. It is poorly exposed in the mapping area and is considered to consist of silt and a dolomitic limonitic siltstone which contains much iron.

3. The third subunit is a 25m thick massive dolomite / limestone. The dolomitic areas show deeply weathered cliffs of yellow-brown colour and are medium bedded whereas the limestone is gray to creamy and fossiliferous.

4. The topmost thinly-bedded subunit consists of about 12m of fossiliferous, oolitic limestone with marl intercalations.

The limestones are very hard and dense. A characteristic feature of this formation is the change of weathering colour from gray to brown.

The base is marked by the change from the yellow-brown sandstone of the Silal Sandstone formation to the medium-bedded white wackestone. The Top is marked by the change of the fourth subunit to a calcareous, borrow-mottled sandstone. Between these units, there are few centimetres of iron pisolitic orange dolomite, clayey mudstones or sandstones which already belong to the Ramla formation.

BANDEL (1981) reported a 43 m thickness for the whole formation at Wadi Umm Butma. Other authors report a range from 50 to 57m of total thickness for this formation. The Dhahab formation is increasing in thickness and percentage of carbonate towards the north.

The sediments of the Dhahab formation are those of a shallow, open marine environment. An oolitic facies indicates a high energy of a shallow subtidal regime which is saturated with $CaCO_3$. The shoreline is considered to be in the south. In general, the environment should be a shallow shelf which was dolomitised later on.

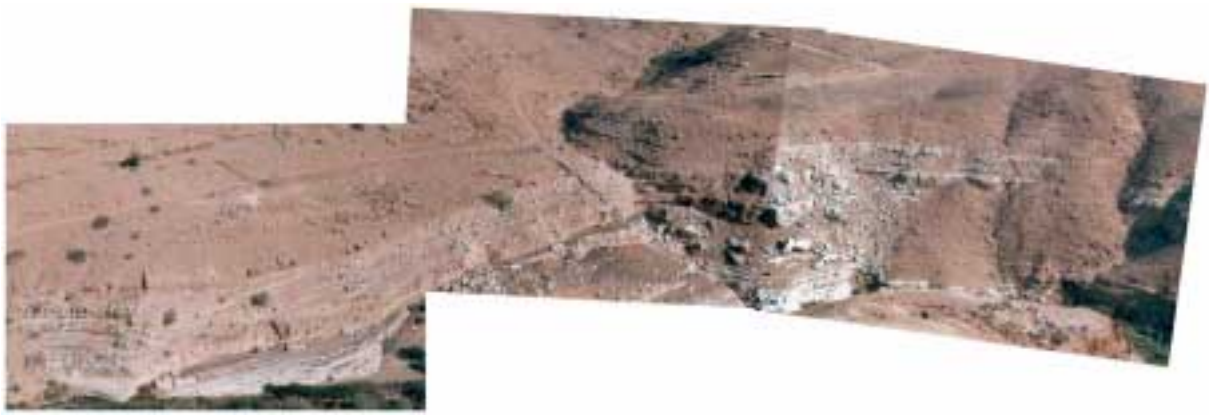

• Fig. 17 Overview of the Dhahab Limestone formation at Tel Dhahab.

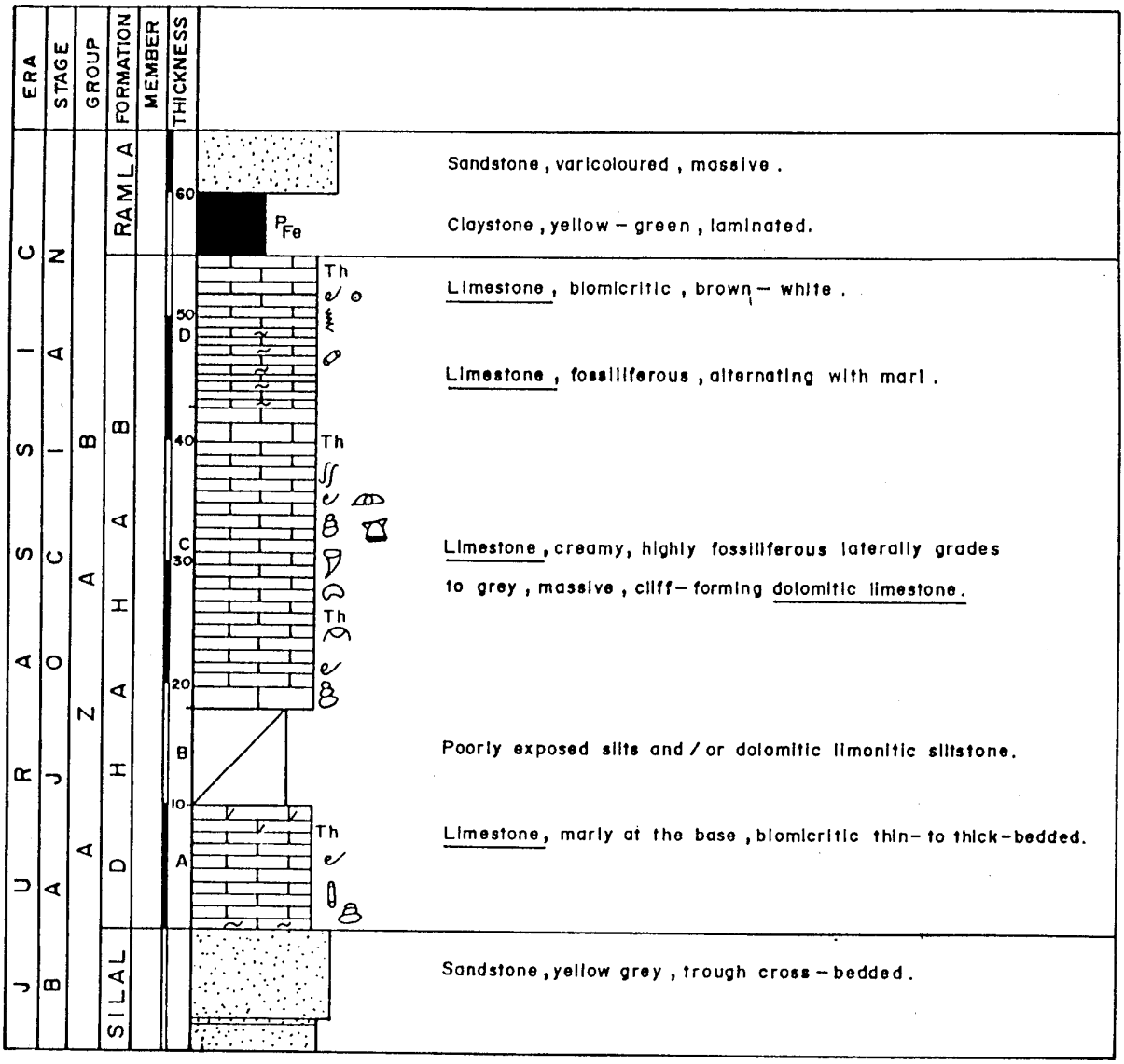

• Fig. 18 Lithological section of the Dhahab Limestone formation in its type area, Tell ed Dhahab (E 215.5, N177.3) (KHALIL, 1992).

As shown in Fig. 19, the main cleavage of the Dhahab Limestone at N3564453 E36753193 appears to be NW-SE and NE-SW.

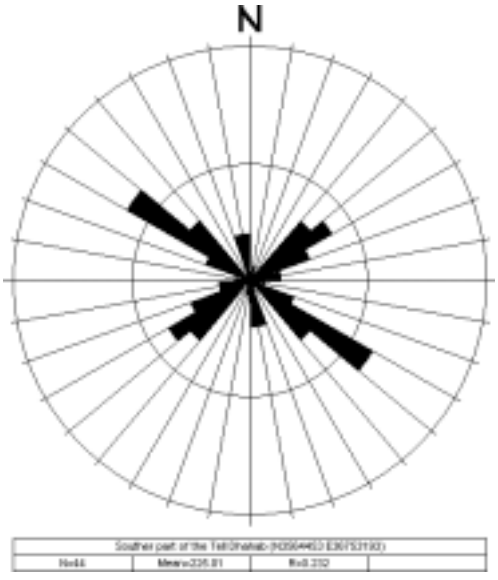

• Fig. 19 Rose diagram of the cleavage for the Dhahab Limestone formation.

4.3.5 Ramla Sandstone Formation

The Ramla Sandstone formation is of siliclastic nature and consists mainly of sandstone and clay with few, thin beds of limestone. It has a total thickness of about 80m. The basal meters show gray claystone with calcareous red siltstone with iron pisoliths. The rest of the formation can be grouped into fining-upward cycles. They start off with a planar cross-bedded sandstone with a thickness of 5-8m. This sandstone is medium- to coarse-grained and occasionally granular. It is followed by a thinly and horizontally bedded, ripple cross-laminated fine- to medium-grained sandstone. The next unit of the cycle is built of a varicoloured siltstone or claystone. These interbeds of ripple cross-laminated fine-grained sandstone usually alternate with this facies. The last unit is built of a dolomitic limestone. It ranges in thickness from 0.5m to 4m. It contains some algal-laminated limestone and bivalves.

The base is marked by the change of the gray-creamy, fossiliferous limestone of the cliff forming Dhahab formation to the few centimetres of iron pisolitic orange dolomite, clayey mudstones or sandstones. The top is defined by the change from the siliclastic facies of the Ramla Sandstone formation to a carbonate facies which consists of creamy fossiliferous mudstone to wackestone.

Intermixed lithologies, sedimentary structures, coal, marine fauna and bioturbation structures show evidence for a tidal environment. The presence of ferruginous ooids suggests a nearby river mouth.

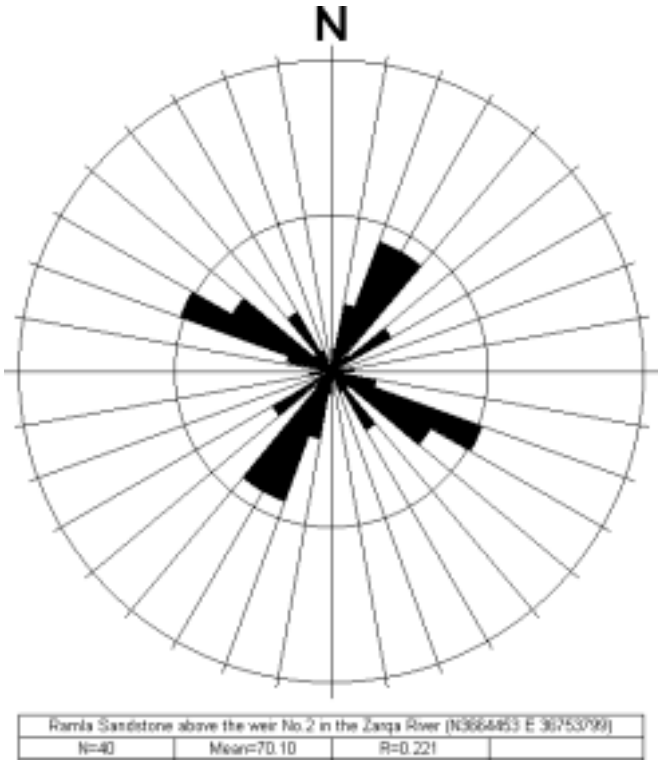

• Fig. 20 Rose diagram of the cleavage for the Ramla Sandstone formation.

As shown in Fig. 20, the main cleavage of the Ramla sandstone at N3664453 E36753799 appears to be NE-SW and NW-SE.

4.3.6 Hamam Formation

The Hamam formation is a mixture of siliclastic and carbonate rocks. Different weathering has created a step-like morphology.

KHALIL & MUNEIZEL (1992) subdivided the formation into nine different subunits (Fig. 21):

1. The basal part consists of gray, fossiliferous, hard limestone. It is followed by about 15m of gray, laminated calcareous clayey mudstone. This mudstone captures macrofossils and is alternating with a red-pink mudstone that captures brachiopods and limy pebbles. The upper 8m are characterised by the presence of bitumen. KHALIL & MUNEIZEL (1992) mentioned a deposit of amber and coaly seams; this was not proven in the mapping area.
2. The basal part of the subunit consists of 13m of yellow-brown, medium-grained, bedded, channelled sandstone, alternating with a fine-grained, thin-bedded sandstone with flaser-bedded, commonly ripple cross laminated clay interbeds. The following about 7m consist, of yellow, fine-grained, massive bedded sandstone alternating with beige to gray fine grained, ripple cross-laminated sandstone. The last 4m are built of gray claystone.
3. The subunit comprises a cream, rippled cross-laminated, fossiliferous, marly limestone that alternates with a white bedded limestone. It has a thickness of about 9 to 10m.
4. This subunit has only a thickness of about only 1 to 2m. It consists of brown, medium-grained, sandstone.
5. This subunit comprises a gray, thick-bedded, fossiliferous, packstone that is alternating with a gray medium bedded, micritic mudstone. It is about 7 to 8m thick.
6. This subunit with a thickness of about 3,5m comprises two massive sandstone beds which are separated by a pisolitic, ironstone.
7. Subunit seven represents 6m of yellow-brown, medium-grained, thin-bedded, sandstone.
8. This subunit consists of a gray, thin-bedded dolomite with a thickness of 2m.
9. The uppermost subunit shows a varicoloured, laminated, non-calcareous clay which was synsedimentary faulted.

The base is set at the first appearance of fossiliferous limestone beds. The top is marked by the change from the varicoloured clay to a dolomitic sandstone of about 2m thickness which belongs to the Mughanniyya Limestone formation. The overall thickness of the Hamam formation is about 75m.

The general deposit environment should be a mixed carbonate-siliclastic shoreline. Subunit 1 represents a shallowing cycle consisting of an intertidal-subtidal environment at the bottom and passing upwards to a swampy, anoxic condition. The other subunits record gradual deepening and shallowing of the sea. The cross-bedded, massive sandstones are considered to be tidal channels or fluvial deposits cut into the tidal, flaser-bedded sandstones.

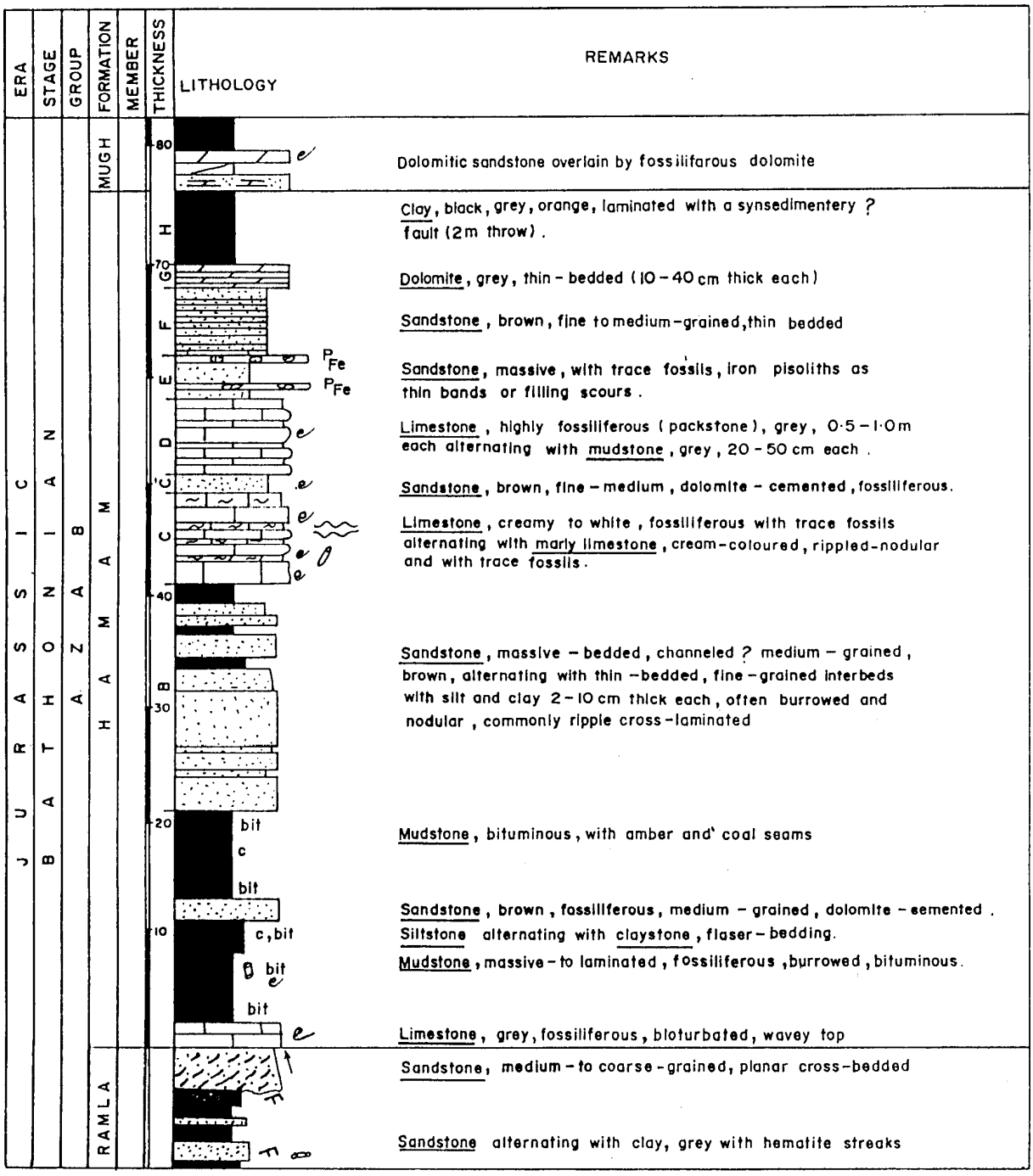

• Fig. 21 Lithological section of the Hamam formation in Wadi al Hamam (E 211.5, N 172.5) (KHALIL, 1992).

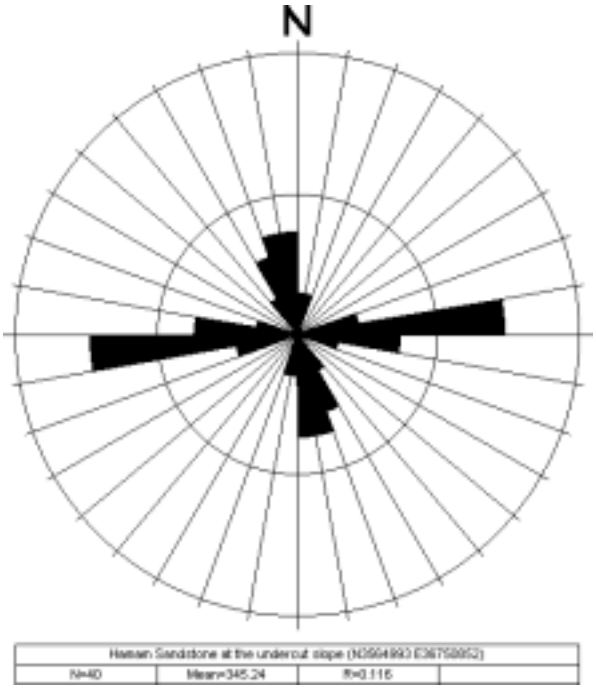

• Fig. 22 Rose diagram of the cleavage for the Hamam Sandstone formation.

As shown in Fig. 22, the main cleavage of the Hamam sandstone at N3564993 E36750852 appears to be NNW-SSE and WSW-ENE.

4.3.7 Mughanniyya Limestone Formation

The Mughanniyya Limestone formation is the uppermost unit of the Jurassic sequence in Jordan. It comprises mainly limestone, marl, clay and dolomite. In the topographic profile, cliffs alternate with a more gentle topography.

BANDEL (1981) subdivided the formation into two subunits: the lower Shaban Member and the upper Tahuna Member (Fig. 23).

The lowermost about 20m of the Shaban Subunit, as described by BANDEL for the Wadi Shaban area, comprise dolomitic sandstones, highly fossiliferous and oolitic limestone / dolomite, gray to pink clays and bedded, fossiliferous, about 13m thick limestones which have thin interbeds of red-orange silty clay. These are followed by about 10m of gray, fine-laminated, fossiliferous clay. The latter is overlain by about 6m of yellow, dolomitic limestone. The limestone is overlain by about 15m of marl that alternates with thin layers of limestone. The uppermost part of the Shaban member is built of about 10m fossiliferous limestone consisting of beds of beige packstone which are alternating with yellow-gray mudstone. In the Wadi Tahuna area which is a tributary of the Wadi Zerqa, the clay beds present in the lower parts of the Shaban Member become marl or marly limestone. The lithology of the rest is almost the same as that of the type area.

The Tahuna Member comprises about 10 to 15m of yellow-green, silty claystone with streaks of limestone, gypsum and allunite, overlain by about 20m of limestone. The latter consist in the basal 5m of fossiliferous mudstone to wackestone, overlain by about 2m of limestone alternating with a

cross-bedded and fossiliferous mudstone-packstone that shows loadcasts. These are overlain by 2m of yellow, argillaceous limestone followed upwards by beige-yellow, brown limestones which change from micritic at the base to packstone textures at the top. The following lithology is a 3m thick gray clay overlain by a light brown, bedded dolomite. The top of the limestone subunit is built of a mudstone bed. It is overlain by 3m of massive-bedded, finely laminated dolomite. The upper 6m of the Mughanniyya Limestone formation are built of a yellow-gray, cross-laminated dolomitic limestone. NW-SE orientated Channels and scours, filled with an upgrading, cross-bedded sandstone can usually be found at the top.

The base is marked by the change from the varicoloured clay from the Hamam formation to a dolomitic sandstone of about 2m thickness from the Mughanniyya Limestone formation. The top is marked by the distinctive change from the cross-laminated dolomitic limestone to the varicoloured sandstones, locally with basal conglomerates of the overlying Cretaceous Kurnub Group. The total thickness of the Mughanniyya Limestone formation is about 110m.

In my opinion, the environment of the Shaban Member should be a low energy shelf with some high energy events. The sediments of the Tahuna Member should be deposited on a muddy shelf with some river mouths near by, local low oxygen levels and mudflats. The high fossiliferous carbonate horizons might have their reason in a storm washover.

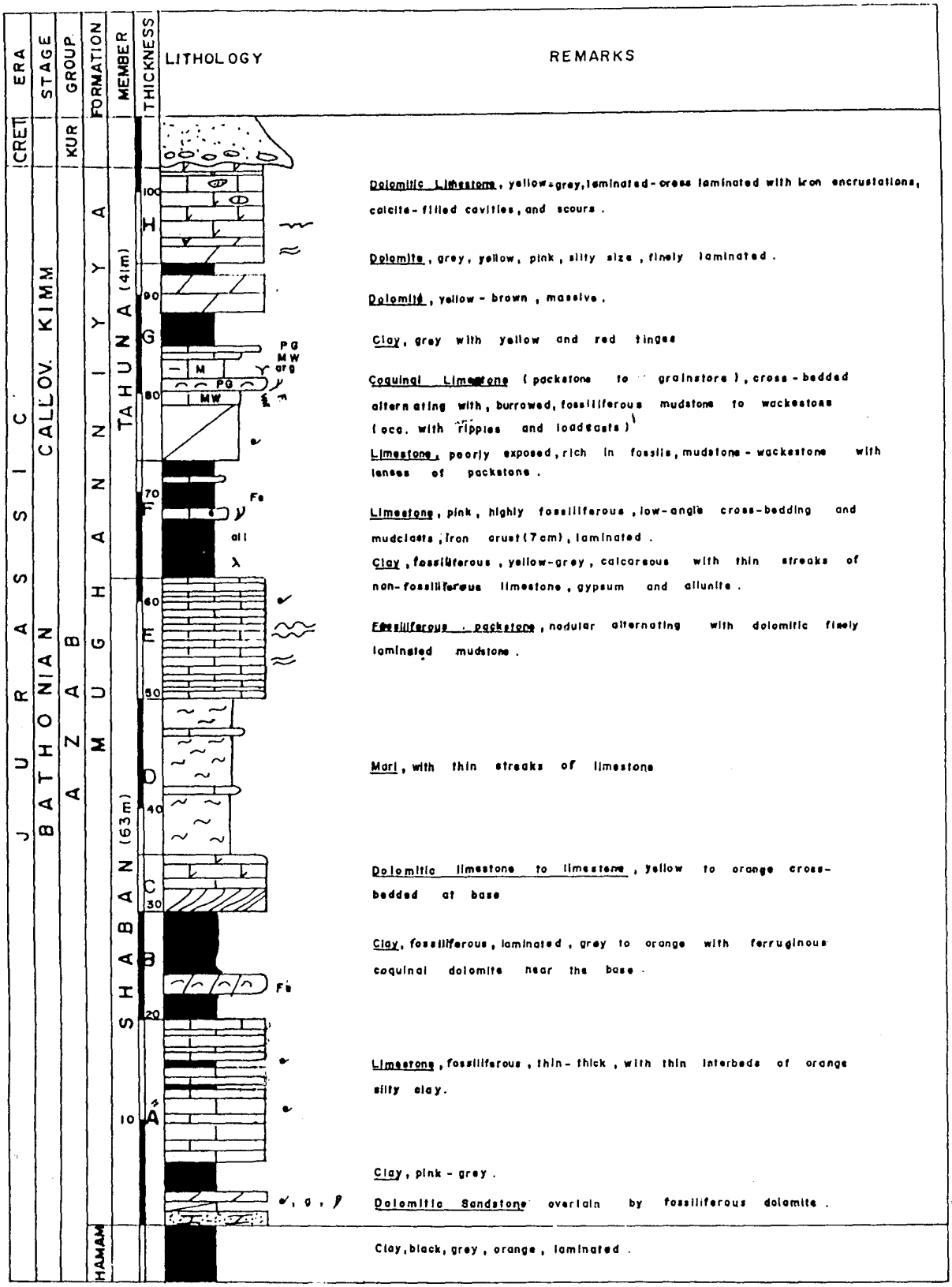

• Fig. 23 Lithological section of the Mughanniyya formation, from the Wadi Shaban area (E 174.5, N 211.0) (KHALIL, 1992).

4.4 Kurnub Sandstone Group

The group in the study area is morphologically characterised by cliff building units and units that are less expressed (Fig. 24). BENDER (1968) subdivide the Kurnub Sandstone Group, but due to its lithology it was not found suitable for the mapping area. The Kurnub Sandstone Group consists of mega cross-bedded, coarse and pebbly, varicoloured quartz arenite (Fig. 25). Fining-up cycles and channels are typical. Sometimes interbeds of thin horizontally bedded red-beige fine-grained sandstones and siltstones appear. Glauconitic sandstones and alunite are common. ABED (1982) reported some coal within the fine-grained units. As well dolomitic cemented sandstones and dolomite appear in the upper parts of the lithological profile in the mapping area. The thickness of the Kurnub Sandstone Group is about 250 to 300m.

The base is marked by the change of the Jurassic carbonates to the Cretaceous sandstones, sometimes with basal conglomerates. The top was outside the mapping area. ABDELHAMID (1995) describes the base of the following Naur Limestone formation as indicated by the presence of a gray-green, shallow marine glauconitic sandstone which unconformably rests on the continental sandstones of the Kurnub group.

The Sediments of the Kurnub Group were built by a meandering river system in an alluvial plain. The interbeds are flood plain deposits and deposits of a shallow marine environment.

←W E→

• Fig. 24 Kurnub Sandstone at N 3565209 E 36757076.

• Fig. 25 Detail view of the Kurnub Sandstone with Mg/Fe-nodules.

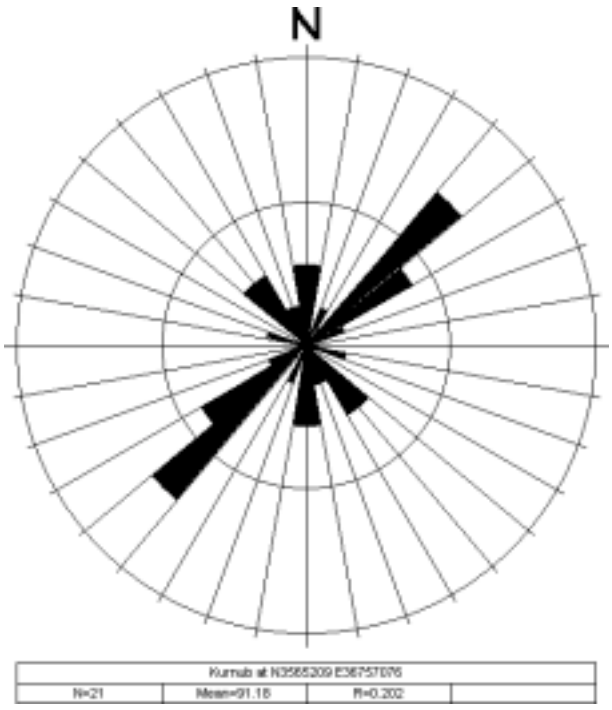

• Fig. 26 Rose diagram of the cleavage for the Kurnub Sandstone formation.

As shown in Fig. 26, the main cleavage of the Kurnub sandstone at N3565209 E36757076 appears to be NE-SW. Two minor ones with N-S and NW-SE could also be measured.

4.5 Ajlun Group

The Ajlun group was only mapped in the south west near the Jordan valley to get a better idea of the tectonic settings.

4.5.1 Naur Limestone Formation

The Naur limestone formation appears in the mapping area due to some fault systems but the complete lithology could not be found.

The formation starts off with a fine grained sandstone which contains in some parts glauconite, silt or clay. It is followed by limestone, marl, chalk and their combinations. Mudstone to wackestone textures, horizontal lamination as well as fossils are common. In the uppermost part there is a shift to packstone texture whereas fossils are abundant, too.

The total thickness can only be estimated to 100 to 150m.

The siliclastic layers at the bottom indicate a shoreline. The carbonates of the formation were deposited under normal marine conditions in a shallow warm sea. This is why a transgression might have occurred.

4.6 Quaternary Sediments

4.6.1 Lisan Marl Formation

This white, light gray formation rests unconformably on strata of Mesozoic and Cenozoic ages. It was mostly mapped together with the Damya formation because of small thickness in the mapping area. The formation consists of two alternating lithofacies: laminated evaporites (gypsum, aragonite, calcite and anhydrite) and massive mudstone (quartz, feldspar, clay minerals). The evaporites are generally thin bedded and varve like. In literature, maximum thicknesses of 35 to 40m are mentioned, which could not be proven in the area. A clear contact to the underlying formations was not found in the mapping area. The sediments were deposited in a lake which had fresh, brackish and saline phases. The evaporites dominate in the upper part of the formation.

4.6.1.1 Damya Sandy Limestone Formation

The formation is characterised by red to brown colour (Fig. 27). However, the boundary to the underlying Lisan Marl formation can be clearly seen. It consists of thin to medium bedded silty limestone to calcareous mudstone. Most of the rounded to subrounded grains are extraclast pellets. In the mapping area it has a thickness of about 4m. Occasionally the formation is overlain by soil. The red colour and the absence of evaporates suggest the sediments' deposit in a fresh water lake.

←E W→

• Fig. 27 Damya Sandy Limestone formation at the mouth of the Wadi Zerqa.

4.6.2 Superficial Deposits

4.6.2.1 Fluviatile Gravels of Pleistocene Age

Small outcrops of pebble to boulder gravel occur above the present drainage system of the mapping area (Fig. 28). The best one is on the northern side at the mouth of Wadi Zerqa. It consists of poorly sorted, subangular to rounded local bedrocks clasts. The presence of calcrete explains that it is partly cemented.

• Fig. 28 Block of fluviatile gravels of Pleistocene age at the mouth of the Wadi Zerqa.

4.6.2.2 Holocene to Recent Sediments

Salt crusts are commonly found in the surrounding of the thermal springs in the Wadi Zerqa, (Fig. 29). Chemical analyses have not been made but in some places the crusts had a slightly salty taste.

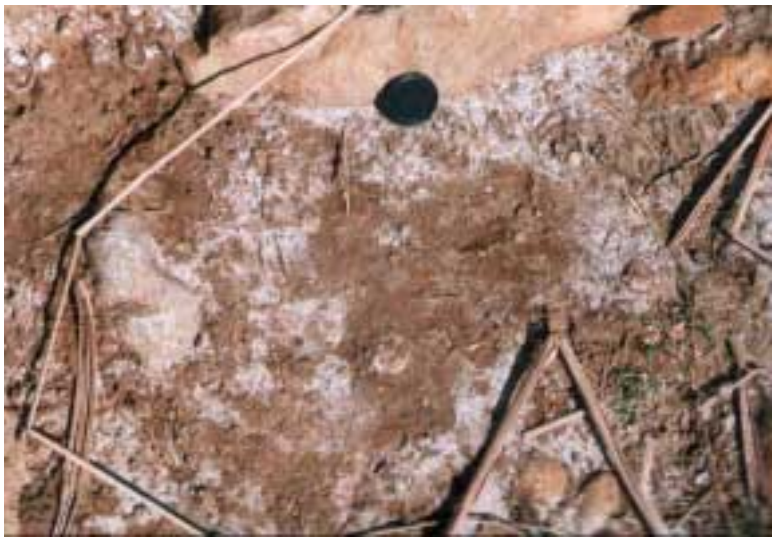

• Fig. 29 Salt crusts in the surroundings of the thermal springs in the Wadi Zerqa.

Alluvium

These sequences of alluvium consist of subrounded, matrix- but mostly clast-supported pebbly gravels which fill the wadi courses (Fig. 30). At the mouth of the wadis alluvial fans can be found. They have thicknesses of more than 10m.

←NW SE→

• Fig. 30 Recent Wadi sediments at a road cut in Wadi Zerqa near the gypsum stone pit.

Soils

Soils are most common along the Wadi sides (inner banks) and in the Jordan Valley (Fig. 31). In the south-east of the mapping area, there are some hollow moulds. Higher precipitation makes them fill up with red soils of terra fusca-rendzina type which tend to calcrete in some places. Generally the soils have little or no profile development.

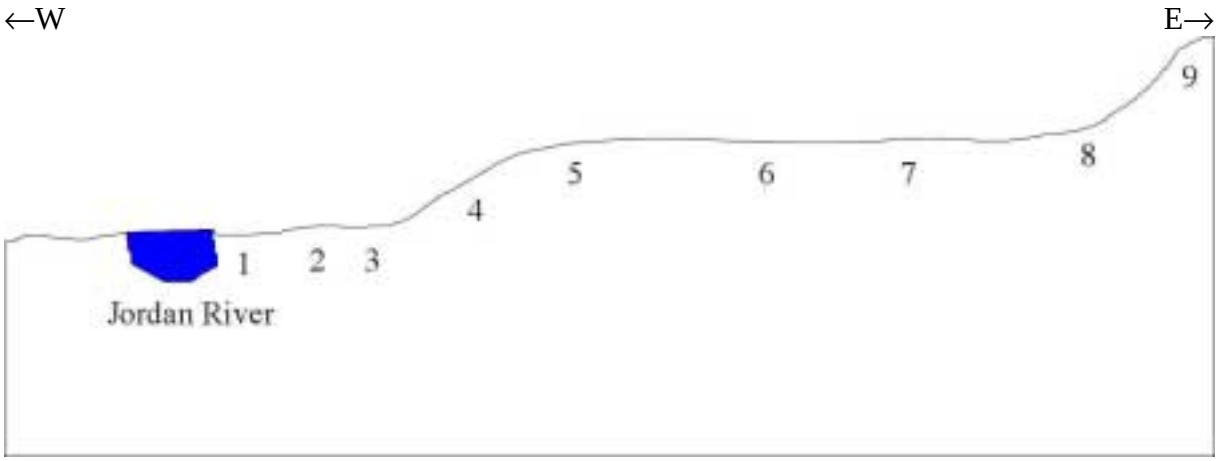

Physiography	Soil Description
1. Levee	Coarse loamy, deep, well drained soil
2. Interlevee	Coarse loamy to loamy-deep, non saline, well drained soil on gently sloping land
3. Terrace	Fine loamy, very deep non saline, well drained soil
4. Katar	Fine loamy clayey, moderately deep to deep, imperfectly drained soil
5. Toe slope eroded	Loamy moderately deep, imperfectly drained soil
6. Toe slope	Loamy shallow to moderately deep imperfectly drained soil
7. Basin	Clayey moderately deep, poorly to imperfectly drained soil
8. Foot slope	Loamy skeletal, moderately deep to deep, well drained soil
9. Back slope	Coarse loamy, skeletal moderately deep, well drained soil

• Fig. 31 Characteristic topsoil types along a west-east cross-section of the Jordan Valley (modified after, AL KUISI, 1998).

4.7 Structural Geology

The mapping area lies on the eastern side of the Dead Sea-Jordan Valley Transform Fault (Fig. 32). It is part of the boundary between the African and Arabian plates. In detail it represents several pull-apart basins (Fig. 33). It is estimated that there was a first stage with 62km of horizontal movement taking place in the latest Oligocene / early Miocene and a second stage with a 45km movement occurring in the Plio-Peistocene and still continuing today. According to WOLF (1998), there is a sinistral movement of 107km today and a large vertical downthrow (up to 1500m). The segments of this fault in the mapping area are covered by Lisan Marl and Peistocene to recent sediments. There are several sub-parallel faults in the mapping area which also roughly extend from south to north. They have downthrows mainly to the west and occasionally to the east.

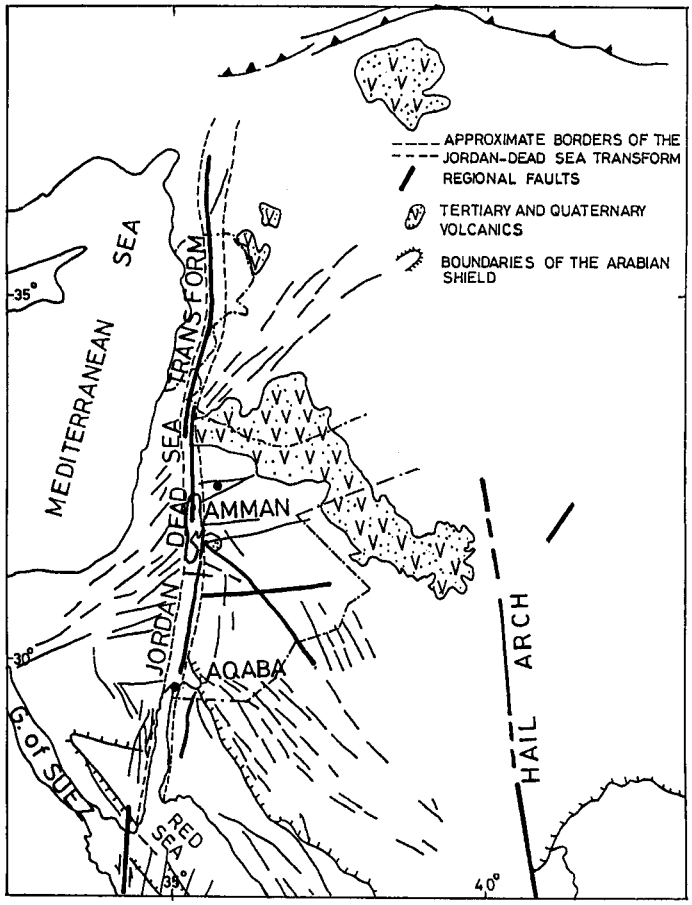

• Fig. 32 Major tectonic elements of the Jordan-Dead Sea transform (ZUHAIR, 1992).

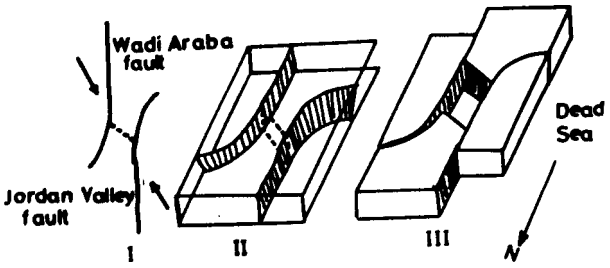

• Fig. 33 Block diagram showing the formation of the Dead Sea (ATALLAH, 1991): I-Fault pattern and direction of compressive stress. II-Faults before movement. III-Faults after movement.

The second major fault system is the so called Zerqa River Fault which strikes E-W (Fig. 34). It has not always been recognizable because of the nature of sandstones exposed on both sides of the valley and the landslips in the surroundings of the river. The minor faults of the mapping area are relatively short and have different amounts and directions of throws. They generally strike NW-SE, NNW-SSE and WNW-ESE and reflect a tensile fracture mechanism.

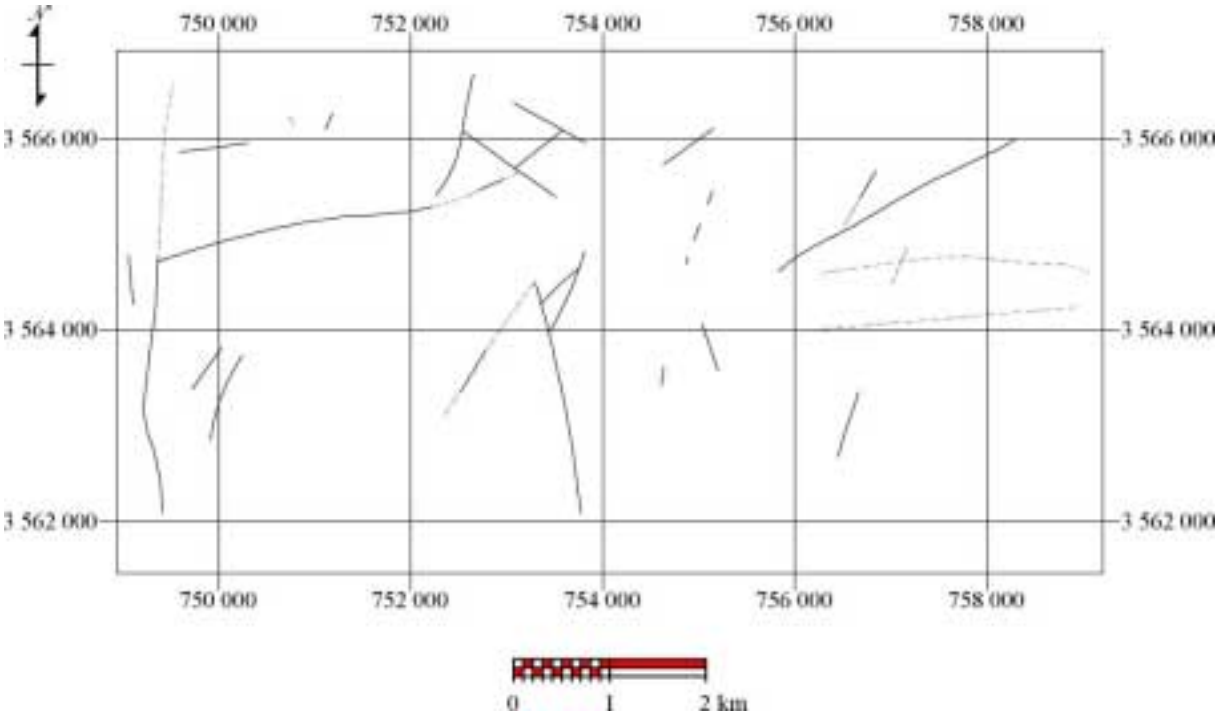

• Fig. 34 Map with the main tectonic elements in the mapping area.

The whole mapping area is influenced by the Zerqa River anticline with a N-S axis plunging to the north and to the south. The Zerqa River Valley and the anticline represent a relief inversion. Any hydraulic properties of the faults could not be seen except for the ones discussed in the hydrochemistry chapter (6.2).

5 Methods

5.1 Geoinformation System

All databases used in this work are based on Microsoft® (http://www.microsoft.com) ACCESS. The program got close to its limits with over 300,000 records in the climate database.

The GIS software used for this work is called TNTmips (http://www.microimages.com). TNTmips is one of the few GIS which can display layers (Raster, Vector, CAD, TIN, Database) in different grid-coordinates in one window, e.g. using ARCINFO, ARCVIEW you would have to recalculate all layers to one system. The problem was to get the parameters of the different grids and datums used in the maps which were available.

5.1.1 Georeference

All topographic maps of the area are based on the Transvers Mercator -System (European Datum), whereas the geological maps are based on the Palestine Grid. The Palestine Grid of 1928 has its origin at station Number 2 where: Φ_0 = 31°18'06.27'' North, Λ_0 = 34°31'42.02'' East of Greenwich, the reference ellipsoid is Clark 1880 where a = 6,378,300.789m, 1/f = 293.466004983713280, and the elevation is set to 98.9m. Another grid from 1933 is based on Cassini-Soldner coordinates. Its origin is in Jerusalem at ϕ_0 = 31°44'02.749'' North and λ_0 = 35°12'39.29'' East of Greenwich + 4.200''E = 35°12'43.490''. According to MUGNIER (2000) the addition of 4.200'' to the longitude is in accordance with the decision in 1928 to adopt values from the French grid, founded in Egypt, for the longitude at the points of junction 73'M and 98'M in the north, and to correct all Palestine longitudes accordingly. The false easting is 170,251.555m, false northing = 126,867.909m. There also exists a military version of this system based on Gauss-Krüger Transvers Mercator. It is identical to the civil Cassini-Soldner grid, except for false easting at false origin where 1,000,000m were added.

5.1.2 Digital Elevation Model (DEM)

For the DEM of the mapping area, the topographic map sheet Es Salt 3154 III with a scale of 1:50,000 was scanned with 600 dpi and imported to the GIS-Software TNT-Mips 6.2. The isohypsometric lines were digitalised for the whole mapping area from these scanned maps. The 1km hydrological corrected DEM from the USGS was used as base for the entire area (http://edcwww.usgs.gov/landdaac/gtopo30/hydro/index.html). To get a better transition to the 1km DEM of the USGS, more and more isophyses were left out approaching the boundaries (Fig. 35). Unfortunately, the map sheet 3154 II was not available during my stay in Jordan, therefore the vector dataset of the mapping area has a hard transition at its eastern boundary.

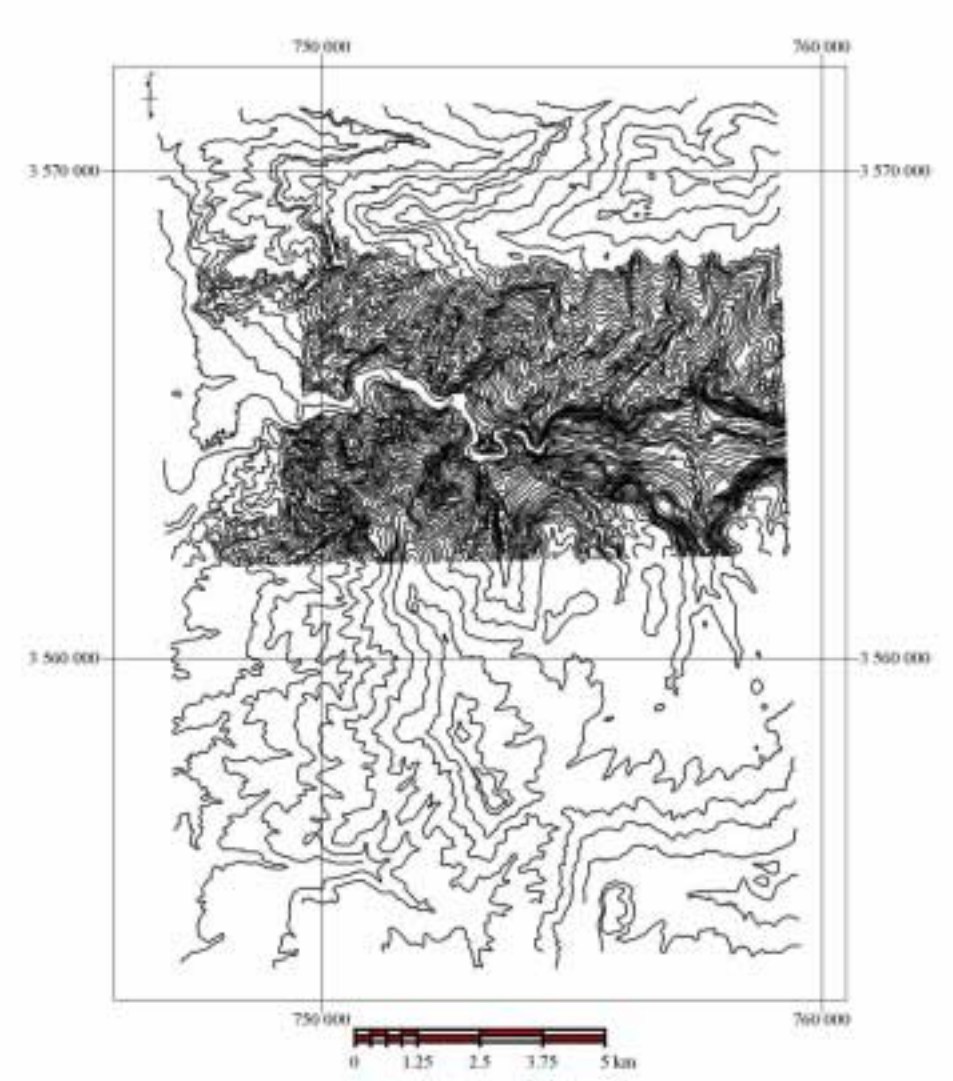

• Fig. 35 Vectorised lines for the DEM.

For converting the vector data, into raster data the surface modelling option of TNT-Mips (Operation: Surface fitting, Method: Minimum Curvature) was used. The output cell size was 50x50m. The curvature was set to linear whereas the remaining parameters were left as default.

The joining of the two DEMs was done by the raster mosaic option in TNT-Mips. The fitting of contrast was done manually in the input file settings. In order to reach the 50x50m of the mapping area DEM, the resampling method was set to bilinear interpolation. The fringe of the mapping area DEM to the underlying USGS DEM was calculated by a function using the elevation average.

The watersheds were calculated by using the produced DEM. They were compared to the watersheds offered by the USGS and modified referring to topographic maps in borders of the mapping area. The main changes were done near the Jordan river, where a more gentle topographic relief appears.

The large subterranean catchment area of the deeper aquifers which almost reach Saudi Arabia being quite large, the area surrounded by the modified watershed was set as model area.

5.1.3 Remote sensing

The remote sensing was done on the basis of satellite images from August 1999. These images cover the complete mapping area but have a lack in the east of the model area. The images were used to get a better idea of the geology, tectonics and hydrology of the mapping area.

Several indices were calculated over the part of the mapping area and the results were proven during the fieldwork. For the calculation of the wetness, greenness and brightness index, the internal formula of TNT-Mips were used. The clay mineral index was set as the quotient of the band 7 to band 5 of the Landsat 7 images. The Iron-oxide was calculated by the division of the red band images (3) through the blue band image (1) of the satellite images.

Unfortunately, no aerial pictures were available to check and correct the topographic maps based on data of 1961 and 1963.

5.2 Hydrochemistry

With reference to the aquifers of the model, it was tried to take as many representative samples as possible from each aquifer. The samples were taken from wells and springs. The hydrodynamic flow pattern shown in Fig. 8 suggests that they should be located close to the mapping area or in the western part of the model area (Fig. 36).

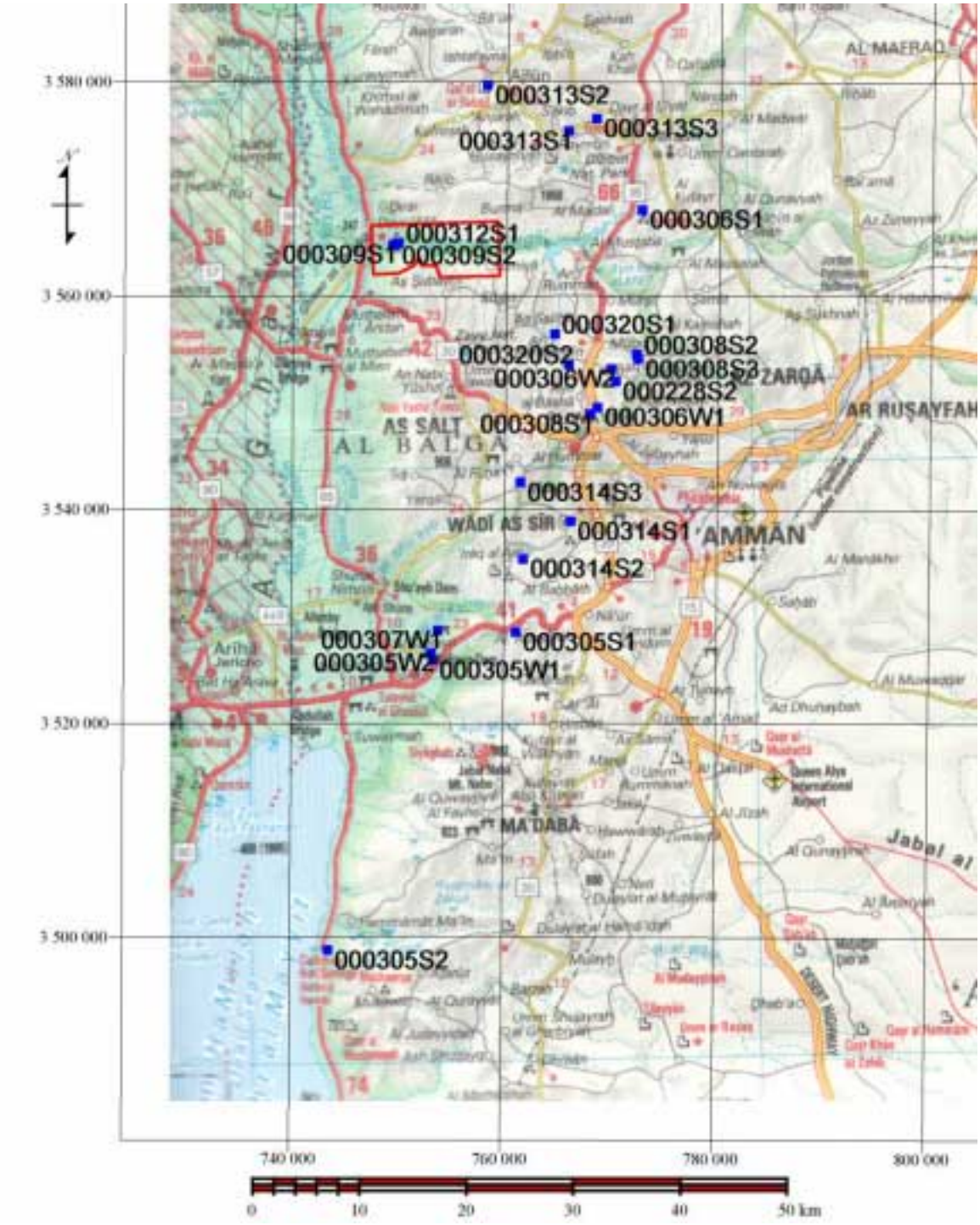

• Fig. 36 Location map of the samples (red line = mapping area).

5.2.1 Sampling

Two wells (000305W1 & W2) and 3 springs (000309S1 & S2, 000312S1) were sampled out of the Zerqa aquifer, stratigraphically followed by the Kurnub sandstone which was sampled on three wells (000306W1 & W2, 000307W1) and five springs (000228S2, 000305S2, 000306S1, 000308S1 & S2). Out of the following A1-A2 aquifer, four springs were sampled (000305S1, 000308S3, 000313S1, 000314S3).

However, the A4 aquifer was only sampled twice (000313S3, 000314S2) on springs and the last aquifer available in the area, A7, was sampled four times on springs (000313S2, 000314S1, 000320S1 & S2). As shown in their names, all samples were taken in March. For more details see App. 7. Before taking the samples, pH, temperature, conductivity, oxygen and redox potential were measured in a flow-cell using a WTW MulitLine P4. Due to a later on recognised malfunction at the WTW MulitLine P4, some of the measurements might be wrong. The measurements were taken observing their stability, which sometimes took quite a long time. At the beginning, it was tried to measure HCO_3^-, CO_2 in the field but the available equipment not being sufficient to do the measuring it was postponed to the laboratory (Fig. 37).

- Fig. 37 Equipment for the HCO_3^- and CO_2 field measurement.

For the laboratory work, the following amounts of water were taken:

- 2x1L in brown glass bottles, unfiltrated, unstabilised
- 1x0.05L in PE bottles, filtrated (200nm)
- 2x0.05L in PE bottles, filtrated (200nm), stabilised (suprapur nitrate acid)

All samples were delivered as quickly as possible to the laboratory and in the meantime were kept cool and dark. Unfortunately, some samples stored in glass bottles were destroyed during their transport to Germany, so not all elements could be determined as shown in App. 7. For the whole model area, as much information as possible has been collected, making reference to environment, well equipment, groundwater table, climate and former chemical analysis.

5.2.2 Chemical determinations

CL^-, NO_3^-, SO_4^{2-}, Li^+, Na^+ Ca^{2+}, Mg^{2+} were determinated with the MERCK / HITACHI D 6000 A at the TU-Bergakademie Freiberg. The carbon acid species (CO_2, HCO_3^-) were also measured at the TU-Bergakademie. For the determination a digital titrator from the firm HACH was used. For the NO2-, PO_4^{3-}, SiO_2 and NH_4^+ measurements the spectralphotometer DR 2000 (HACH) at the TU-Bergakademie was used. F^- was detected with an ion sensitive electrode in combination with the pMX 3000 from WTW. Fe was measured with a photometric method. Problems occurred due to the fact that the prefabricated indicator (HACH) included sulphites as reduction agent. Once the indicator had been added to the samples, precipitations disturbed the photometric method. So a L(+)-ascorbin acid (500mg/25mL) was used as a reduction agent and 1,10 –Phenanthrolin-Hydrochlrid-Monohydrat was used indicator. The measured values seem to be quite low, inspite of the fact that some wells and springs have iron crusts at the outflow. So it is possible that most of the iron was taken away by the filtering with 200nm.

AL, V, Cr, Mn, Co, Ni, Cu, Zn, As, Cd, Hg, Ti, Pb, Th, and U were determinated with the ICP-MS in Tharandt, Germany.

Generally the samples with the highest chemical measurements are all samples from the Zerqa aquifer (000305W1, 000309S1, 000309S2, 000312S1) and some samples from the Kurnub aquifer (000305S2, 000306W2, 000306S1). Compared to the legal requirements of the German law (TrinkwV. 1990), Cl, SO_4, Na, K, Mg, NH_4, Mn and As show a high concentration. Some samples having been taken from thermal springs, this comparison may be neglected.

5.2.3 Statistical treatment

The chemical analysis on the purpose of interpretation was divided into different groups by using cluster analysis (STATISTICA, method: K-means, cases). The cluster analysis was done with all available samples. In order to avoid any dealing with missing values, only the variables which were determined over all samples are taken into consideration (aquifer, conductivity, temperature, pH; O_2, CO_2, HCO_3, F, Cl, SO_4, NO_2, PO_4, SiO_2, Na, K, Ca_2, Mg_2, NH_4, Al, V, Cr, Co, Cu, Zn, As, Tl). The resulting matrix contained 21 cases with 26 variables.

The significancy of the clusters was calculated by using the one-factor variogram analysis of the program JOKER (method ANOVA). The harmonic mean was preferred as an output value. A significancy of 0.05 (5%) is regarded acceptable. The calculation was made for the clusters 3 to 10, due to the fact that a subdivision of 21 cases in more than 10 groups is regarded useless.

5.2.4 Isotopes

The stable isotopes deuterium (^{2}H) and oxygen (^{18}O) were determined (Tab. 4) by the GSF - Forschungszentrum für Umwelt und Gesundheit (Prof. Seiler).

• Tab. 4 $\delta^{18}O$ and deuterium measurements and the calculated excess of the samples.

sample ID	$\delta^{18}O$ (‰)	$\delta^{2}H$ (‰)	excess $_{local}$ (‰)	aquifer
000305S1	-5.67	-25.6	21.1	A1/2
000308S3	-5.54	-27.8	17.8	A1/2
000313S1	-6.80	-33.0	23.1	A1/2
000314S3	-6.24	-29.0	22.4	A1/2
000313S3	-6.30	-32.5	19.4	A4
000314S2	-5.86	-26.8	21.5	A4
000313S2	-6.61	-32.4	22.1	A7
000314S1	-5.95	-27.9	21.2	A7
000320S1	-5.17	-25.3	17.3	A7
000320S2	-5.64	-27.5	19.0	A7
000305S2	-5.24	-37.6	5.6	K
000306W1	-5.88	-29.3	19.2	K
000306W2	-4.11	-20.9	13.0	K
000306S1	-6.10	-44.0	6.3	K
000307W1	-5.34	-24.6	19.4	K
000308S1	-5.99	-29.3	20.0	K
000308S2	-5.51	-28.0	17.5	K
000305W2	-5.35	-25.6	18.6	Q
000305W1	-5.36	-31.5	12.7	Z2
000309S1	-6.56	-40.9	13.1	Z2
000309S2	-6.32	-38.9	13.2	Z2
000312S1	-5.87	-35.6	12.8	Z2

This data was plotted together with the meteoric water line published by ROZANSKI et al., 1993 in a diagram.

$$\delta^{2} = 8.17(\pm 0.07) \bullet \delta^{18}O + 11.27(\pm 0.65)\ ^{0}/_{00}$$

The global meteoric water line not fitting the samples, a local meteoric water line was calculated out of the data published by the International Atomic Energy Agency for the Irbid station (http://www.iaea.or.at/programs/ri/gnip/gnipmain.htm).

$$\delta^{2} = 8.2446 \bullet \delta^{18}O + 21.859\ ^{0}/_{00}$$

The local meteoric water line is almost parallelly shifted to the global meteoric water line, it is diluted.

The plotting of the samples along the line is used to distinguish the recharge environments of the samples. This has its reasons in the fact that the heavy isotopes ^{2}H and ^{18}O are enriched at the beginning of the rain and in higher altitudes the average temperature is lower so that precipitation will be isotopically depleted. According to CLARK & FRITZ (1997), the depletion varies between –0.10 to –0.20 $^{0}/_{00}$ per 100m rising in altitude for the Oman and –0.31 $^{0}/_{00}$ for western Italy. The distance of the samples from the line is used to detect evaporation effects after the infiltration of the meteoric water. Therefore the deuterium excess $d_{exlocal}$ ($d_{exlocal} = \delta^{2}H - 8.2446 \bullet \delta^{18}O$) has been calculated and was used as a scale for the effect of evaporation. The higher d_{ex} differs negatively from 21 $^{0}/_{00}$ (correction of the local meteoric water line), the higher the evaporation effect was.

Tritium (^{3}H) was measured by Prof. Hebert, Inst. für Angewandte Physik at the TU-Bergakademie Freiberg. Unfortunately some samples have been destroyed during the transport from Jordan to Germany.

For detailed isotopic studies time series (~2a) of samples should be done.This could not be realised as time was to short during my fieldwork.

5.3 Numerical groundwater model

The numerical groundwater model is calculated with FEMWATER. FEMWATER is a three-dimensional finite element computer model for simulating density-dependent flow and transport in variably saturated media. Additionally, the graphical user environment GMS was used to perform the groundwater simulation. Within GMS 2.1, the modules subsurface characterization, mesh, map and FEMWATER were available. Running on a PIII with Microsoft® Windows 98SE, GMS 2.1 seems to have several bugs, e.g. 3D meshes and the fluid properties files can not be saved and have to be regenerated every time building and running the model.

The types of elements supported by FEMWATER are shown in Fig. 38. Each of the elements is linear; quadratic elements are not supported. As tetrahedrons do not perform as well as the other types, prisms are used in the model.

The boundary conditions supported by FEMWATER include dirichlet (specified head), flux, flux gradient and variable boundaries (rainfall, evaporation and seepage). In each case, the prescribed values can be either constant or vary within time.

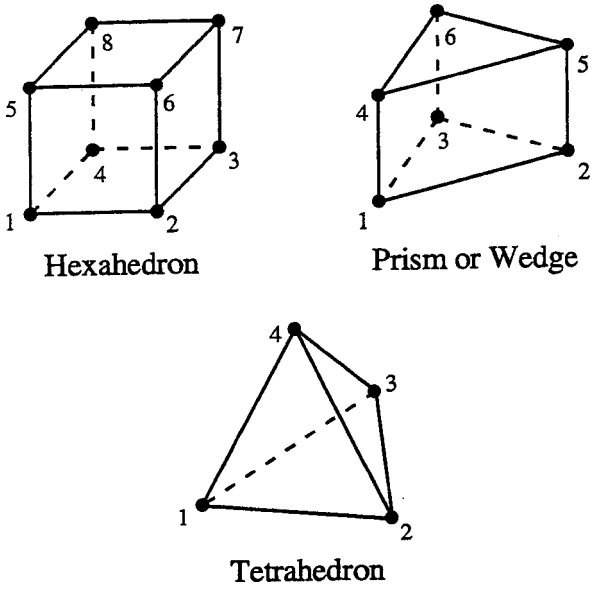

• Fig. 38 The types of elements supported by FEMWATER.

5.3.1 Geological model

Contour maps of the bases of the aquifers / aquitard were used to get a geological model. The maps have a scale of 1:250,000 and are published by the Water Authority Jordan (WAJ) & Institute for Geoscience and Natural Resources (Germany) BGR 1993 in the Palestine Grid. The following contour maps were available (App. 10-App. 13):

- Structure contour map base of Kurnub aquifer
- Structure contour map base of A1/A6 unit
- Structure contour map base of A7/B2 aquifer
- Structure contour map base of B3 aquitard

These maps are based on borehole data published in the technical papers and reports of the WAJ (1967-1995). At first the maps were redrawn, scanned and vectorised in TNT-Mips 6.2. Trying to import them as line AutoCAD files into GMS 2.1, points had to be manually (App. 15-App. 19) taken from the scanned maps and imported into the modelling software due to a software failure. The Zerqa aquifer system that may be important either for its chemistry or the flow analyses was added by interpolation based on drilling reports of deep oil wells. 1400m (Z1 and Z2) were added (App. 14) in the north and east, 1100m in the southwest whereas in the southeast of the model area the group was eroded (Fig. 39).

As some geological units crop out in the model area and FEMWATER can not handle this kind of data, the thickness was reduced to 0.01 to 0.03m depending on the numbers of layers for each unit. The number of layers was reduced to the number of aquifers / aquitards occurring in a unit, e.g. A7/B2 was calculated with 2 layers.

Tectonic elements, especially faults, were not taken into consideration because of a lack of information about their properties and influences on the flow model.

This data was imported as dxf files into GMS and converted to 3D TINs. After triangulation, they were calculated together with the grid as 3D meshes.

5.3.1.1 Geological stratigraphy

The stratigraphy of the model area will only be described by groups and is added to the stratigraphy of the mapping area.

5.3.1.1.1 Zerqa Ma'in Group

ANDREWS (1992) gave this group the name of "Ramtha Group", which seems to be a good choice taking into consideration that different classifications contain the name of "Zerqa" or "Zerqa Ma'in".

According to ANDREWS (1992), the most important lithofacies of this group are:

1. clastics (interbedded shales, siltstones and crossbedded, flaser-bedded and bioturbated sandstones),
2. aragillaceous, fossiliderous, limestone or dolomite, often interbedded with shale or marl,
3. oolitic, peloidal and bioclastic carbonates and
4. anhydrite and halite interbedded with shale and thin carbonates (Abu Ruweis formation, chapter 4.2.1).

The group is divided into the Suwayma formation, Hisban formation, Mukheiris formation, Salit formation and the Abu Ruweis formation which was discussed before.

The distribution and thicknesses of the group can be seen in Fig. 39.

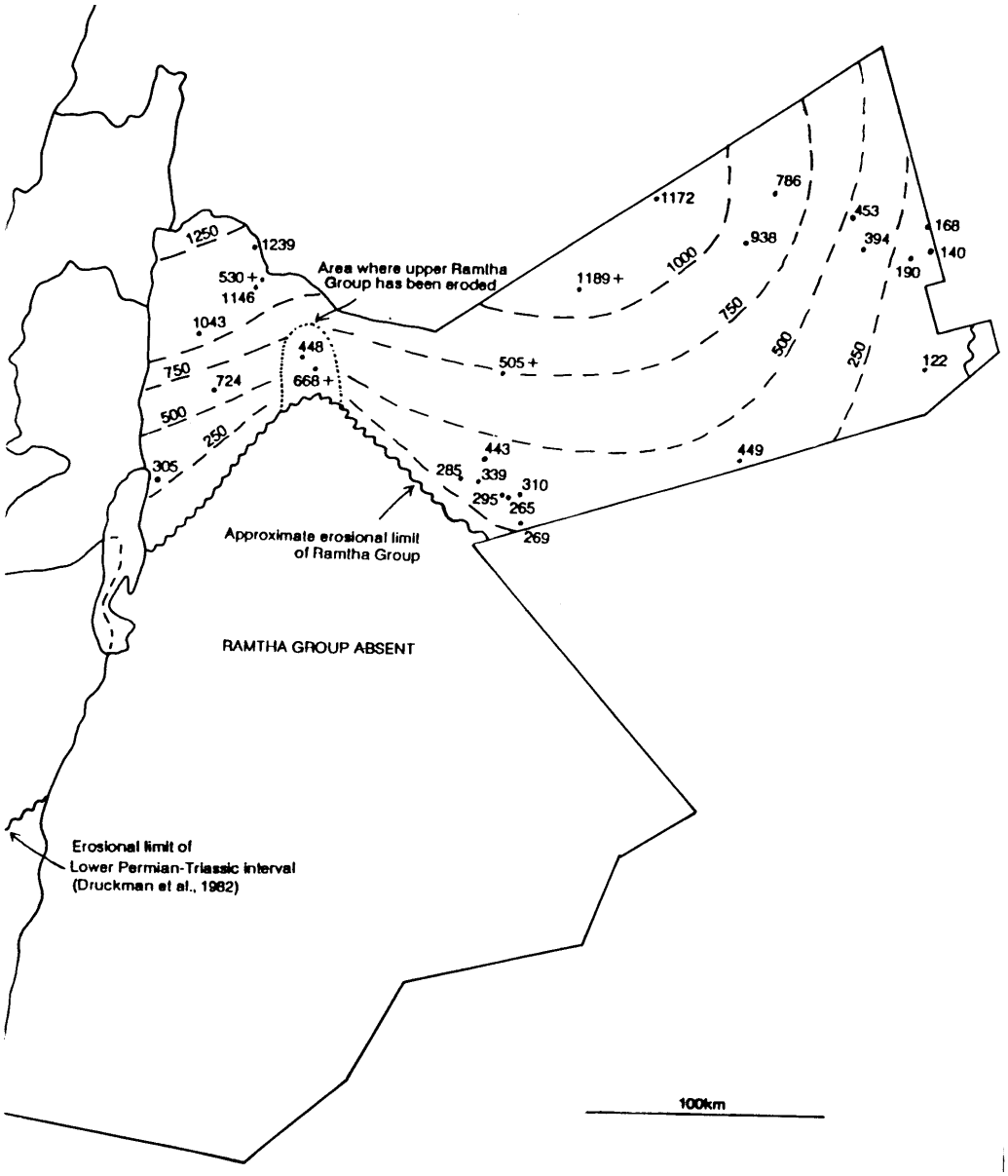

• Fig. 39 Isopach of the Ramtha Group (Triassic) in Jordan (ANDREWS, 1992).

5.3.1.1.2 Ajlun Group

The Ajlun Group is subdivided into the northern parts of Jordan in the Naur (A1-2), Fuheis (A3), Hummar(A4), Shuayb(A5-6) and Wadi as Sir (A7) limestone formation. The Group is very important as a reservoir for the oil industry, as an aquifer and as a source of clay for cement. It predominantly consists of limestone, limestone and shale and / or marl. A1-A6 have a total thickness of 350 to 400m decreasing to the south and east. The A7 forms a major aquifer especially in the cavernous upper 20m. It also consists predominantly of well-bedded, massive limestone with more or less dolomite, marl, gypsum, chert and clasitic components. The Wadi as Sir formation has an average thickness of 240 to 250m, although the figures differ a lot due to faulting and the attached missing sections. The base of the Ajlun Group is set where the Kurnub Sandstone is overlain by limestone, whereas the top is set by a change from marls and dolomites to sandstones, belonging to the Belqa Group. The Ajlun Group records a major transgression of the Tethys Ocean to south and east. The sediments were deposited in a carbonate-dominated, inner to mid shelf environment, interrupted by some deeper water events.

5.3.1.1.3 Belqa Group

The Belqa group is the youngest part handled in the model. It is subdivided into the Wadi um Ghudran (B1), Amman (B2), Muwaqqar (B3), Rijam (B4) and the Shallala formation (B5). However, recent authors (ANDREWS, 1992) may take a different division but due to the fact that the main aquifers / aquicludes are well described this work deals with the older division. The Balqa Group consists of limestones and marls with varying amounts of chert and phosphatic rocks. All formations have a variable thickness. However, the thicknesses always decrease towards the south. Most of the sediments were deposited at the shelf of the Tethys Ocean whereas the water depth was variable. The occurrence of phosphate might have its reasons in the high organic productivity in the Ocean.

5.3.2 Water balance

The deeper aquifers have, except for some small outcropping areas, no recharge from precipitation. Downward leakage from the overlaying aquifers and aquitards feeds these aquifers (Fig. 8). The outflow of the deeper aquifers occurs at springs in the outcropping area. It is estimated that most of the volume is dissipates unnoticed into the Jordan Rift. However, the potentiometric surface of the Kurnub Aquifer is in some places higher than that of the Wadi Es-Sir (A1) aquifer system so that an upward leakage into the A1/A6 aquifer system is possible. The same is assumed for the Zerqa / Kurnub aquifer system (Fig. 9).

The upper aquifers can be recharged directly from precipitation. They form the most important and extensive aquifer system in Jordan. Various pumping tests (GTZ, 1977; RIMAWI,1985) proved that the aquifer system is anisotropic and heterogenous (transmissivity ranges from 7.0 to 8000m²/d). This might have its reasons in faults, fractures and the cavities as described in (5.3.1.1.2). The caverns might be built due to the mixing of different water types.

The calculations of the groundwater recharge are based on a database provided by the WAJ. It contains almost daily measurements with different starting dates (oldest one 01.10.37 AL0019 (Fig. 40)) for 129 stations within and around the study area, nine of them being evaporation stations (Fig. 41).

5.3.2.1 Precipitation

The amount of precipitation was calculated by using a database (Fig. 41). To avoid mistakes (e.g. growth of cities), cumulative curves were calculated (Fig. 40).

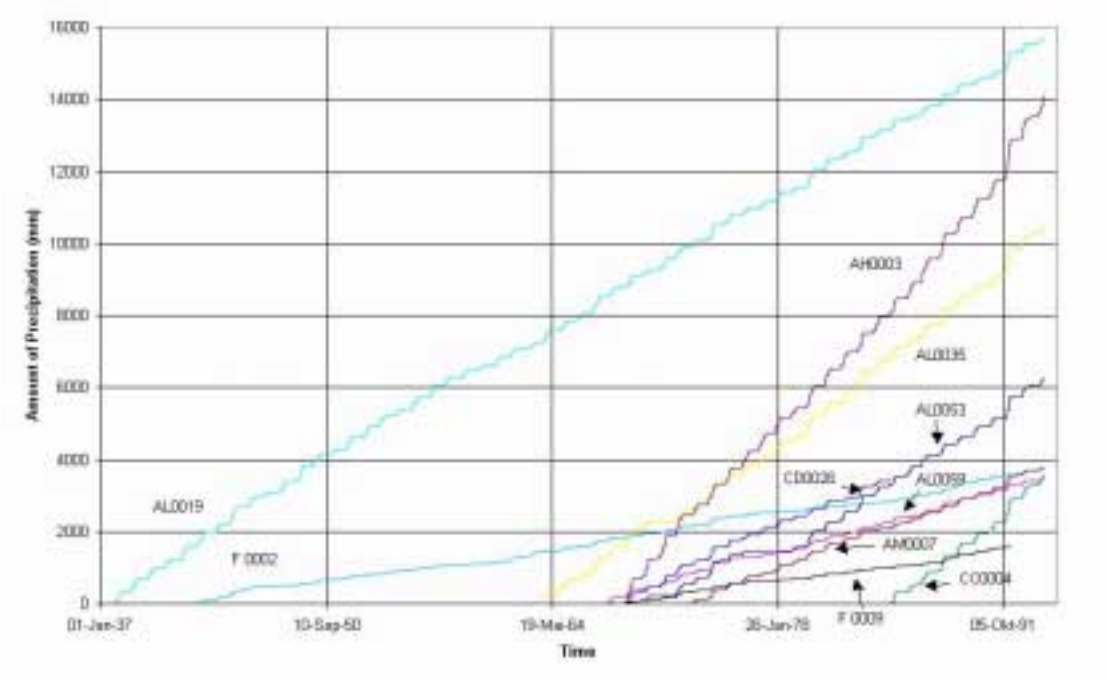

• Fig. 40 Cumulative curves of selected meteorological stations in the model area.

It can be clearly seen that in some years (e.g.1991), there is a peak in the amount of rainfall. This peak represents “wet” years. The gradient of the lines stays more or less the same.

From this data, the yearly average was calculated and an isohyete map was calculated by using SURFER 6 with kriging. The variogram settings were taken from a model composed with VARIOWIN. The map was imported to TNT-Mips and converted to a raster by using a linear minimum curvature (Fig. 42).

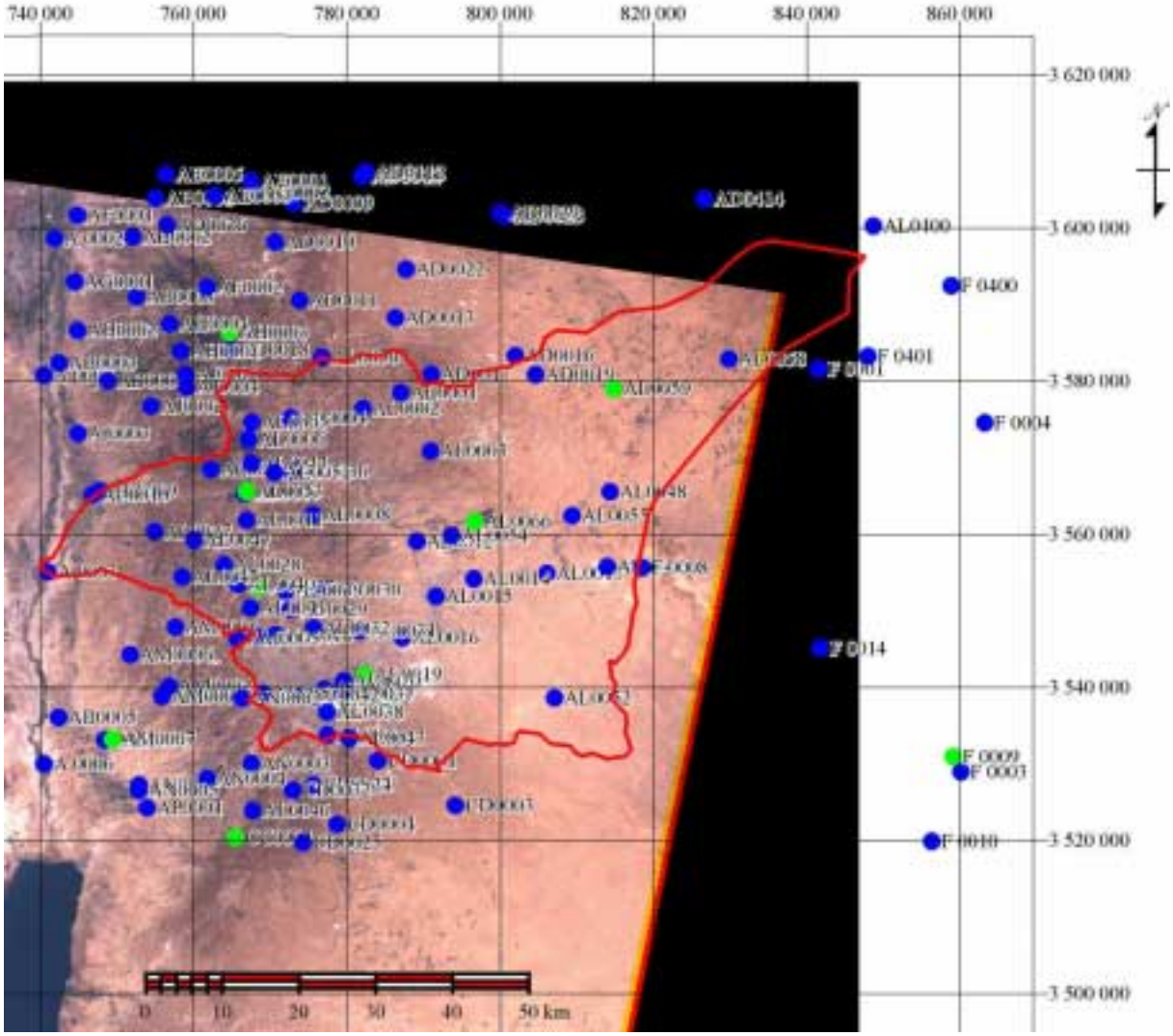

- Fig. 41 Location map of meteorological stations in the study area.

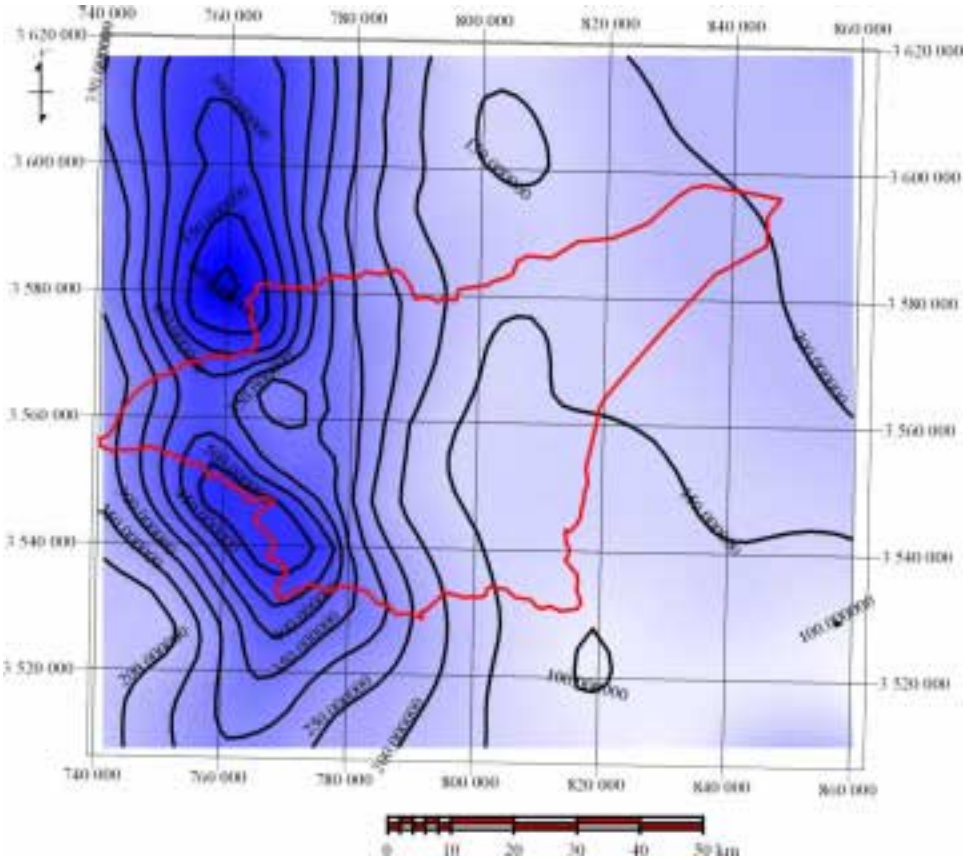

• Fig. 42 Raster and vector file of the precipitation in the study area.

5.3.2.2 Evaporation

Due to a lack of information, the evaporation was taken out of the climate database, in which it appears as potential evaporation. In order to avoid any dealing with missing values, only measurements over a longer period of time for each station were taken into consideration. As there are only a few stations in the study area, it was tried to correlate the evaporation with the altitude or the geographical position. As shown in Tab. 5, there is no significant correlation between the position or the altitude of an evaporation station in the study area and the potential evaporation.

• Tab. 5 Correlation between potential evaporation and the altitude or geographic position (SPSS).

		PE	**PGN**	**PGE**	**ALT**
PE	Pearson correlation	1.0	0.987	0.923	0.059
	Sig. (2-tailed)		0.101	0.252	0.962
	N	3	3	3	3
PGN	Pearson correlation	0.987	1.0	0.851	-0.099
	Sig. (2-tailed)	0.101		0.353	0.937
	N	3	3	3	3
PGE	Pearson correlation	0.923	0.851	1.0	0.439
	Sig. (2-tailed)	0.252	0.353		0.711
	N	3	3	3	3
ALT	Pearson correlation	0.059	-0.099	0.439	1.0
	Sig. (2-tailed)	0.962	0.937	0.711	
	N	3	3	3	3

5.3.2.3 Groundwater recharge

The Groundwater recharge was calculated by a simple model using the following equations:

$$\theta_{new} = \theta_{old} + PE \bullet EF + P$$

with:

θ = water content
PE = potential evaporation
EF = evaporation factor
P = precipitation

In cases the new water content was higher than the estimated field capacity, the difference was added to the groundwater recharge and the water content was set equal to the field capacity.

The groundwater recharge was calculated for the stations AH0003, AL0019, AL0035, AL0053 and AL0059, as the other evaporation stations in the study area have no precipitation readings. Due to the small number of stations, the areas of influence of each evaporation station were not calculated with the Thiessen-method. Geomorphological facts were taken into consideration.

5.3.2.4 Runoff and Discharge

The main part of the runoff is stored in the King Talal Dam. At normal water level it stores $89*10^6 m^3$. However, the evaporation of the reservoir surface is approximately 2000mm/yr, which equals 5,5 mm/d (Tab. 6).

• Tab. 6 Flow data from 1984 to 1988 on King Talal Dam (WAJ, 1988).

year	inflow ($10^6 m^3$ per year)				Zerqa river (%)	outflow ($10^6 m^3$ per year)			reservoir volume ($10^6 m^3$)
	Zerqa river	tribu-taries	rain-fall	total		outflow	evap.	total	
1984	53.868	7.188	0.312	61.368	87.8	48.120	2.844	50.964	20.820
1985	48.636	9.252	0.264	58.164	83.6	68.628	2.988	71.616	7.055
1986	63.024	5.436	0.228	68.688	91.8	46.224	1.728	47.964	27.531
1987	53.292	4.668	0.216	58.176	91.6	56.928	3.168	60.096	25.605
1988	100.824	6.084	0.612	107.52	93.8	74.688	5.304	79.992	53.230
Average	63.929	6.526	0.326	70.783	89.7	58.918	3.206	62.126	26.848

It is estimated that 95% of the baseflow and 80% of the flood flow originates above King Talal Dam.

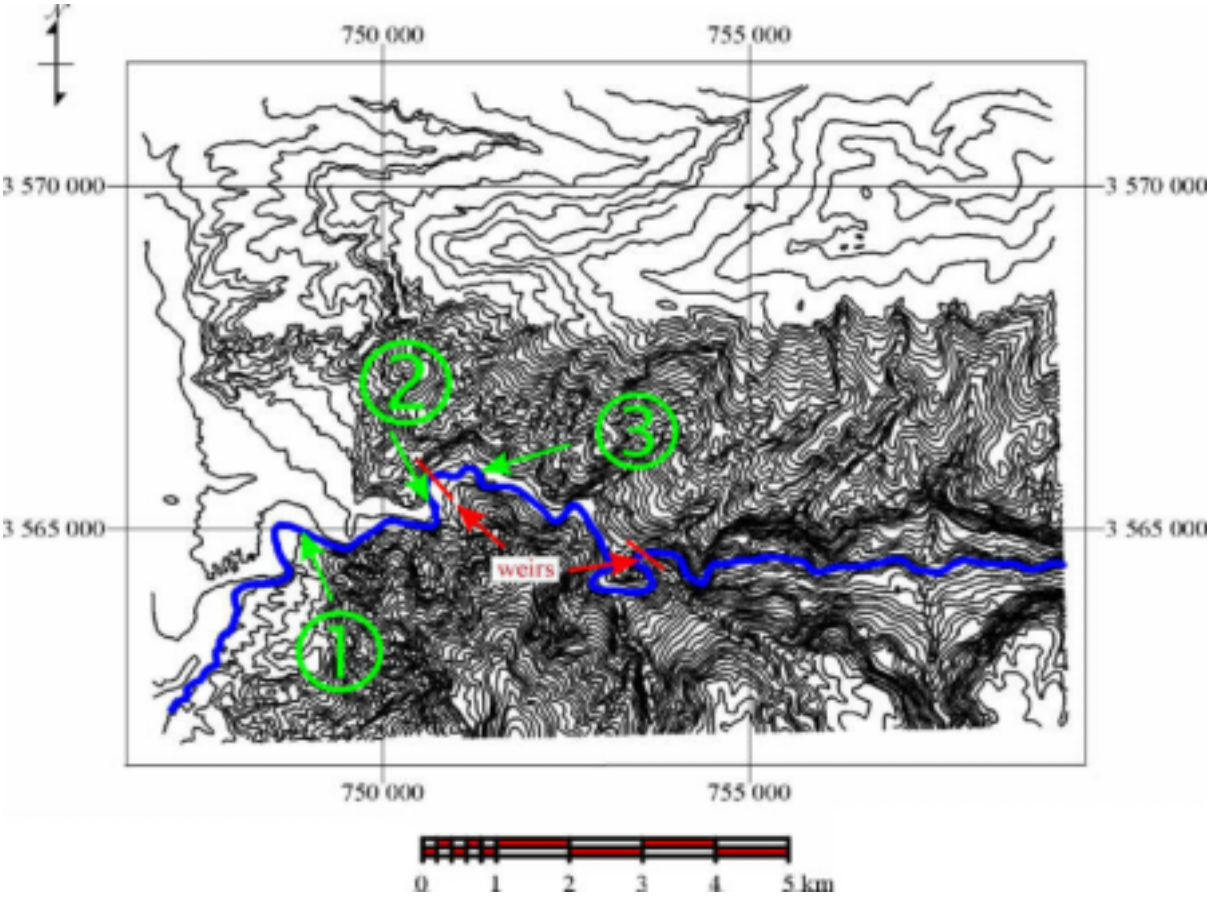

• Fig. 43 Location map of the weirs downstream King Talal dam.

• Fig. 44 ① Wadi Zerqa downstream the last weir and downstream of the springs (~4m wide).

• Fig. 45 ② Wadi Zerqa downstream the last weir and upstream the springs (~1m wide).

• Fig. 46 ③ Wadi Zerqa above the last weir.

• Tab. 7 Results of flow measurements in the Zerqa river(JICA, 1995).

location	date	upstream flow (L/s)	downstream flow (L/s)	difference (L/s)	discharge from King Talal dam (m³/s)
Wadi Zerqa	22.09.94	600	1,450	850	3,6
Wadi Zerqa	24.09.94	600	1,326	726	3,6
Wadi Zerqa	11.10.94	960	1,670	710	4,5
Wadi Zerqa (Damieh)	24.09.94		445		
Wadi Zerqa	07.01.95	620	1,220	600	2-3
Wadi Zerqa	10.01.95	65	500	435	0
Wadi Zerqa (Damieh)	8.01.95		620		
Wadi Zerqa (Damieh)	11.01.05		525		

The baseflow from the Zerqa Group into the Zerqa river is the difference between upstream and downstream flow measurement. As the flow past the last weir (Fig. 43) can almost be set to 0, the inflow from the Zerqa Group to the river downstream of the weir is the measured flow at Damieh. Data concerning discharge from springs in study area was not available. A database was created, in order to calculate the groundwater abstraction from the different aquifers.

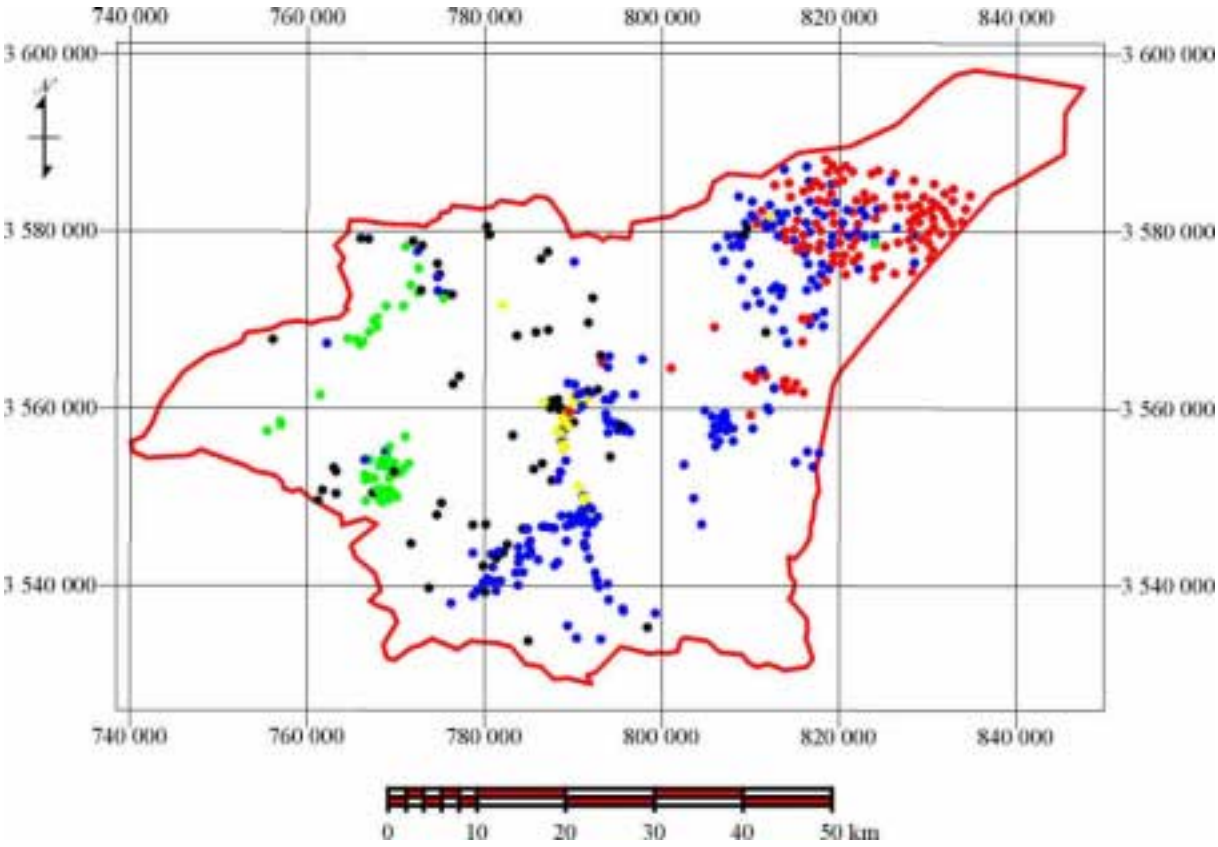

• Fig. 47 Map of wells in the study area discharging groundwater from different aquifers. (Basalt, Kurnub, A7/B2, A1/A6, Alluvium).

The database contains the information of 513 wells from the year 1993 (Fig. 47). In cases that wells discharge from several aquifers, the total amount of discharge is divided through the numbers of aquifers, due to a lack of information.

5.3.3 Design of the Finite-Element grid

The grid Fig. 48 was composed by GMS 2.1. The watershed calculated from the DEM and corrected according to the topographic maps was used as an outside boundary. It was tried to get smaller cells to the west, towards the mapping area. At the beginning, due to the large area and the available data, the borders of the cells in the west were set to a length between 1500 to 2000m, whereas 4000 to 5000m (max. 8000m) were established in the eastern part. As calculation took very much time, the grid was rebuilt to larger cell sizes later on.

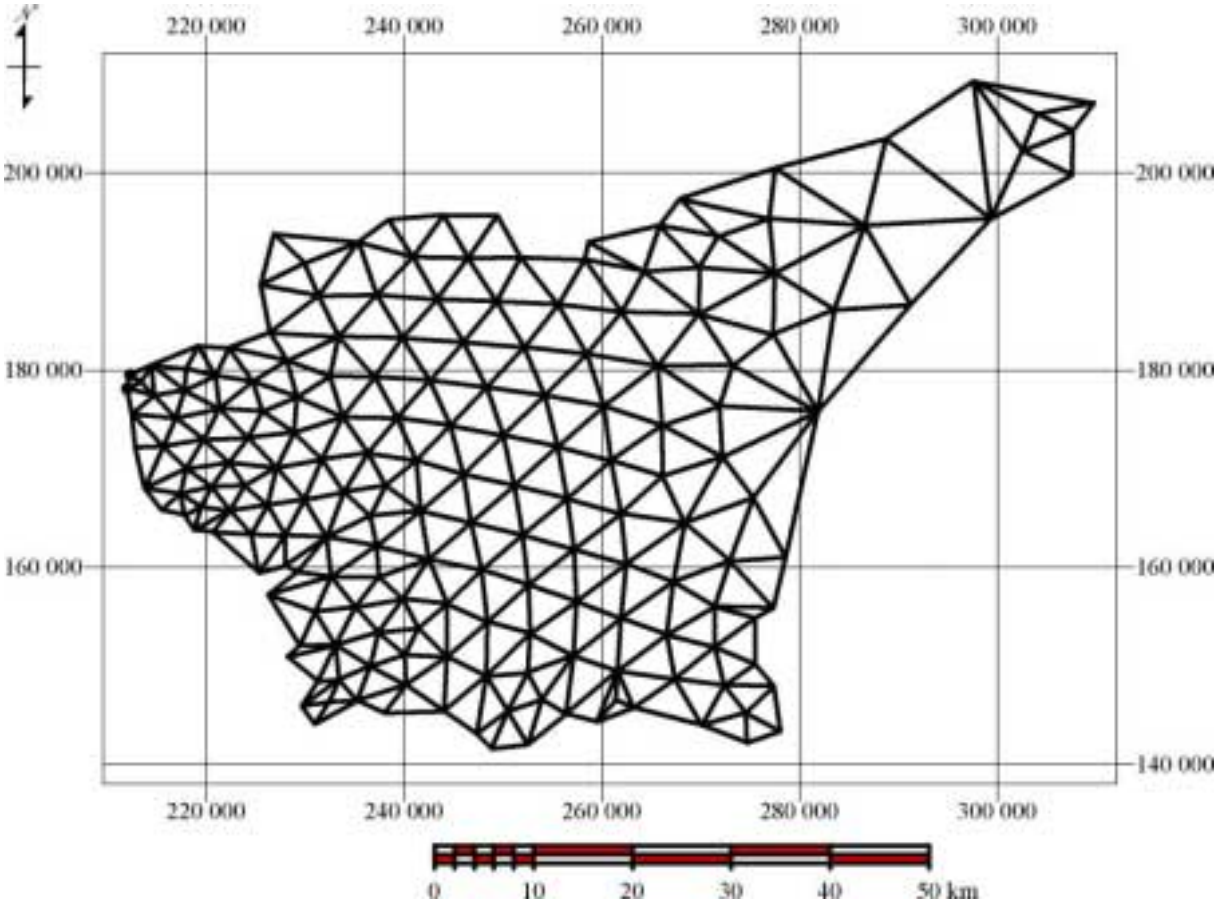

• Fig. 48 Finite-Element grid of the model.

5.3.4 Boundaries

For the settings of the lateral boundaries a database was created which contains all measured watertables records of wells and springs which were available either from literature or collected during my stay in Jordan. Unfortunately, only a small amount of data was available for the deeper aquifer system so that the boundaries were set similar to those of the upper aquifers. Due to the conditions of the steady state model only constant head (dirichlet head) and no flow boundaries were assigned (Fig. 49-Fig. 51). The constant head boundary was taken were the groundwater head was known or could be interpolated. The no flow boundary was set either if the flow line is almost parallel to the border of the model or if the aquifer thins out as discussed in chapter 5.3.1.

For the vertical boundaries (Fig. 52) the results of the groundwater recharge model (6.3.2) were used. They had to be changed during the calibration of the model (chapter 6.3.5). Due to a lack of information, it is assumed that the base of the model is represented by a impermeable strata.

It is estimated that the abstraction of the wells discussed in chapter 6.3.3 and the natural discharge of the aquifers as well as the groundwater recharge due to the King Talal dam (chapter 5.3.2.4) has no influence on the model due to its large scale and grid.

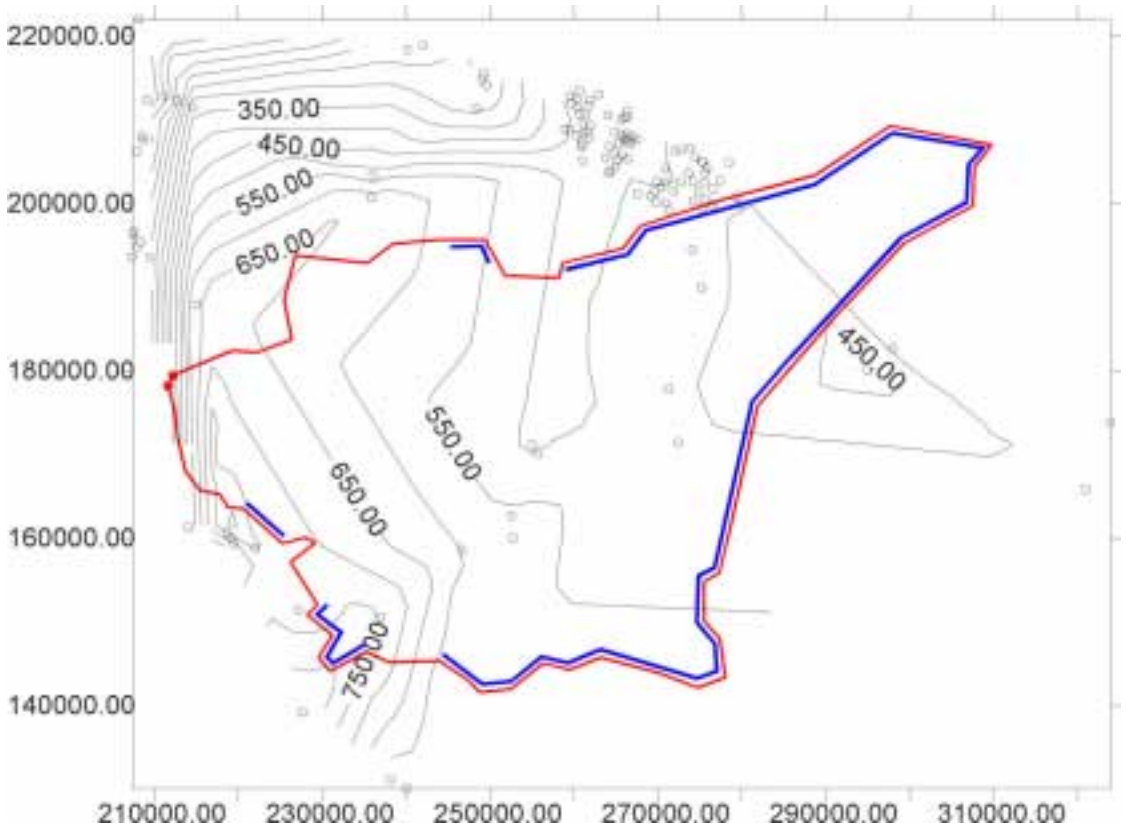

• Fig. 49 Boundary settings and groundwater level contour map of the A7/B2 aquifer. (red line = model area, blue lines = dirichlet head boundary).

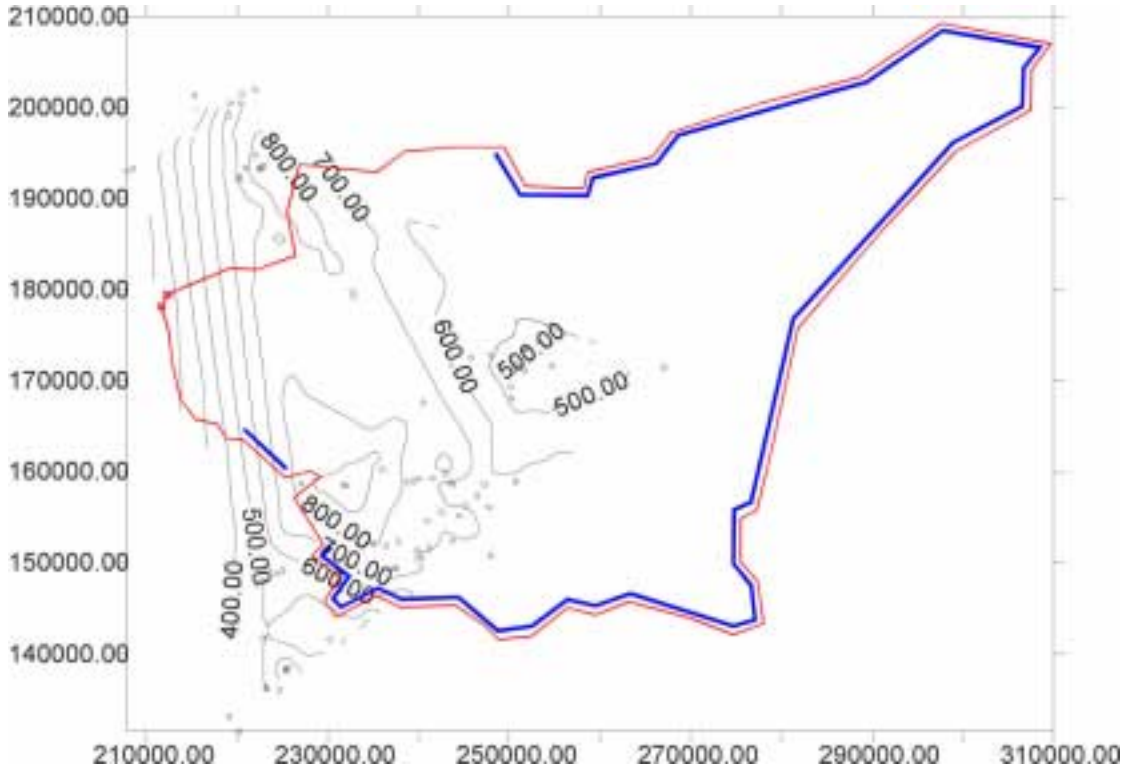

• Fig. 50 Boundary settings and groundwater level contour map of the A1/B6 aquitard. (red line = model area, blue lines = dirichlet head boundary).

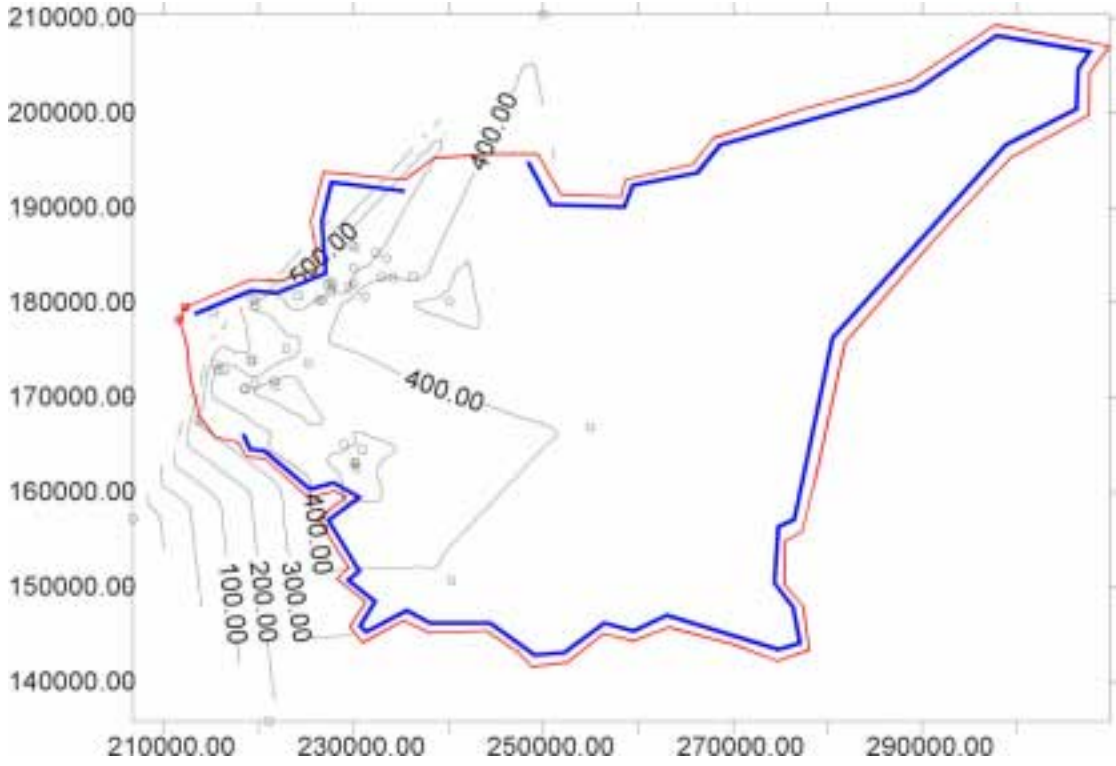

• Fig. 51 Boundary settings and groundwater level contour map of the Kurnub aquifer. (red line = model area, blue lines = dirichlet head boundary).

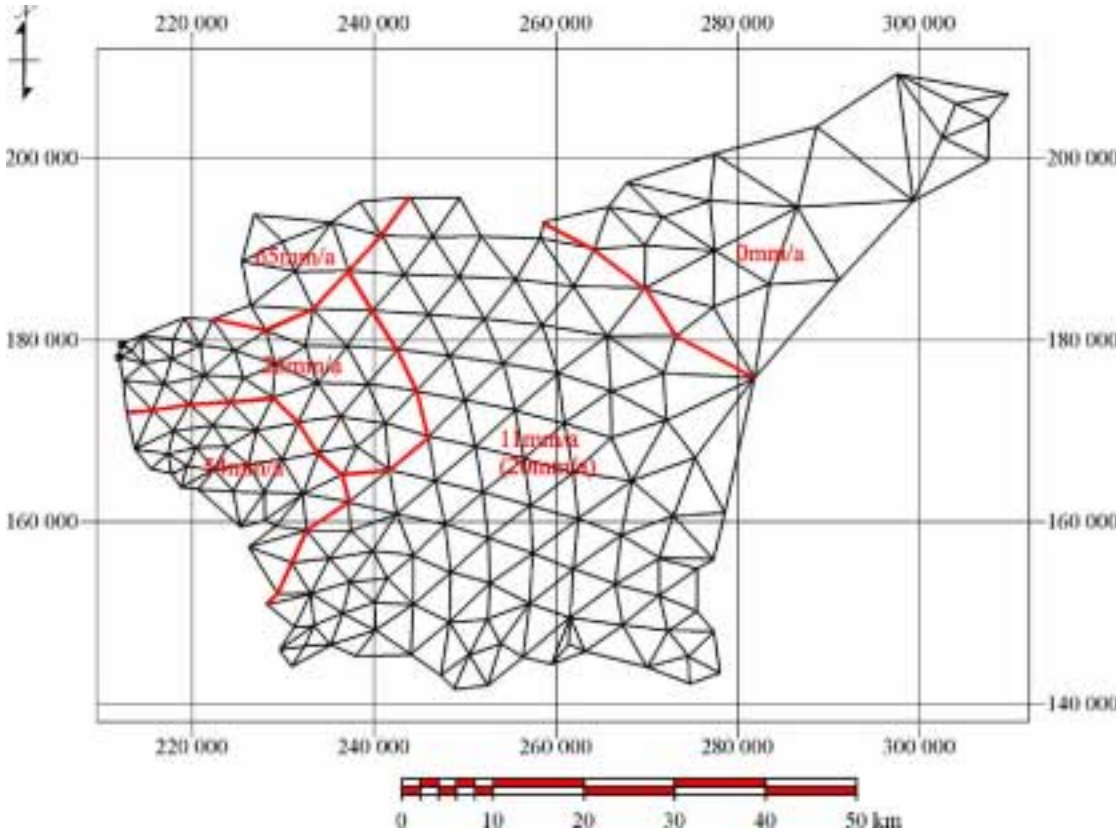

• Fig. 52 Vertical boundaries as the result of the groundwater recharge model.

6 Results

6.1 Geoinformation System

6.1.1 Digital Elevation Model

In Fig. 53, the composed digital elevation model and the corrected watersheds can be seen. The number of vertexes was first reduced in TNT-Mips and later on again after the import into GMS. This was necessary because of the long calculation time of the model.

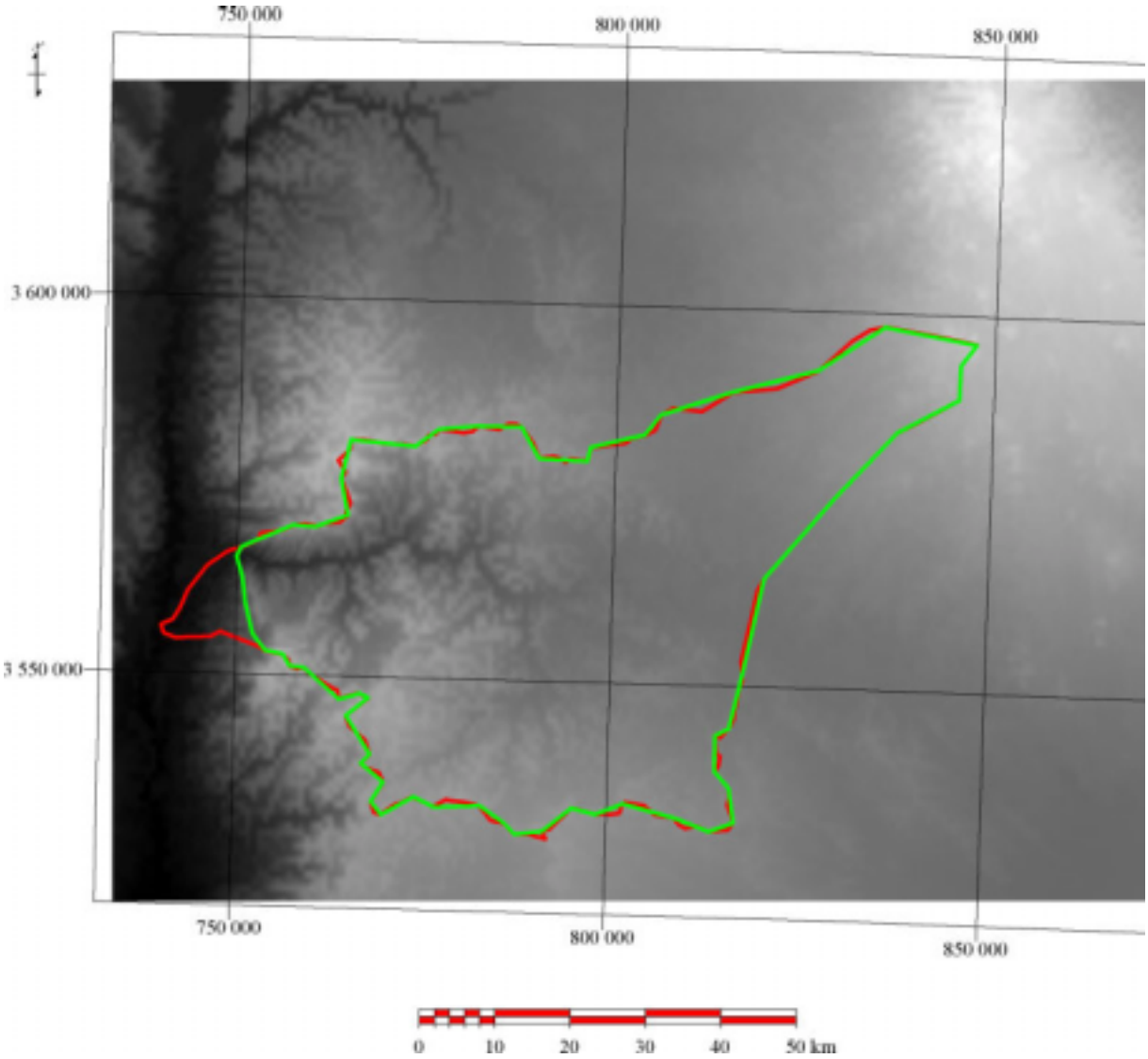

• Fig. 53 Raster file of the DEM (50x50), the red line shows the computed watershade the green line is boundary of the model.

6.1.2 Remote sensing

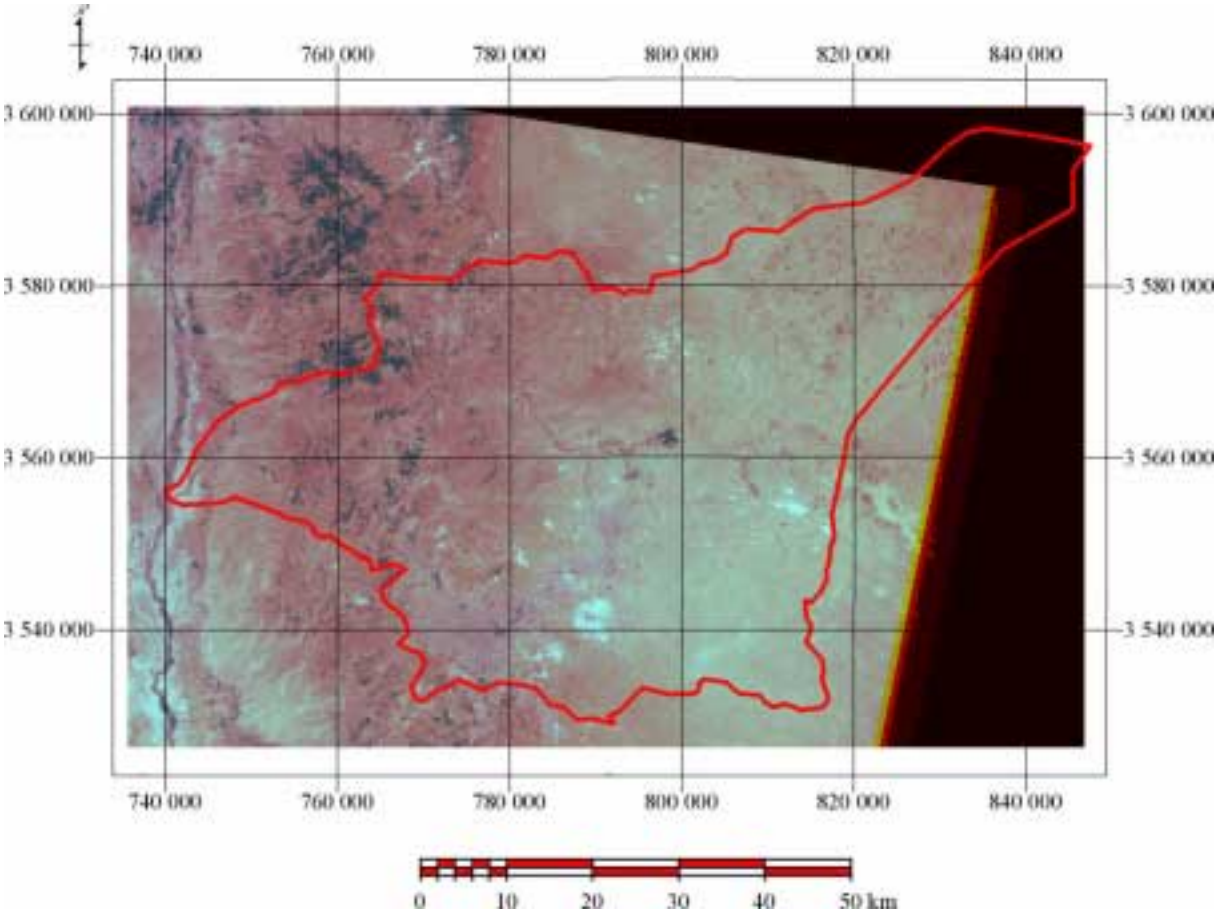

• Fig. 54 Brightness index calculated with TNT-Mips shown as RGB brightnes, 2, 1.

Fig. 54 shows the brightness index calculated with TNT-Mips. The reddish areas lying in the west are the brighter ones because of the occurrence of limestones of the Mesozoic rock units. The black areas in the highlands represent the vegetation or ponds which can also be seen in greenness and wetness index. The greenness index (Fig. 55) might lead to the interpretation that the whole highlands area is covered by vegetation. However, vegetation is widely spread except for some smaller forests. Within the Jordan Valley the vegetation is represented by farms. The wetness index was used to find springs around the mapping area. However, most of the bluish areas in Fig. 56 represent irrigated landsides or ponds as well as areas with trees due to the fact that trees reduce the evaporation of the soil. However, the King Talal Dam and the sewage plant near Zerqa can be clearly seen. As shown in Fig. 57, most of the iron oxide containing minerals (red colour) appear to be in the eastern part of the model area. This has its reason in the Basalt flows at the boarder to Syria. According to the clay mineral index (Fig. 58), most of the clay minerals represented by red colour appear to be in the highlands. As well as there are some more to the west representing clay minerals in soils or layers in a geological strata. However, there should be more clay minerals shown in the clay mineral index but this could be the reason of spectral information of clay and the period of time (August, 1999) in which the image was taken, which means the spectral information varies between wet or dry clay.

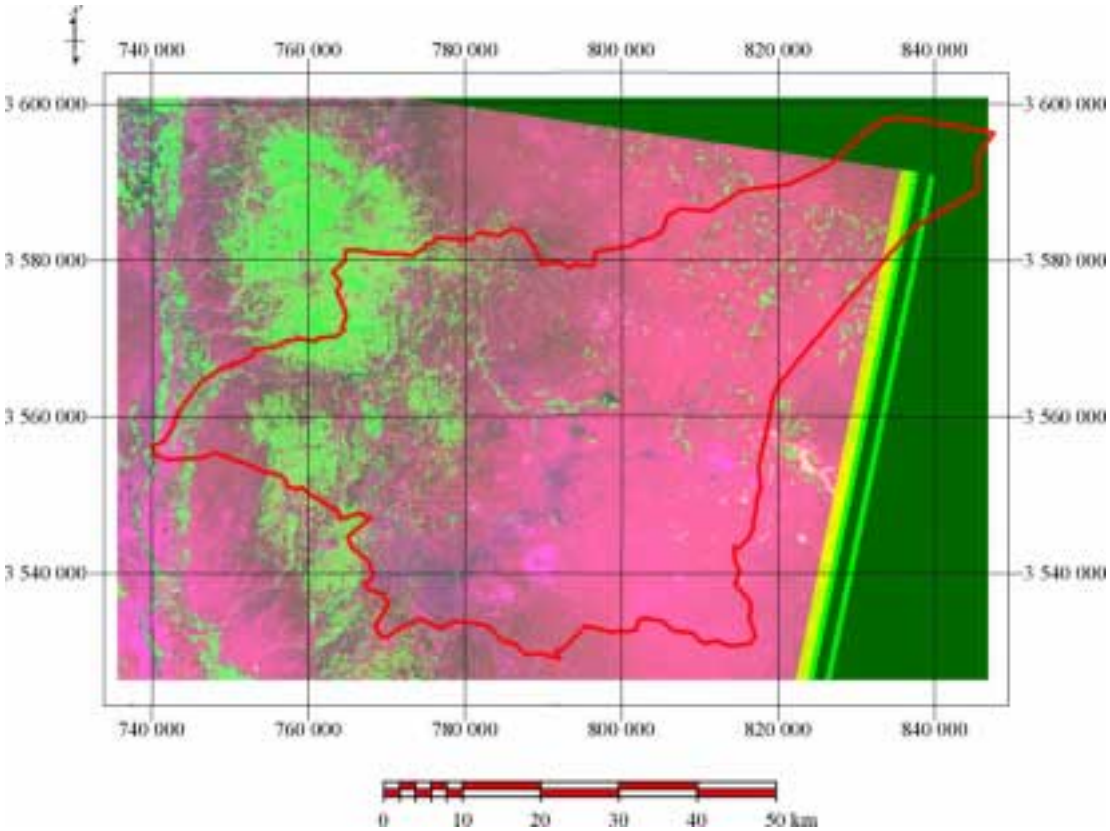

• Fig. 55 Greenness index calculated with TNT-Mips shown as RGB 3, greenness, 1.

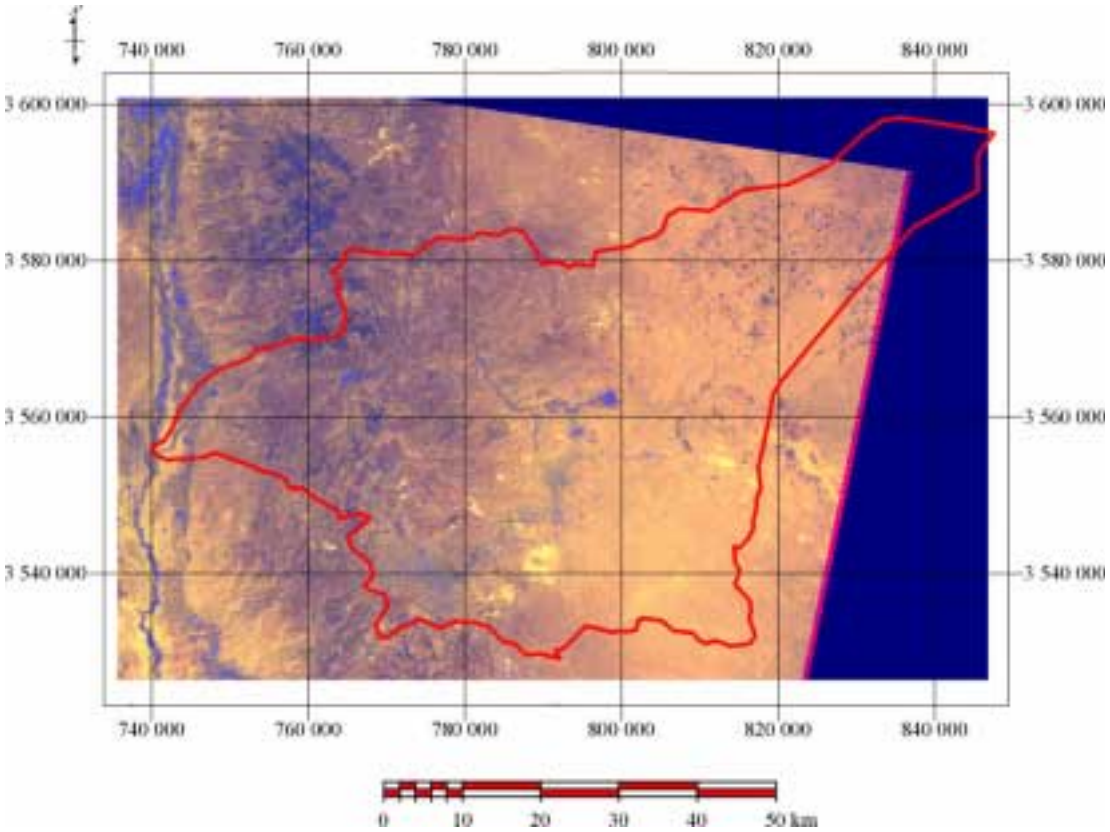

• Fig. 56 Wetness index calculated with TNT-Mips shown as RGB 3, 2, wetness.

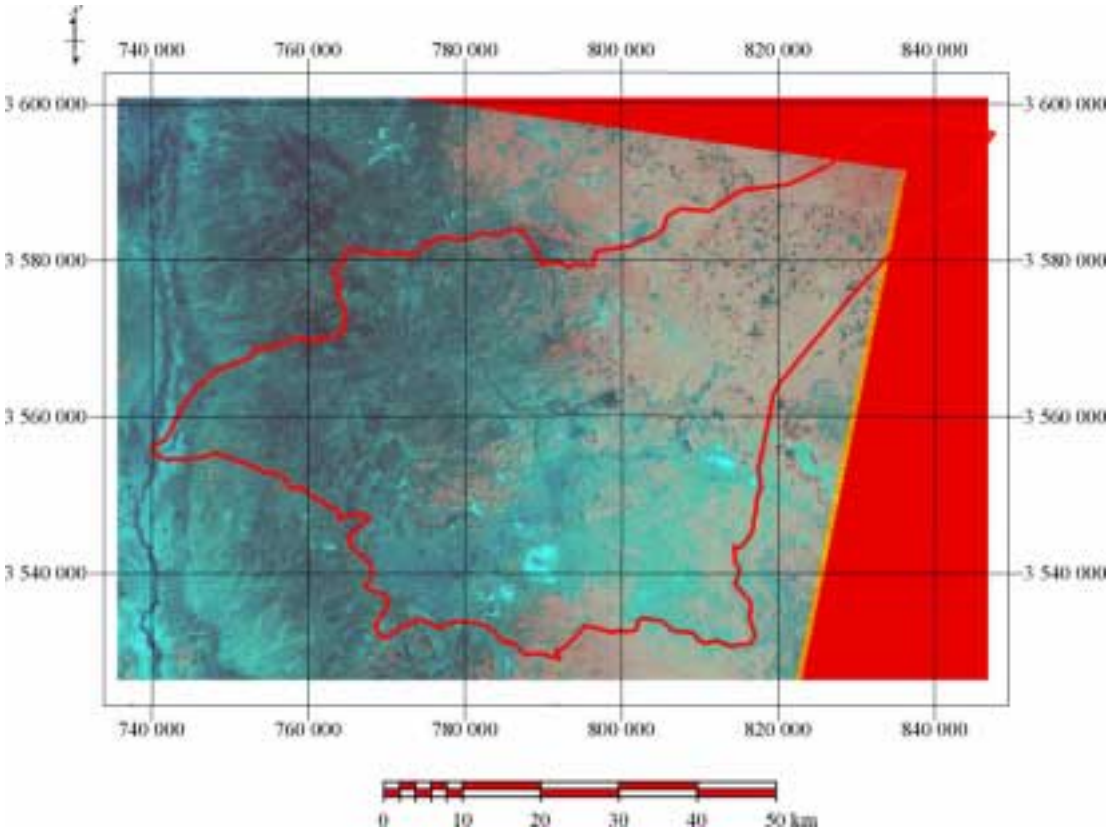

• Fig. 57 Iron oxide index calculated with TNT-Mips shown as RGB iron oxide index, 2, 1.

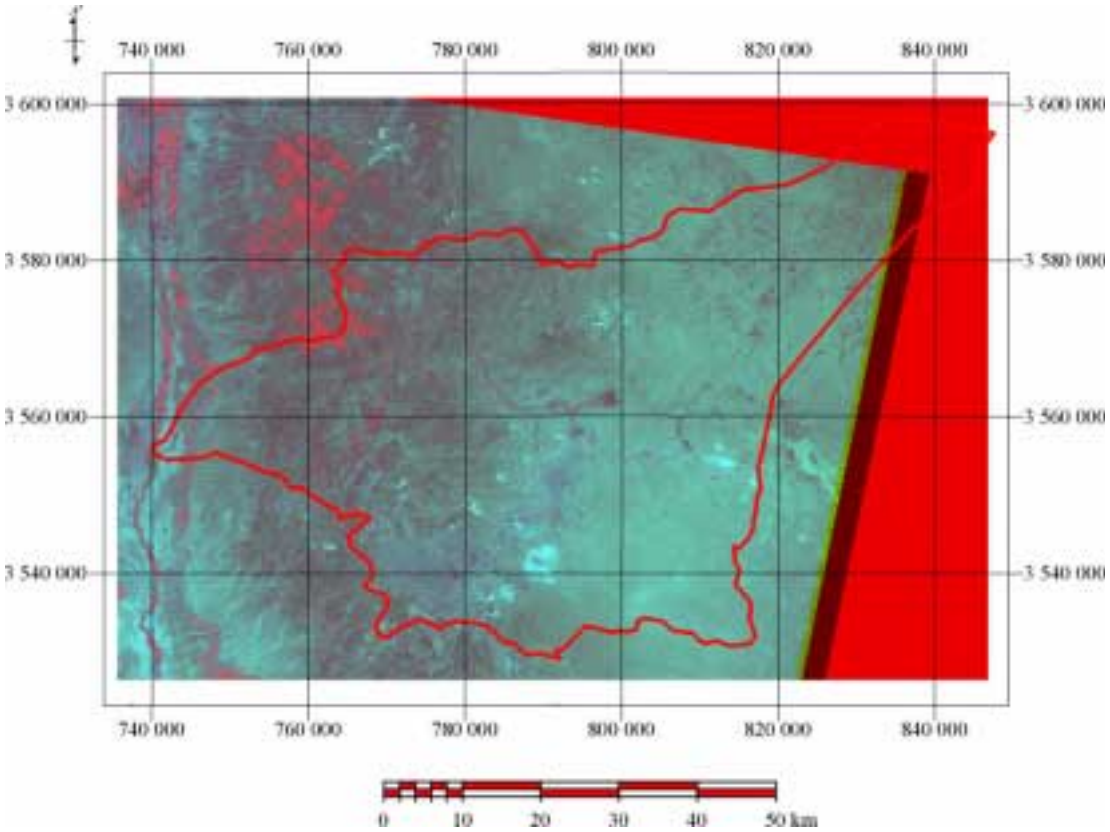

• Fig. 58 Clay mineral index calculated with TNT-Mips shown as RGB clay mineral index, 2, 1.

6.2 Hydrochemistry

6.2.1 Statistical treatment

Tab. 8 shows the clusters and the samples in each of them. It is remarkable that there is a split at the beginning into one cluster with several samples and many smaller ones with up to two samples.

- Tab. 8 Entire cluster analysis 21 cases with 26 variables, method: K-means. The different colours represent different aquifers.

02	1, 2, 3, 4, 5, 6, 7, 8, 9, 10, 11, 14, 15, 16, 17, 18, 19, 20, 21																		12, 13	
03	1, 2, 4, 5, 6, 7, 8, 9, 10, 11, 15, 16, 17, 18, 19, 20, 21																3, 14		12, 13	
04	1, 4, 6, 8, 9, 10, 11, 15, 16, 17, 18, 19, 20, 21													2, 5, 7			3, 14		12, 13	
05	1, 4, 6, 8, 9, 10, 11, 15, 16, 17, 18, 19, 20, 21													2, 7		3, 14		5	12, 13	
06	1, 6, 15, 16, 17, 19, 21						2, 7		3, 14		4, 8, 9, 10, 11, 18, 20							5	12, 13	
07	1	2, 7		3, 14		4, 8, 9, 10, 11, 18, 20				5		6, 15, 16, 17, 19, 21							12, 13	
08	1	2, 7		3, 14		4, 8, 10, 11, 20			5		6, 9, 16, 18, 19					12, 13		15, 17, 21		
09	1	2, 7		3, 14		4, 8, 20		5	6, 16, 19			9, 10, 11, 18				12, 13		15, 17, 21		
10	1	2, 7		3, 14		4, 8, 20		5	6, 16, 19		9	10, 11, 18				12, 13		15, 17, 21		
11	1	2, 7		3, 14		4, 20	5	6, 16, 19		8	9	10, 11, 18				12, 13		15, 17, 21		
12	1	2, 7		3, 14		4, 20	5	6, 16, 19		8	9	10, 11		12, 13			15, 17, 21			18
13	1	2, 7		3, 14		4, 20	5	6, 16, 19		8	9	10	11	12, 13			15, 17, 21			18
14	1	2, 7		3, 14		4, 20	5	6, 16, 19		8	9	10	11	12, 13			15, 17		18	21
15	1	2, 7		3, 14		4, 20	5	6, 19	8	9	10	11	12, 13			15, 17		16	18	21	
16	1	2, 7		3, 14		4, 20	5	6	8	9	10	11	12, 13			15, 17		16	18	19	21
17	1	2, 7		3, 14		4, 20	5	6	8	9	10	11	12, 13		15	16	17	18	19	21	
18	1	2, 7		3, 14		4	5	6	8	9	10	11	12, 13		15	16	17	18	19	20	21
19	1	2	3, 14		4	5	6	7	8	9	10	11	12, 13		15	16	17	18	19	20	21
20	1	2	3	4	5	6	7	8	9	10	11	12, 13		14	15	16	17	18	19	20	21
21	1	2	3	4	5	6	7	8	9	10	11	12	13	14	15	16	17	18	19	20	21
	000305 S1	000305 S2	000305 W1	000305 W2	000306 S1	000306 W1	000306 W2	000307 W1	000308 S1	000308 S2	000308 S3	000309 S1	000309 S2	000312 S1	000313 S1	000313 S2	000313 S3	000314 S2	000314 S3	000320 S1	000320 S2

As shown in Tab. 9, there is no cluster without a not significant element. In clusters 8 to 10, SiO_2 is not significant. In cluster 7, NO_2 and Aluminium are not significant, either. In the 6. cluster the significancy of the harmonic mean of the variable aquifer is above the limit. As well, NO_2, PO_4^{3-} and Al are above 5% while SiO2 is slightly lower. Cluster 5 is similar to cluster 6, except that the aquifers and Aluminium are significant whereas Zn is not. In cluster 3 and 4 the temperature, NO_2, PO_4^{3-} SiO2 and Zn are not significant. In cluster 3 also the variables aquifer and Ti are above the limit.

Considering that the water temperature should be a significant parameter since there are thermal springs sampled and analysed, clusters 3 and 4 are rejected.

• Tab. 9 Significancy for the main clusters. red numbers (>0.05 (5%)) are not significant. AM = arithmetic mean, HM = harmonic mean.

	3 AM/HM	4 AM/HM	5 AM/HM	6 AM/HM	7 AM/HM	8 AM/HM	9 AM/HM	10 AM/HM
Aquifer	0.014/0.057	0.005/0.042	0.013/0.024	0.031/0.148	0.001/0.004	0.002/0.1	0.0/0.0	0.0/0.001
EC	0.0/0.0	0.0/0.0	0.0/0.0	0.0/0.0	0.0/0.0	0.0/0.0	0.0/0.0	0.0/0.0
T°C	0.085/0.188	0.006/0.057	0.017/0.029	0.0/0.0	0.0/0.0	0.0/0.0	0.0/0.0	0.0/0.0
pH	0.001/0.007	0.0/0.003	0.0/0.0	0.0/0.0	0.0/0.0	0.0/0.001	0.0/0.0	0.001/0.002
O2(%)	0.0/0.001	0.0/0.0	0.0/0.0	0.0/0.0	0.0/0.0	0.0/0.0	0.0/0.0	0.0/0.0
O2(mg/L)	0.0/0.002	0.0/0.0	0.0/0.0	0.0/0.0	0.0/0.0	0.0/0.001	0.0/0.0	0.0/0.0
HCO_3	0.0/0.0	0.0/0.0	0.0/0.0	0.0/0.0	0.0/0.0	0.0/0.0	0.0/0.0	0.0/0.0
F^-	0.0/0.001	0.0/0.001	0.001/0.001	0.002/0.006	0.001/0.004	0.003/0.005	0.006/0.006	0.002/0.002
Cl^-	0.0/0.0	0.0/0.0	0.0/0.0	0.0/0.0	0.0/0.0	0.0/0.0	0.0/0.0	0.0/0.0
SO_4	0.0/0.0	0.0/0.0	0.0/0.0	0.0/0.0	0.0/0.0	0.0/0.0	0.0/0.0	0.0/0.0
NO_2	0.011/0.053	0.032/0.071	0.075/0.085	0.142/0.286	0.239/0.491	0.0/0.0	0.0/0.0	0.0/0.0
PO_4^{3-}	0.195/0.150	0.349/0.222	0.058/0.079	0.113/0.28	0.01/0.003	0.013/0.007	0.03/0.012	0.021/0.009
SiO_2	0.672/0.684	0.827/0.811	0.002/0.013	0.003/0.049	0.143/0.112	0.21/0.164	0.205/0.151	0.083/0.070
Na^+	0.0/0.0	0.0/0.0	0.0/0.0	0.0/0.0	0.0/0.0	0.0/0.0	0.0/0.0	0.0/0.0
K^+	0.0/0.0	0.0/0.0	0.0/0.0	0.0/0.0	0.0/0.0	0.0/0.0	0.0/0.0	0.0/0.0
Ca^{2+}	0.0/0.0	0.0/0.0	0.0/0.0	0.0/0.0	0.0/0.0	0.0/0.0	0.0/0.0	0.0/0.0
Mg^{2+}	0.0/0.0	0.0/0.0	0.0/0.0	0.0/0.0	0.0/0.0	0.0/0.0	0.0/0.0	0.0/0.0
NH^{4+}	0.0/0.0	0.0/0.0	0.0/0.0	0.0/0.0	0.0/0.0	0.0/0.0	0.0/0.0	0.0/0.0
Al	0.007/0.009	0.02/0.019	0.048/0.036	0.096/0.158	0.12/0.28	0.001/0.003	0.003/0.005	0.007/0.012
V	0.0/0.0	0.0/0.0	0.0/0.0	0.0/0.0	0.0/0.0	0.0/0.0	0.0/0.0	0.0/0.0
Cr	0.0/0.0	0.0/0.0	0.0/0.0	0.0/0.0	0.0/0.0	0.0/0.0001	0.001/0.001	0.0/0.001
Co	0.0/0.0	0.0/0.0	0.0/0.0	0.0/0.0	0.0/0.0	0.0/0.0	0.0/0.0	0.0/0.0
Cu	0.0/0.0	0.0/0.0	0.0/0.0	0.0/0.0	0.0/0.0	0.0/0.0	0.0/0.0	0.0/0.0
Zn	0.844/0.9	0.154/0.166	0.271/0.245	0.0/0.0	0.0/0.0	0.0/0.0	0.0/0.0	0.0/0.0
As	0.0/0.0	0.0/0.0	0.0/0.0	0.0/0.0	0.0/0.0	0.0/0.0	0.0/0.0	0.0/0.0
Ti	0.708/0.773	0.007/0.01	0.02/0.018	0.0/0.0	0.0/0.0	0.0/0.0	0.0/0.0	0.001/0.0

The Orthophosphate concentration is considered to be significant, all determinations lying within the natural range shown in Tab. 10 and no anthropogenic influence being evident. Clusters 5 and 6 can not be used as a result.

• Tab. 10 PO_4^{3-} concentrations in the precipitaion of Jordan (RIMAWI & SALAMEH, 1991)

Station	PO_4^{3-} (mg/L)
University of Jordan	0.125
Ruseifeh	1.799
Khalidiya	0.71

The fact that Aluminium and Silicium are not significant might have its reason in the fact that the analysed samples were filtered with 200nm so some of the Al- and Si- complexes and colloids were filtered away.

The fact that the significancy of NO_2^- is above 5% for all clusters from 3 to 7 has its reasons in a mixture of influences. The main ones are the N_2 and NO_2^- exhalations in the thermal springs and the anthropogenic influences (fertilizer denitrification). Due to this and the fact that NO_2^- is meta stable, it is not taken into account.

Nevertheless, a number of eight clusters is possible but considering the reasons mentioned above it is believed that a seven cluster model fits best. One remarkable observation is the close correlation with the electric conductivity (EC) as shown in Tab. 11. As the EC is a result of the ions in a sample, the model is quite near to the chemical composition.

• Tab. 11 Correlation of cluster model 7 with the aquifers and the electric conductivity(EC).

ID	Aquifer	EC(µs/cm)	Cluster
000305S1	A1/2	167	1
000320S2	A7	440	7
000313S3	A4/A7	471	7
000313S1	A1/2	503	7
000314S3	A1/2	609	7
000306W1	Kurnub	615	7
000313S2	A7	655	7
000308S1	Kurnub	753	5
000314S2	A4	817	5
000308S3	A1/2	880	5
000308S2	Kurnub	917	5
000307W1	Kurnub	958	5
000305W2	Quartär	1050	5
000320S1	A7	1077	5
000305S2	Kurnub	1625	2
000306W2	Kurnub	1836	2
000306S1	Kurnub	3160	6
000305W1	Zerqua	4930	3
000312S1	Zerqua	5390	3
000309S2	Zerqua	11220	4
000309S1	Zerqua	12160	4

A closer examination of the cluster model reveals a number of important observations. The samples from the Zerqua aquifer are divided into two groups, cluster 3 & 4. Cluster 4 representing the sample of the so called “Spring No.1” and the “Men spring”. They are located close to one another at the mouth of the wadi Zerqua. The sample of the spring called “Women” which is situated about 300m to the ENE of the Men spring is in cluster 3 together with a sample of a well near the Kafrain dam. The reason for the grouping might be that the springs of cluster 4 might be influenced by a fault system near by, which is also indicated by the high volume of gas appearing together with the water in the pond. However, the spring and the well of cluster 3 should in turn of it represent a closer chemical finger print of the water from the Zerqa aquifer. The samples 000305W2 and 000307W1 are equally remarkable. Whereas the first one comes from an irrigation well downstream the Kafrain dam and, as I was told, is only situated in the wadi gravel, the second one is an observation well of the Kurnub aquifer upstream the Kafrain dam. Its chemistry being highly comparable (App. 7), it is not believed that the irrigation well only gets water out of the wadi gravel. Unfortunately, no data about this well was found in databases or literature and no total depth could be measured due to active pumping, either. However, these two samples belong to the cluster group 5 which is the largest one. It contains 7 samples of the aquifers of the Ajlun group and the Kurnub sandstone. Samples 000308S1 and 000308S2 are both samples from springs in the Baqua region. The springs discharge at a foot of a hill so some interaction with the interflow can not be excluded. However, it is not believed that they represent “pure” Kurnub samples, which is indicated by the low electric conductivity and the Tritium measurements. Cluster group 2

represents two samples of the Kurnub aquifer. 000305S2 is a sample from a thermal spring called Sara close to the Dead Sea near the wadi Zerqa Ma'in whereas sample 000306W2 was taken out of a well near Baqua about 60km to the NNE of the spring. This is remarkable because one sample (000306W1) of a well near by penetrating the Kurnub aquifer has different chemical fingerprints and is situated in cluster group 7. A sample (000320S2) from a spring called "Um Dananir" in cluster 7 is also situated in the Baqua region and discharges from the A7 aquifer. Due to this and the fact that the sample 000306W1 has the lowest temperature (~11°C) which is lower than the average year air temperature the well might be situated in another aquifer, but no Tritium occurrence was measured, which indicates a deeper aquifer system. However, group 7 contains 6 samples which are all from the Ajlun group except for the previously discussed one.

6.2.2 Hydrogeochemical results

The following chapter is sorted by a decrease of the electric conductivity and the statistical clusters discussed in chapter 6.2.1.

As shown in Fig. 61, the two highly mineralised (average EC: 11690 µS/cm) samples of cluster 4 belong to an alkaline water type with prevailing sulphate-chloride (LANGGUTH classification). Due to its thermal character and its high mineralisation, it can not be used as drinking water without water treatment (desalination) and therefore won't be discussed. The method published by the US SALINITY LABORATORY STAFF (1954) was used for its classification as irrigation water. This method considers the risk of salinity and the risk of sodium (SAR-Index = sodium absorption ratio) because high sodium concentrations cause problems for the pH and soil texture. The SAR is calculated by :

$$SAR = \frac{Na\frac{mmol(eq)}{L}}{\sqrt{\frac{Ca\frac{mmol(eq)}{L} + Mg\frac{mmol(eq)}{L}}{2}}}$$

As shown in Fig. 60, the samples of cluster 4 plot in the field C4-S4, which means that there is a very high risk of salinity and sodium for the soils. So a use as irrigation water must be rejected, too.

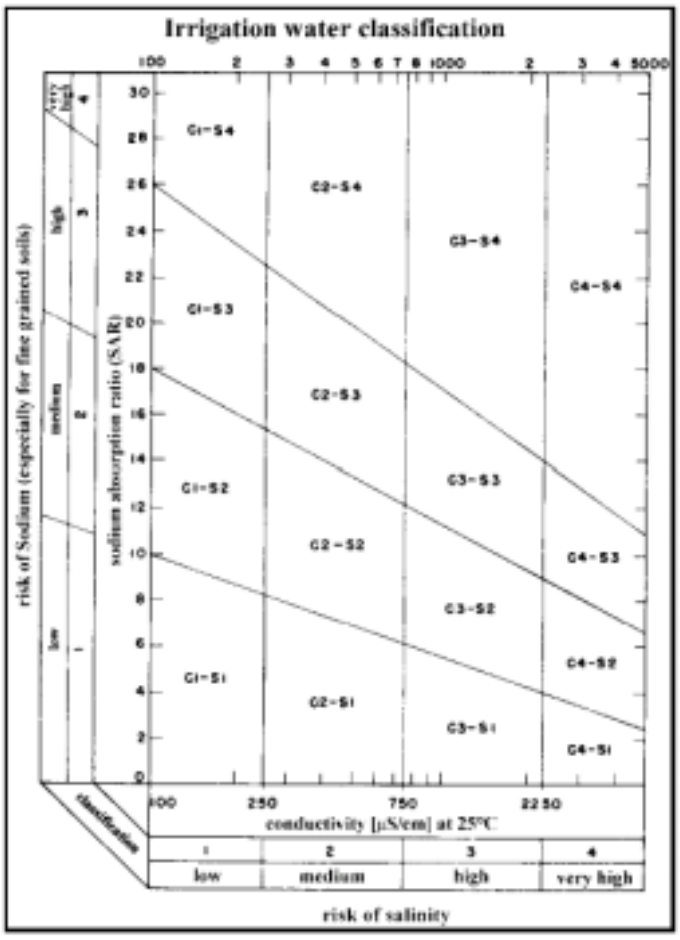

• Fig. 59 Classification scheme for irrigation water (US SALINITY LABORATORY STAFF, 1954).

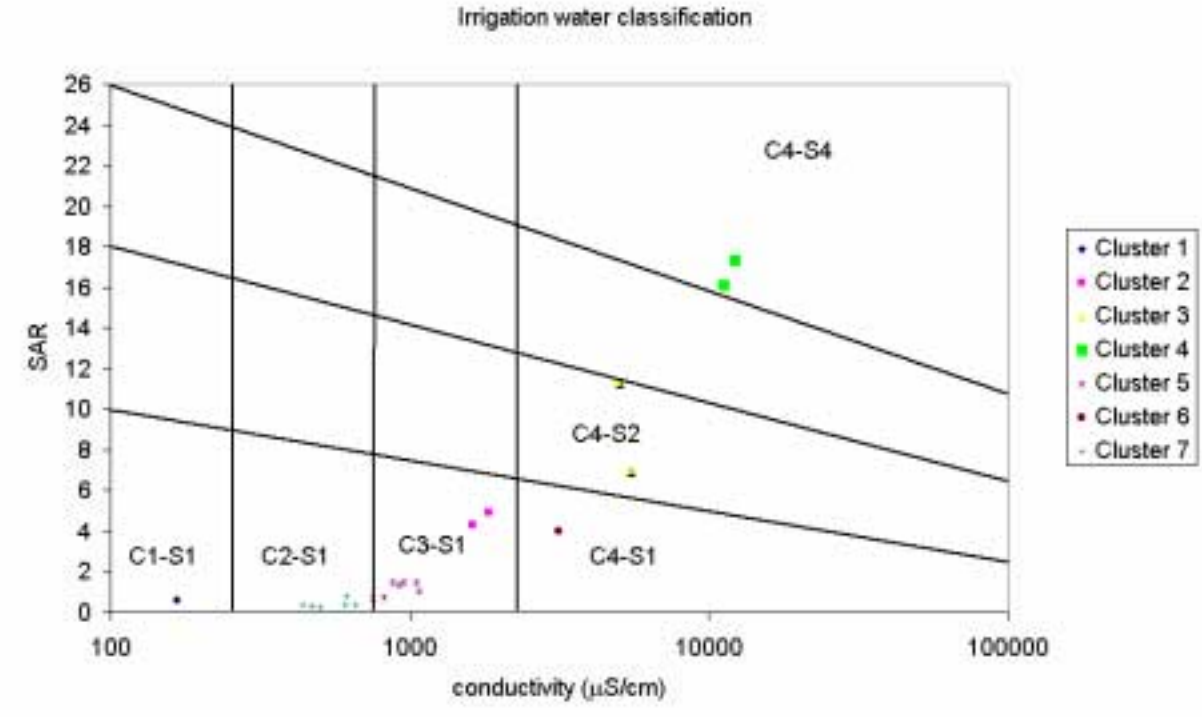

• Fig. 60 Plotting of the samples in the classification scheme for irrigation water.

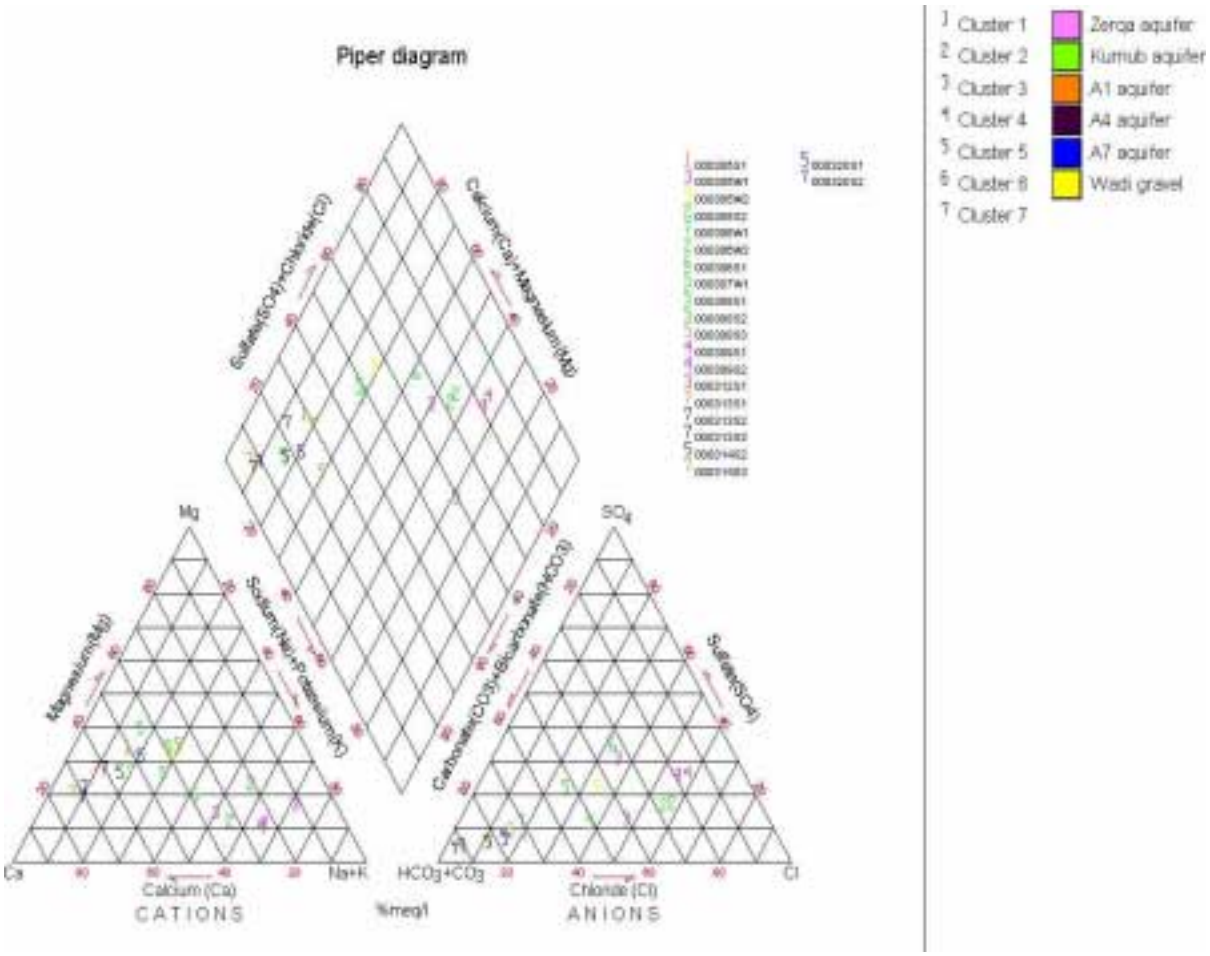

• Fig. 61 Piper diagram for the analysed samples. (Symbols are the clusters, colours are the aquifers).

These two samples contain high concentrations of CL^-, SO_4^{2-}, Na^+, K^+, $Ca^{2+,}$ Mg^{2+} and As. The exhalations of a nearby fault system might be the reason for the high concentrations of NO_2^-.

According to the PhreeqC model (App. 9), the most oversaturated minerals for the group are the iron minerals Hematit and Magnetit as well as Phyllosilicates such as Montmorillonit, Kaolinite and K-Mica. This is proven by the presence of iron crusts near and in the springs where the water was sampled (Fig. 62).

The spring's temperature which is about 34.5°C in this cluster might be explained by the geothermal gradient of the rift valley and the spring's location at -220m below sea level and an average yearly air temperature of about 20°C. Therefore an influence of the nearby fault system can neither be rejected nor assumed.

• Fig. 62 Iron crusts at the thermal springs at the mouth of the wadi Zerqua.

The two samples of cluster 3 also belong to an alkaline water type with prevailing sulphate-chloride. The reason for their different plotting is given by their different Ca^{+} concentration. Calcium is the only element that varies this much. The samples are not as highly mineralised as those of cluster 4 (average EC: 5160 µS/cm). The samples of cluster 3 are oversaturated by the same mineralphases as the samples of cluster 4 but the saturation indices are slightly higher. The samples are undersaturated in mineralphases containing heavy metal ions like $Zn_3O(SO_4)_2$, $(UO_2)_3(PO_4)_2$:4w, UF_4:2.5H_2O (for all SI > -30). A slight undersaturation was calculated for mineralphases containing Ca, Mg, and CO_x.

Again a purpose as drinking water without water treatment (desalination) and irrigation water (Fig. 60) must be rejected due to the very high risk of salinity and a medium risk of sodium for the soils.

Cluster 6 is represented by one sample (000306S1) of the Kurnub aquifer. The sample has an electric conductivity of 3160 µS/cm. It represents an earth alkaline water with an increased portion of alkalies with prevailing sulphate. This sample is oversaturated by mineralphases containing iron (Hematit, Magnetit, Goethit) and copper (Cuprous Ferrit, Cupric Ferrit) as well as clay minerals and micas. It is undersaturated by mineralphases containing As, Ni, and Zn. Carbonates are slightly under saturated, too. According to the irrigation water classification, the sample lies in the field C4-S1 (Fig. 59-Fig. 60), which means that there is a very high risk of salinity but a low risk of sodium for the soils. For the purpose of drinking water a water treatment should be installed to reduce the concentrations of Cl, SO_4, Na, Mg, Mn and As. However, the discharge of the spring being low, this does not seem to be economic.

Both samples of Cluster 2 again belong to an alkaline water type with prevailing sulphate-chloride. The oversaturated mineralphases are similar to those of cluster 3 except that saturation indices are a bit lower. Along the spring where sample 000305S2 was taken, the presence of iron crusts may justify this calculation (Fig. 63). In the case of undersaturation Cu is getting more important compared to the other clusters whereas U gets less significant. As shown in Fig. 60, there is a high risk of salinity and a low risk of sodium for the soil (C3-S1), if the water is used as irrigation water. Reaching about 52°C, sample 000305S2 has had the highest temperature taken during the field work. For the purpose of drinking water, a water treatment should be installed reducing the concentration of Cl, NO_3, Na, K, Mg, and As and in case of this spring the temperature should be reduced. At least this might not be discussed nowadays. Increasing water demands in Jordan will lead to a discussion in the future, as the high temperature might deliver a part of the energy needed for this process.

• Fig. 63 Thermal spring where the sample 000305S2 (Ain Sara) was taken.

Mostly all samples of cluster 5 are also situated in the C3-S1 (Fig. 60) field near those of cluster 2. The average EC is 921,71 µS/cm. The samples around the Kafrain dam (000307W1, 000305W2) and a sample of a spring near Baqua (000308S2), which all come from the Kurnub aquifer, are of an earth alkaline water type with an increased portion of alkalies prevailing sulphate. The rest of the samples in cluster 5 contain normal earth alkaline water or earth alkaline water with an increased portion of alkalies but always prevailing bicarbonate. As shown in the piper diagram (Fig. 61) sample 000308S1 does not contain prevailing sulphate although, as I have been told, it is supposed to come from the Kurnub aquifer. In my opinion, either the sample has been mixed up with other, e.g. meteoric water or the sample is out of another aquifer (could not be clearly seen because of a concrete wall). However, the sample has Tritium which should be untypical for the lower aquifer system. Both samples of the Kafrain dam show similar saturation indices for the oversaturated mineralphases like the previously discussed clusters (Hematit, Magnetit and Phyllosilicates), except for the observation that Cuprous Ferrite and Cupric Ferrite, both mainly

existing of copper and iron, are oversaturated too. According to calculation, minerals containing zinc are the most undersaturated ones, whereas carbonates seem to be slightly under saturated. The mineralphases Apatit, Leonhardit ($Ca_2AL_4Si_8O_{24}x7H_2O$), Tremolit, K-Mica and clay minerals are the most oversaturated mineralphases of the remaining samples. However, mineralphases containing As, U, Cu and Zn were calculated to be the most undersaturated ones, whereas carbonates were just slightly undersaturated.

Compared to the drinking water limitations either of Jordan, Germany or the WHO guidelines (App. 8), potassium is the only element analysed that might be a problem. The samples of the Kurnub are generally higher mineralised than the other ones within this cluster.

According to the piper diagram, all samples of cluster 7 are of a normal earth alkaline water with prevailing bicarbonate (Fig. 61). The oversaturated mineralphases are Apatit, Leonhardit, Phyrophyllit, K-Mica and Kaolin. Carbonates are slightly undersaturated, whereas minerals containing As, U, and Cu are the most undersaturated ones. According to Fig. 60, all samples have a medium risk of salinity and a low risk of sodium if the water is used for irrigation. Compared to the drinking water limitations and guidelines, none of the analysed elements is striking. The two samples enriched by zinc in this cluster are samples 00306W1 and 000314S3. The occurrence of zinc might has its reason in an anthropogenic influence due to the nearby townships and settlements (industry, fertilizer, pumps).

Cluster 1 is only represented by one sample (000305S1) of the A1/2 aquifer. With 167µS/cm it has the lowest electric conductivity of all samples collected during the fieldwork. This is why it plots in the C1-S1 field of the irrigation water classification (Fig. 59). This means that there is a low risk of salinity and sodium for the soils. In the piper diagram, the sample plots in the field of normal earth alkaline water with prevailing bicarbonate together with the samples of cluster 7. The sample is oversaturated with the mineralphases Apatit, Leonhardit, Phyrophyllit, Tremolit, K-Mica and Kaolin and mostly undersaturated with minerals containing As, U, Zn and Cu, too. Carbonates again are slightly undersaturated. Compared to the drinking water limitations and guidelines (App. 8), none of the analysed elements is remarkable.

6.2.3 Isotopes

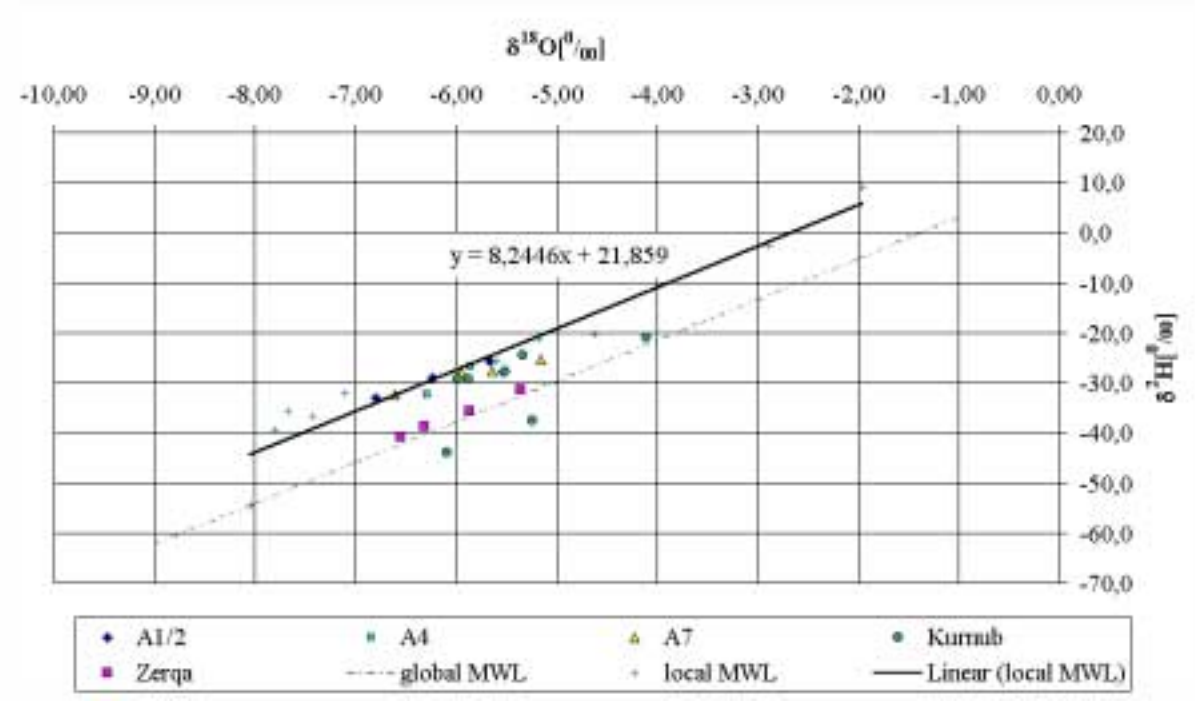

• Fig. 64 $\delta^{18}O$ and $\delta^{2}H$ diagram.

The most striking plots are made by the samples of the Zerqa group (Fig. 64). They are situated along a parallel line to the meteoric water lines with $\delta^{18}O$ values from –5.36 ‰ to –6.56 ‰ and $\delta^{2}H$ ranges from –31.5 ‰ to –40.9 ‰. The excess to the local meteoric water line is around 13.0. This can be interpreted as an environment change in the recharge area. However, the samples having been taken in a short period of time and the locations of the samples being almost close together, this interpretation might be wrong. It is more likely that the samples are influenced by an interflow process from the wadi and the nearby fault system (degasification in the headpool). The high excess indicates strong evaporation effects but as the recharge area of the groundwater is close to Saudi Arabia, it has no Tritium and plots near the global meteoric water line, the evaporation effects in former times might not have been that high.

The samples of the Kurnub aquifer have $\delta^{18}O$ values from –4.11 ‰ to –6.10 ‰ and $\delta^{2}H$ ranges from –20.9 ‰ to –44.0 ‰. The calculated $d_{exlocal}$ is widely spread and ranges from 5.6 ‰ to 20.0‰. This data should be a function of leakage from and to the Kurnub Aquifer as well as there might be some mistake due to the interflow in the springs (000308S1) or a take in of younger groundwater because of pumping (000306W2). This is also shown in the Tritum measurements (Tab. 12).

The samples of the A1/2 aquifer have $\delta^{18}O$ values from –5.54 ‰ to –6.8 ‰ and deuterium has a range from –25.6 ‰ to –33.0 ‰. Calculated excesses with an average of 21.12 ‰ are strongly remarkable. They plot to the right of the local meteoric water line, which means that the samples are diluted. The local meteoric water line being a trend line and the calculated excess being just a bit higher, the dilution can be neglected in favour of statistical background.

The ranges of $\delta^{18}O$ and $\delta^{2}H$ in the samples of the A4 aquifer system are quite similar to those of the A1/2 aquifer. Nevertheless, the average of the excesses is 20,49 ‰ and therefore slightly under the local meteoric water line. The samples are almost not influenced by evaporation.

The samples of the A7 aquifer system have $\delta^{18}O$ values which range from –5.17 ‰ to –6,61 ‰ whereas the $\delta^{2}H$ values have a range from –25.3 ‰ to –32.4 ‰. The average of the excesses is 19.88 ‰, which means that the samples are influenced by an evaporation effect.

For all samples except 000306W2, the calculated recharge area lies within explainable altitudes.

• Tab. 12 Results of the Tritium measurement.

ID	Aquifer	Tritium	±
		(T/T.E.)	(T/T.E.)
000305S1	A1/2	2.70	0.50
000305W1	Zerqua (2)	0.00	0.30
000305W2	Quartär	2.70	0.50
000305S2	Kurnub	0.00	0.30
000306W1	Kurnub	0.00	0.30
000306W2	Kurnub	1.10	0.50
000306S1	Kurnub	0.00	0.30
000307W1	Kurnub	-0.30	0.30
000308S1	Kurnub	3.40	0.40
000308S2	Kurnub	3.10	0.40
000308S3	A1/2	1.00	0.20
000309S1	Zerqua (2)	0.20	0.30
000309S2	Zerqua (2)		
000312S1	Zerqua (2)	0.40	0.30
000313S1	A1/2	5.80	0.60
000313S2	A7	5.80	0.60
000313S3	A4/A7	6.60	0.70
000314S1	A7		
000314S2	A4	4.60	0.50
000314S3	A1/2		
000320S1	A7		
000320S2	A7	2.87	0.50

As shown in Tab. 12, the samples of the Zerqa aquifer contained almost no Tritium, so the water has probably not been in touch with meteoric water for some time. Unfortunately, no Tritium model could be calculated, no input model data being available for this region. Most of the Kurnub aquifer samples do not contain any Tritium, either. The Tritium measurements of the three Kurnub aquifer samples (000306W2, 000308S1, 000308S2) might be explainable, too, by a closer examination of the sampling site.

Sample 000306W2 was taken from a well situated almost in the center of the Baqua depression. As the Kurnub aquifer is partly exposed in this depression, a local recharge with meteoric water containing tritium can not be rejected. However, it can be assumed that the water from the Kurnub aquifer is mixed up with water from the surrounding hills due to the depression's character.

Samples 000308S1 & S2 were also taken from the Baqua depression. The springs are situated near the foots of the surrounding hills. Their position and a large concrete wall possibly damming up younger meteoric water (Fig. 65, Fig. 66), probably lead to a mixture.

It should be mentioned that the geology at the sampling site was not clearly recognisable due to the wall and fault systems, so that the aquifers that should have been worked out in this area could not be treated in the time given for the field work.

• Fig. 65 Ain Mubis, sampling site of the sample 000308S2.

• Fig. 66 Sampling site from the sample 000308S1, beside the road Amman - Baqua.

All samples of the Ajlun aquifer contain Tritium, which might be explained by the circumstance that all samples were taken at springs so that the aquifer also is exposed and a local recharge with young meteoric water is presumable. As well there might be a mixing due to tectonic systems or karst as described in 5.3.1.1.2.

6.3 Numerical groundwater model

6.3.1 Geological model

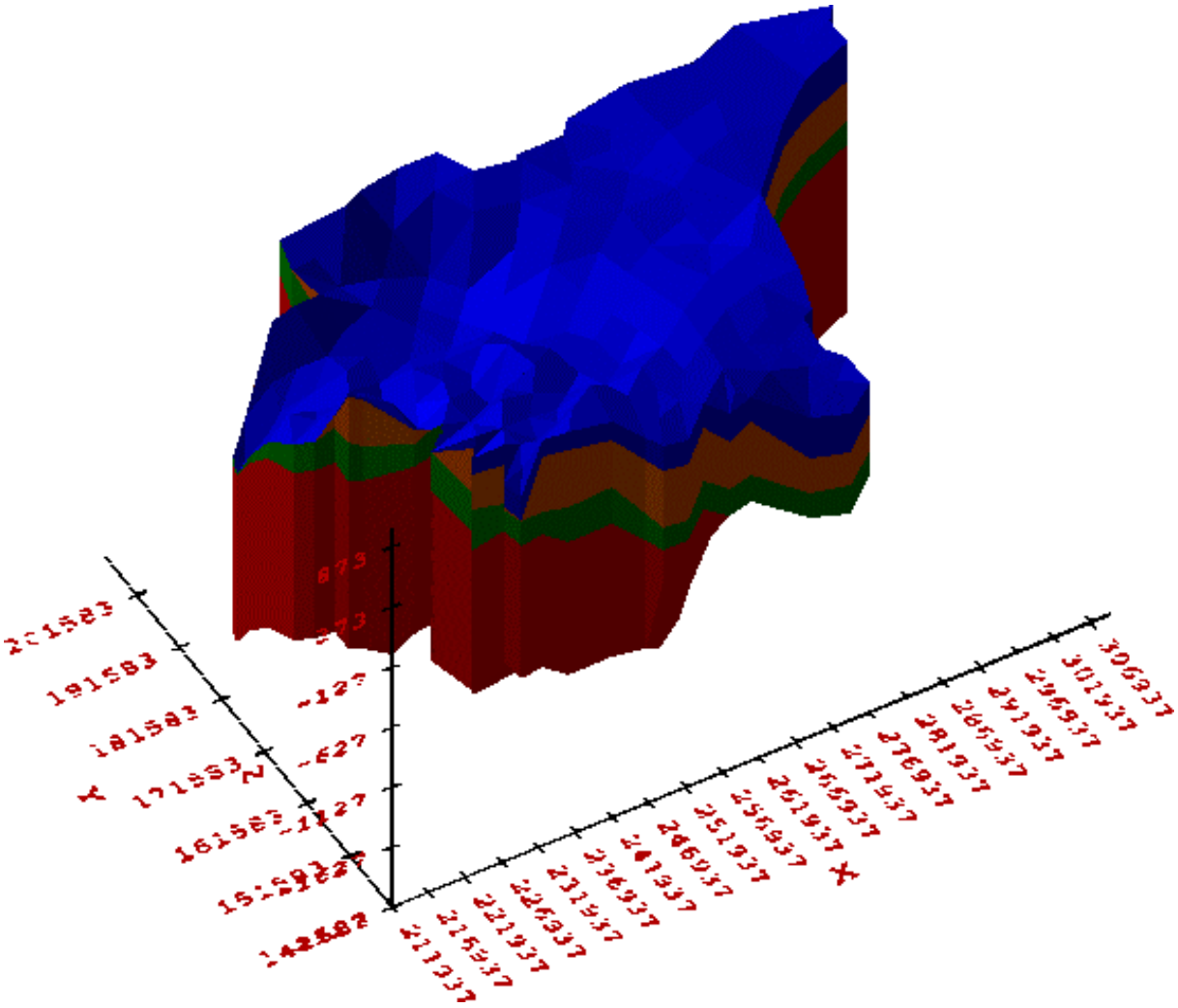

• Fig. 67 XYZ view of the geological model.

Unfortunately, there was no opportunity to get better plottings out of GMS 2.1, at least the main features can be seen. In Fig. 67, the entire covering is blue, which indicates that the A7/B2 aquifer covers the whole model, but this is only the effect of the minimum thickness of 0.01m described in chapter 5.3.1. At the western boarder (closed to the y-axis), the pinch out zones of the units can be seen. In Fig. 68 and Fig. 69, the eroded part of the Zerqa aquifer in the center of the model can be recognised. As well the shift in the dipping direction near the boarder to Syria can be seen.

During the calibration of the model it was tried to get rid of the areas with a 0.01m thickness where the geological stratas crop out. Therefore several efforts have been made. At the beginning it was tried to assign a new highly pervious material to these areas (Fig. 70). Secondly, all elements of the 3-dimenional meshes belonging to the outcropping zones were deleted (Fig. 71). However, none of these efforts led to a satisfying result so that the original model was used for further investigation.

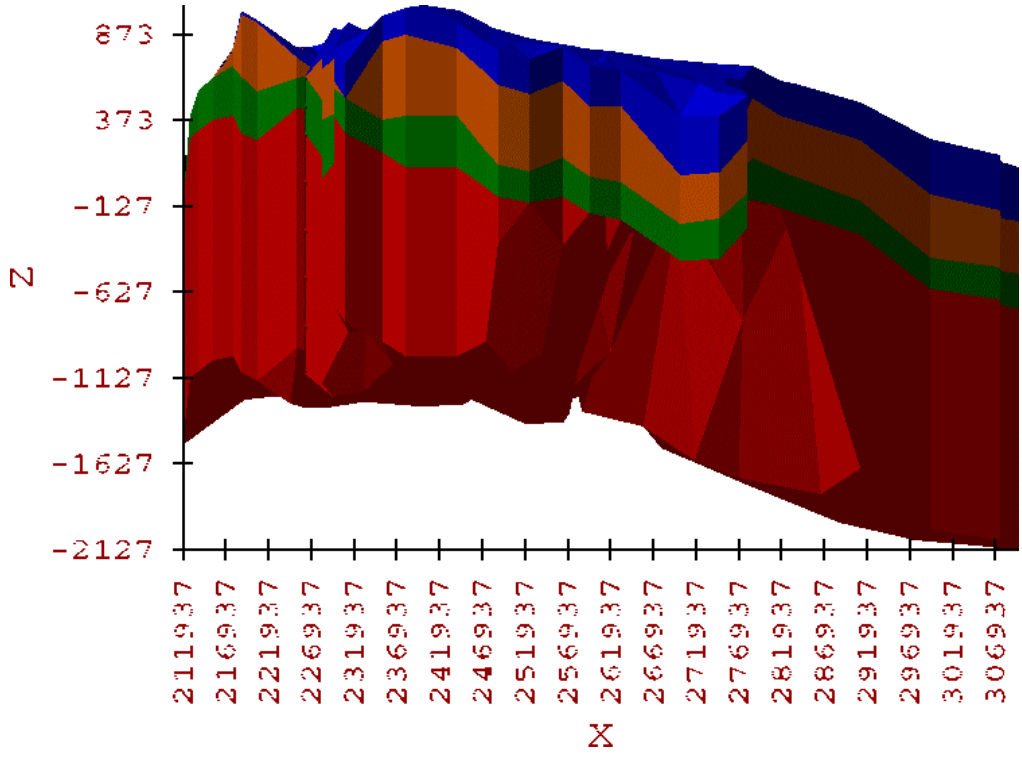

• Fig. 68 XZ view of the geological model.

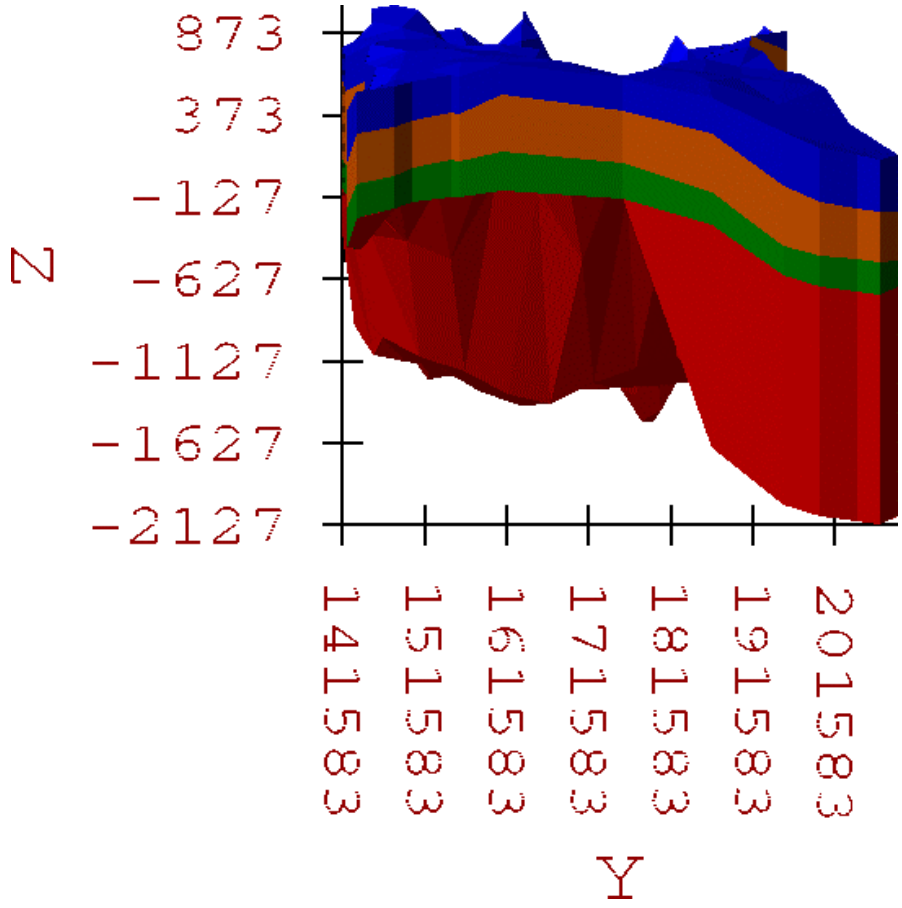

• Fig. 69 YZ view of the geological model.

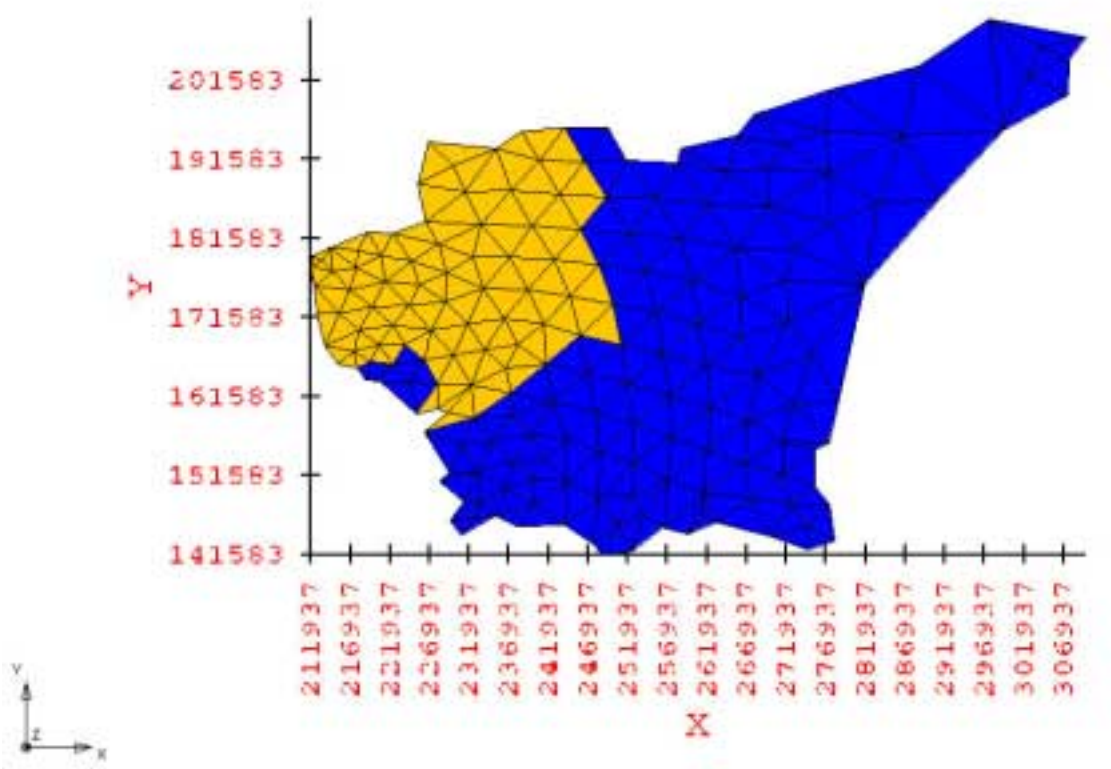

• Fig. 70 XY view of the geological model with the assigned highly pervious material (yellow).

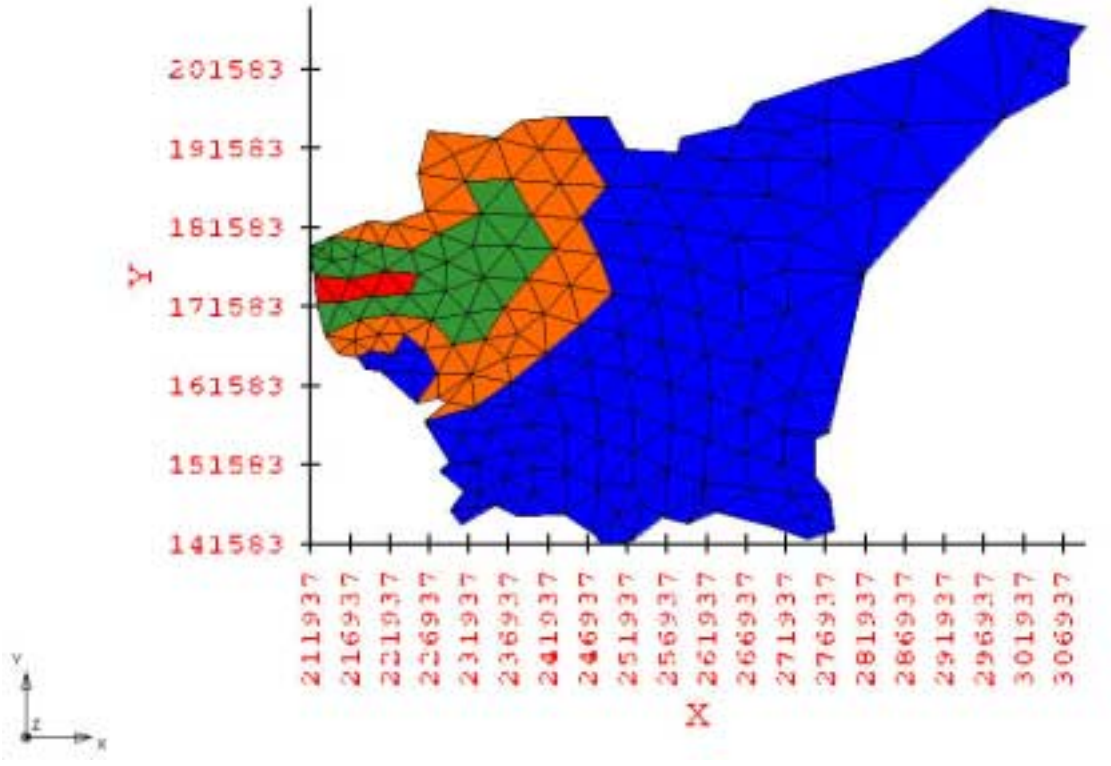

• Fig. 71 XY view of the geological model after the outcropping zones were deleted.

6.3.2 Groundwater recharge

As shown in Tab. 13, the groundwater recharge varies between 0 to about 65mm/a. Station AL0059 is the most eastern one in the study area and the local groundwater recharge might have its reasons in the morphological situation discussed in chapter 3.2. However, even a change of the parameters in the model within acceptable ranges will have the same result.

• Tab. 13 Results of the groundwater recharge model.

Station ID	evaporationfactor	groundwater recharge(mm/a)
AL0053	0.8	26
AL0059	0.8	0
AL0019	0.8	11
AL0035	0.8	54
AH0003	0.8	65

The other calculated values seem to be, according to EL-NASER (1991), within suitable ranges for the area.

6.3.3 Runoff and Discharge

6.3.3.1 Kurnub Aquifer

• Tab. 14 Calculated discharge from the Kurnub aquifer.

UNIT1	UNIT2	Total ABS (m^3/yr)	Number of wells	Min. ABS (m^3/yr)	Average ABS (m^3/yr)	Max. ABS (m^3/yr)	Std. Dev.	Variance
K		9625230	50	180	192504.6	864000	152535.10	23266957804.93
K	A1/A6	394650	2	193050	197325	201600	6045.75	36551250
K	A7/B2	604800	1	604800	604800	604800		

The total discharge from the Kurnub is set to 10,124,955 m^3/yr.

6.3.3.2 A1/A6

• Tab. 15 Calculated discharge from the A1/A6 aquitard.

UNIT1	UNIT2	Total ABS (m^3/yr)	Number of wells	Min. ABS (m^3/yr)	Average ABS (m^3/yr)	Max. ABS (m^3/yr)	Std. Dev.	Variance
A1/A6		12446090	64	840	194470.15	855000	182046.83	33141049407.91
A1/A6	A7/B2	1267920	4	155520	316980	518400	163869.61	26853249600
A7/B2	A1/A6	815400	2	59400	407700	756000	492570.58	242625780000
BS	A1/A6	262800	1					
K	A1/A6	394650	2	193050	197325	201600	6045.76	36551250

The total discharge from the A1/A6 was set to 13,816,475 m^3/yr.

6.3.3.3 A7/B2

• Tab. 16 Calculated discharge from the Kurnub aquifer.

UNIT1	UNIT2	Total ABS (m^3/yr)	Number of wells	Min. ABS (m^3/yr)	Average ABS (m^3/yr)	Max. ABS (m^3/yr)	Std. Dev.	Variance
A7/B2		65222898	228	200	286065.34	1641600	288937.34	83484787568.04
A7/B2	A1/A6	815400	2	59400	407700	756000	492570.58	242625780000
A1/A6	A7/B2	1267920	4	155520	316980	518400	163869.61	26853249600
ALL	A7/B2	955200	6	23250	159200	399000	149727.88	22418439000
B4/B5	A7/B2	259200	1	259200	259200	259200		
BS	A7/B2	16507320	41	144000	402617.56	1270200	194491	37826750563.90
K	A7/B2	604800	1	604800	604800	604800		

The total discharge from the A7/B2 was set to 75,427,818 m^3/yr.

6.3.4 Initial conditions

First of all, the run options in GMS had to be defined. The type of simulation was set to flow only steady state. As a solver, the pointwise iterative matrix solver was selected. The other options like weighting factor or quadrature selection were left as default. The initial conditions in GMS were set to cold start with a pressure head computed from the constant heads as they were set as boundaries. The iteration parameters were left as default. In the fluid properties, 1000kg/m^3 was set as density of the water. The viscosity was set to 4.68 kg/m/hr. The compressibility of water was set to 3.410^{-17} m-hr^2/kg and the acceleration due to gravity was set as 1.2710^8 m/hr^2. The boundaries were assigned as discussed in chapter 5.3.4. According to LIN H.J. ET AL. (1997), the variable boundary conditions were used for the groundwater recharge. Later on during calibration, they were changed to a constant flux boundary because no unsaturated zones were modelled. The material properties for the beginning of the calibration were taken out of literature (EL-NASER (1991), KHDIER (1997), JICA (1995)) (Tab. 17).

• Tab. 17 Initial material parameters for the steady state flow model.

	A7/B2	A1/A6	Kurnub	Zerqa
permeability (m/hr)	2.5	0.0025	0.16128	0.018

Problems occurred when trying to find parameters for the compressibility of the rock units. So for the purpose of an idea, a linear regression was made with the values found in DEPARTMENT OF DEFENSE (1998) (Fig. 72). Although the unsaturated zone should not be taken into consideration, FEMWATER does not run without any parameters concerning the unsaturated zone head. This is why the internal van Genuchten curve generator of GMS was used to compute the curves for the moisture content, relative conductivity and the water capacity of the unsaturated zone.

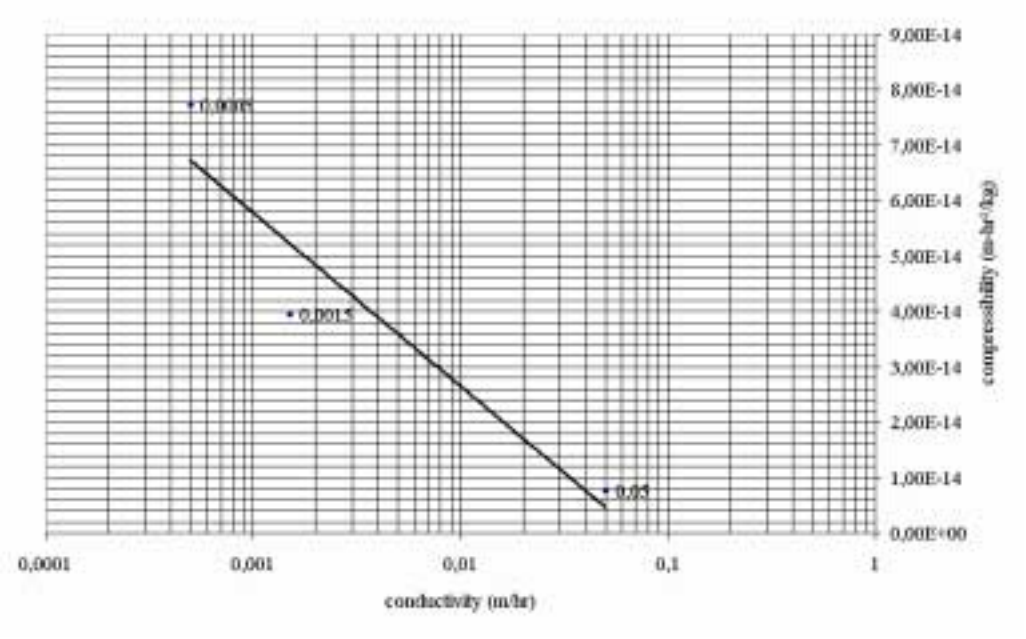

- Fig. 72 Linear regression of the conductivity vs. compressibility according to the data of DEPARTMENT OF DEFENSE (1998).

6.3.5 Calibration of the model

For the calibration of the model, observation points were added into a map layer in GMS. The observation points were taken out of the database which was already used for the constant head boundaries. Unfortunately, no observation point was available for the Zerqa aquifer within the model area. As discussed in chapter 5.3.4, no observation points where available in the eastern part of the model area except those of the A7/B2 aquifer, either. Due to the scale of the model and the fact that several parameters were not available, the aim of the calibration was set to ±50m.

During the calibration of the model it was found out that a change between flux variable and constant flux boundaries for the groundwater recharge had almost no influence on the calibration but increased the calculation speed by a factor of about 1:20. Therefore the calibration was made with constant flux boundaries for the groundwater recharge. Running several models with different material properties it became evident that the groundwater recharge in the central part of the model was to low. This is why the groundwater recharge boundary formally assigned with 11m/a (Fig. 52) was finally reassigned with 20mm/a. The reason for this is the lack of information concerning the evaporation (chapter 5.3.2.2) and soils whereas the precipitation input data could be calculated well enough (chapter 5.3.2.1).

Problems appeared because of 0.01m thick generated layers where the geological formation normally is eroded. As described in chapter 6.3.1, it was tried to either delete or to assign a highly pervious material to this region. However, it was possible as geological model but getting a pressure head file from FEMWATER over the whole model area was impossible. Subsequently, the groundwater recharge could only be assigned to the A7/B2 layer so that the deeper aquifers had no direct recharge as the A1/B6 aquitard lies in between. As a result the pressure head of the deeper aquifers is to low. However, the differences in the pressure head in this region of the model might have its reasons in numerical problems of the solver due to the low thickness.

The only way for calibrating the model is to change the material properties or the constant head boundaries. However, the assigned constant head boundary of the A7/B2 seem to fit with regard to the aim of the calibration. The A1/A6 aquitard should at least be saturated with water and due to the general hydrodynamic flow pattern (Fig. 8), there is a leakage from the Kurnub aquifer to the A7/B2. As a result of this and a lack of information no changes where made at the A1/A6 aquitard and the Kurnub aquifer boundaries. The only aquifer where changes of the constant head boundaries seem to be more likely is the Zerqa aquifer. Lowering the constant head boundary is estimated to be useless as this would lower the pressure head which is too low anyway.

However, the most effective way to calibrate the model was to change the material properties in which the A1/A6 aquitard played a the major role. Therefore several models were computed and checked with the observation points. The deviation from the observation points to the computed pressure head file was calculated by GMS. This calculation could only be done for the uppermost layer of the model. However, switching off a layer of the geological model and seeing the pressure head of a deeper layer did not change the deviation of the observation points. Therefore it was tried to do this manually, but it is almost impossible to get the exact pressure head within a certain point in GMS. However, the contour function and the possibility to created iso-surfaces within GMS were used to get an idea.

Calibration had to be aborted due to a lack of time. The aim of the calibration that the deviation is less the 50m was not totally reached due to the discussed problems. However, two models were calibrated with regard to the problems. One with regard to the pressure head of every single geological layer (model 1)and another one with regard to the observation points and the total pressure head file (model 2).

The best fitting material properties of the two calibrations are shown in Tab. 18.

• Tab. 18 Material properties assigned in the best fitting models.

	A7/B2	A1/A6	Kurnub	Zerqa
conductivity (m/hr) of the model 1	0.8	$5.0*10^{-6}$	0.3	0.005
conductivity (m/hr) of the model 2	0.7	$8*10^{-5}$	2.0	0.05

As shown in Fig. 73, the calibration with regard to the observation points (Tab. 19) is best for the Kurnub aquifer and the A7/B2 aquifer. Increasing the conductivity of the A1/A6 would lower the pressure head within the A1/A6 and would increase it with the Kurnub and Zerqa aquifer but it would lower it within the A7/B2. Increasing the conductivity of the A1/A6 and decreasing the one of the A7/B2 to avoid the lowering would not make much difference because a lower amount of water provided by the groundwater recharge will reach the lower aquifers. However, it is estimated that changing the observation points of the A1/A6 would lead to another result but unfortunately, no data of water levels in wells situated more to the east were available. Therefore springs were taken and as shown in Fig. 73, GMS caused problems in calculating the deviation for the springs Birein and Yajuz.

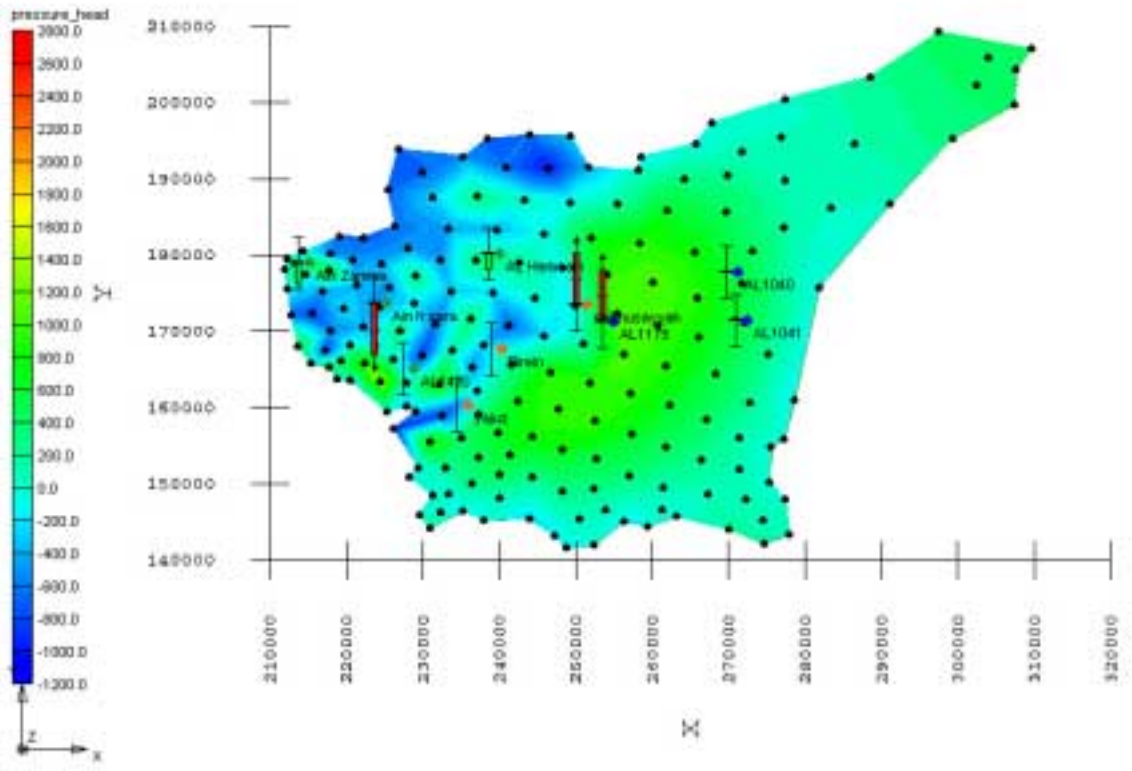

• Fig. 73 Pressure head of the model with the regard to the observation points (model 2).

The massive pressure draw down within the A7/B2 in the western part is supposed to be the result of the 0.01m thick layers. They disappear within the lower aquifer systems which cover the whole area. Therefore it is assumed that the model with regard to the observation points and the total pressure head file is not sufficiently suitable.

• Tab. 19 Differences to the observed water level for calibration 2.

Observation point	Aquifer	observed water level (masl)	difference to the observed water level (m)
Ain Zamma	Kurnub	120	-76
Ain h Sara	Kurnub	435	-453
Ain Hammam	Kurnub	275	-58
Seil husayyah	A1/A6	450	330
AL1175	A7/B2	489	583
AL1040	A7/B2	511	-3
AL1041	A7/B2	517	13

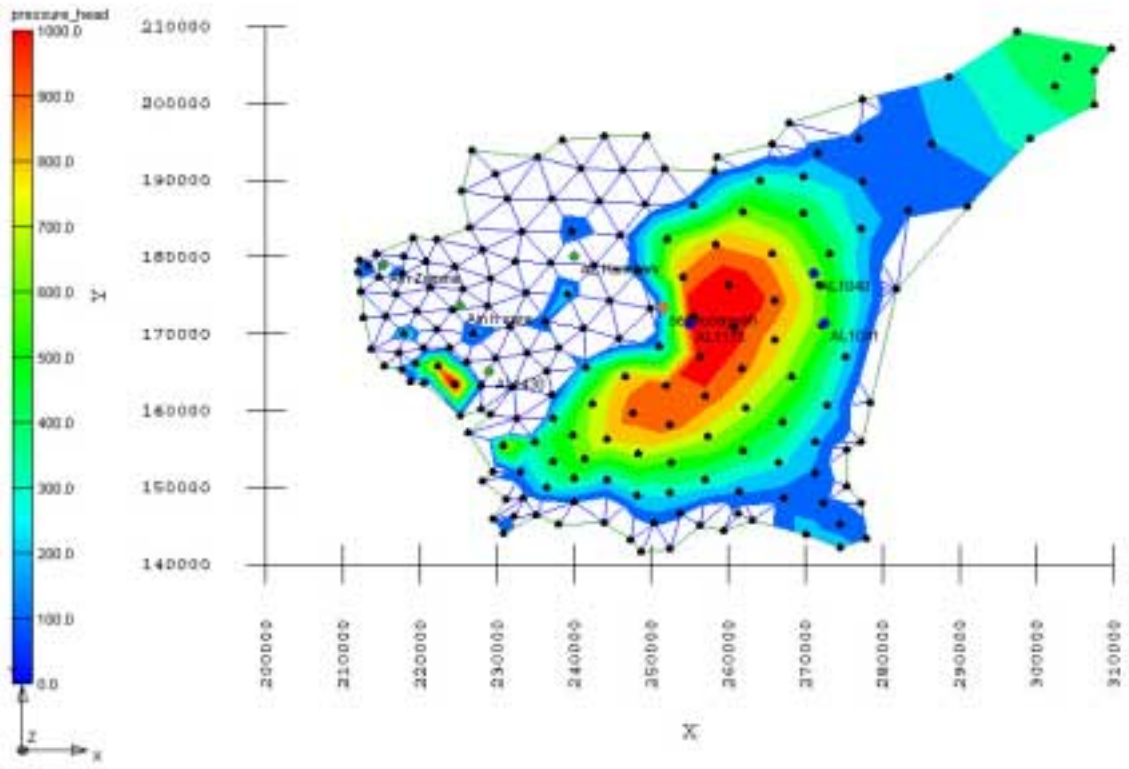

• Fig. 74 XY view of the pressure head calculated for the A7/B2.

The calibration with regard to the pressure head of every single aquifer took more time due to the previously discussed problems. Unfortunately, no table with the deviations can be provided as GMS does not have a function to get the pressure head in one single point. However, as shown in Fig. 74, the observation points AL1040 and AL1041 seem to be fitting, whereas the pressure at AL1175 is to high. However, the high pressure in observation point AL1175 is supposed to have its reasons in the scale of the model. In fact an intense draw down of the pressure appears to be more to the west of the observation point and the high pressure area is represented in the groundwater contour map too. As shown in Fig. 75, the pressure of the A1/A6 observation point almost fits. The nearby draw down has its reasons in the outcropping of the geological layers. As mentioned above, with more observation points and especially wells situated in the eastern part the calibration would be easier and might be of higher quality. All pressure heads concerning the Kurnub aquifer (Fig. 76) provided by the model seem to be too low (~100-200m). It was tried to get a better solution, however without a result. The massive high pressure around N160000 and E230000 could not be explained within the time schedule. It might have its reasons in the dirichlet head boundaries. All models show a higher pressure zone in the north east. However, observed groundwater levels were not available for this area so they were interpolated. Another reason might be that the geological layers dip to the NE in this area, which was the result of interpolation, too (App. 10-App. 19).

It is supposed that the calibration with regard to the pressure head of every single geological layer fits. It is remarkable that the pressure head of the Zerqa aquifer as shown in App. 27 is around -200m in the mapping area where two springs (~-220m) are situated as described in chapter 5.2.

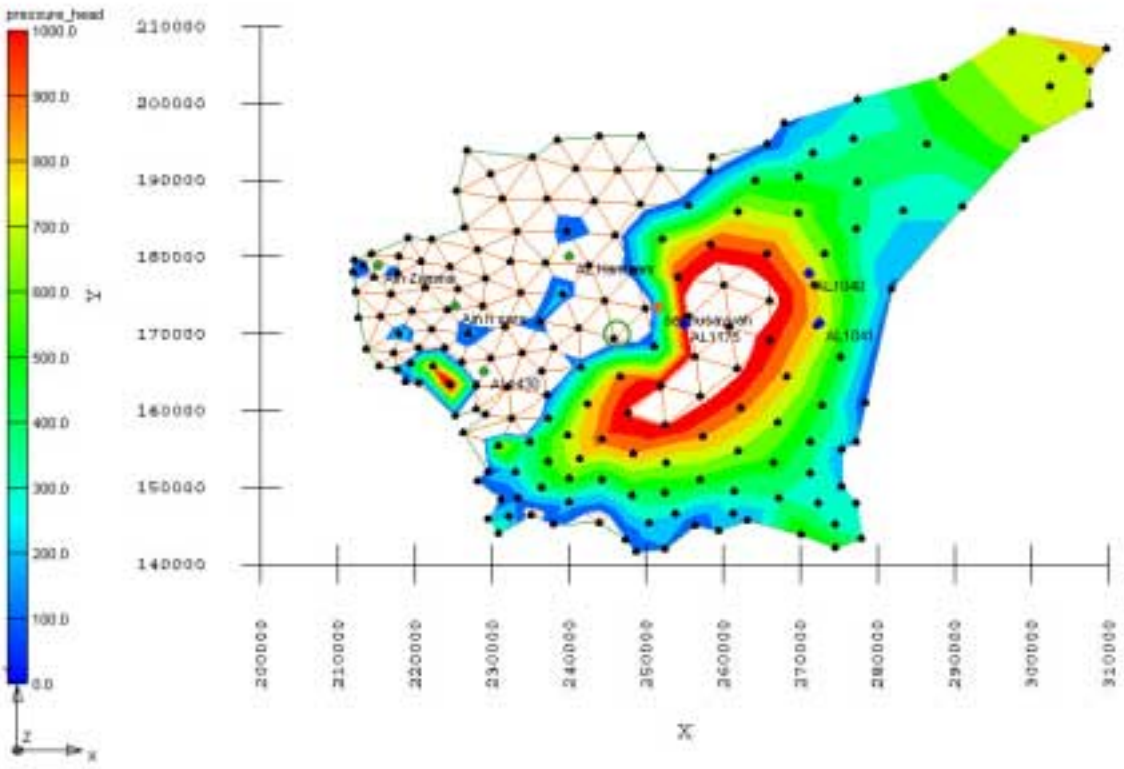

• Fig. 75 XY view of the pressure head calculated for the A1/A6.

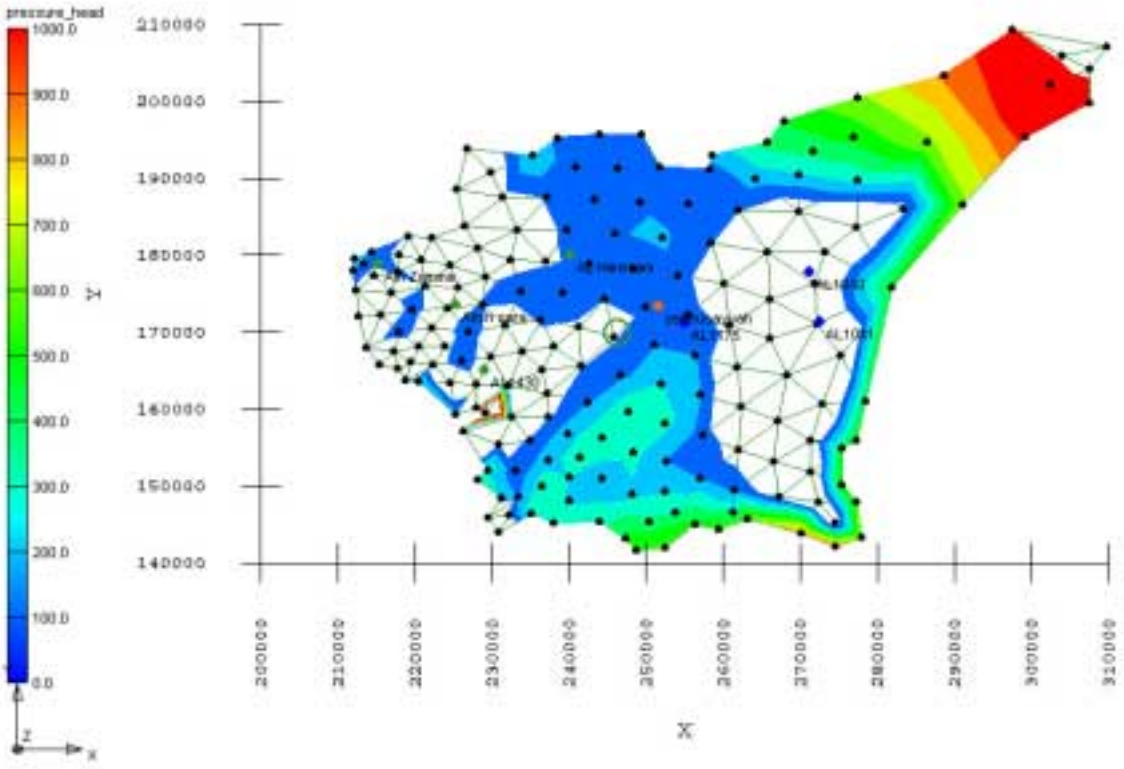

• Fig. 76 XY view of the pressure head calculated for the Kurnub.

7 Recommendations

With regard to the area of interest in this work and the scheduled time and available data, this work can only provide an overview of the groundwater situation within the Wadi Zerqa catchment area. Referring to increasing drinking water demands in Jordan, a detailed study over a longer period of time is recommended, especially for the mostly unused deeper aquifer system.

With a long term chemical study of the wells in the area especially for the trace elements and the exact knowledge of the geological settings and the petrographic features of the aquifers, it should be possible to get detailed fingerprints for the different water types. This data can be used for a PHREEQC mixing model to get detailed information about the leakage. A first study like this was done by EL-NASER (1991) for an area more to the north and only for the upper aquifer system. However, with the chemical determinations provided in this work a solution with a PHREEQC mixing model might be possible but is regarded as inaccurate. Not all field measurements could be done at the sampling place and the samples were not analysed fast enough as they had to be determinated in Germany. These were the main problems in the treatment of the hydrochemistry in this work. However, a study of Strontium and Lithium isotopes of the thermal springs might lead a conclusion about the origin of the thermal water. It was tried to handle this but unfortunately, it was not possible within the time schedule and with the available technical equipment. Furthermore a determination of pesticides and their residues as well as fertilizers were not subjects of this work.

Several problems had to be faced during the construction of the model but could be solved to a large degree. However, the model can only provide one out of many solutions as many subjects were not taken into consideration because of a lack of information or the time schedule. First of all, more information about the water table of the deeper aquifers and the A1/A6 aquitard for the construction of the boundaries and the calibration of the model would be desirable. Although FEMWATER is a finite element density dependent model, the salinity and subsequently the density of the different water types were not taken into consideration. With regard to the geological model, it might be useful to take a closer look at the major tectonic elements and their influence on the hydrological model. As a result, this would certainly lead to a longer calculation time and a finer grid in which the discharge from the aquifers and the infiltration of the King Talal dam can be taken into consideration. As well, more input data concerning the groundwater recharge model would improve the results of the model.

It should be mentioned that GMS 2.1 seems to have several bugs, so that it is recommended to use the version 3.1 or even shift to another graphical interface for constructing the model.

8 Literature

Abdelhamid, G. (1995) : The geology of Jarash area (Map Sheet 3154-I). - Geol. Bul., Vol.30; Amman, Jordan (Natural Resources Authority).

Abed (1982) : Dispoitional environments of the early Cretaceous Kurnub Sandstones, north Jordan. - Sedmimentary Geology, Vol. 32.

Abu-Ajamieh, M.M., Bender F.K., Eicher R.N. (1988) : Natural resources in Jordan. - 224p., 6 maps; Amman, Jordan (Natural Resources Authority).

Ajamieh, M.A. (1980) : The geothermal resources of Zerqa Ma'in and Zara. - Amman, Jordan (Natural Resources Authority).

Al Kuisi, M. (1998) : Effects of irrigation water with special regards to biocides on soils and groundwater in the Jordan Valley area. – Münstersche Forschung zur Geol. und Paläont., Vol. 84 : 173p., 137fig., 66tab.; Münster.

Amireh, B. (1987) : Sedimentological and petrological interplays of the Nubian series in Jordan with regard to paleogeography and diagenesis. – Ph.D Dissertation, University of Braunschweig.

Andrews, I.J. (1991) : Palaeozoic lithostratigraphy in the subsurface of Jordan. - Geol. Bul., Vol. 2; Amman, Jordan (Natural Resources Authority).

Andrews, I.J. (1992) : Permian, Triassic and Jurassic lithostratigraphy in the subsurface of Jordan. - Geol. Bul., Vol. 4; Amman, Jordan (Natural Resources Authority).

Andrews, I.J. (1992a) : Cretaceous and paleogene lithostratigraphy in the subsurface of Jordan. - Geol. Bul., Vol. 5; Amman, Jordan (Natural Resources Authority).

Atallah, Dr. M. (1991) : Origin and evolution of the Dead Sea. - Geol. of Jordan, 15 - 19, 4fig.; Amman, Jordan (Goethe-Institut).

Awad, N. (1990) : The groundwater quality downstream of King Talal dam as affected by the water quality of the dam. - Master Thesis, 121p.; Amman.

Bandel, K. (1981) : New stratigraphical and structural evidence for lateral dislocation in the Jordan Valley connected with a deslocation of Jurassic rock. - Jordan. N. Jb. Geol. Paläont., Abh. 161 : 271-308p.; Hannover.

Bandel, K., Khoury, H. (1981) : Lithostratigraphy of the Triassic in Jordan. - Facies Vol. 4, 1-12p.

Bender, Dr. F. (1968) : Geologie von Jordanien. - Beiträge zur Reg. Geol. der Erde, Vol. 7 : 230p., 173fig., 16tab., 1 geol. map, scale 1:250,000; Berlin-Stuttgart (Gebrüder Borntraeger Verlag).

Clark I., Fritz P. (1997) : Enviromental isotopes in hydrogeology. - 327p.; New York (Lewis Publishers).

Davis J, F. (1973) : Statistics and data analysis in geology. - 550p.; New York (John Wiley & Sons).

Department of defense (1998) : GMS v2.1 Tutorials - Bringham Young University.

Department of defense (1998a) : GMS v.21 Reference manual - Bringham Young University.

El-Naser, H. (1991) : Groundwater resources of the deep aquifer systems in NW-Jordan: hydrogeological and hydrogeochemical quasi 3D Modelling - Forschungserg. aus dem Bereich Hydrogeol. und Umwelt, Vol. 3 : 144p., 42fig., 27tab.; Würzburg.

Fadda, E.H. (1991) : The geology of the Sahab area. - Geol. Bul., Vol. 17; Amman, Jordan (Natural Resources Authority).

Fournier, R.O., Potter, R.W. (1982) : A revised and expanded silica geothermometer. - Geothermal Resources Council Bul. Vol. 11; p. 3-9.

GTZ: Agrar & Hydrotechnik & GTZ (1977) : National water master plan of Jordan. - Vol. 4; Essen, Hannover.

Japan International Cooperation Agency (JICA) (1995) : The study on brackish groundwater desalination in Jordan. - Yachiyo Engeneering CO., Ltd, and Mitsui Mineral Development Engineering CO., Ltd., (main & support interim report) - 318 p.; Tokyo, Japan.

Khalil, B., Muneizel, S.S. (1992) : Lithostratigraphy of the Jurassic outcrops of north Jordan. - Geol. Bul., Vol. 21; Amman, Jordan (Natural Resources Authority).

Khalil, I. (1993) : The geological framework for the Harrat Ash-Ahaam basaltic super-group and its volcanotectonic evolution. - Geol. Bul., Vol. 25; Amman, Jordan (Natural Resources Authority).

Khdier, K. (1997) : An assessment of regional hydrogeological framework of the Mesozoic aquifer system of Jordan. - Ph.D. Thesis, 426p.; Birmingham.

Lin H.J. et al. (1997) : FEMWATER : A three dimensional finite element computer model for simulating density-dependent flow and transport in variably saturated media. - Software manual, distibution unlimited. 142p.

Merkel, B. & Sperling, B. (1996) : Hydrogeologische Stoffsysteme Teil I. - DVWK-Fachausschuß, Bonn, 324p., 83 fig., 102 tab., 17 coloured graph.; Bonn.

Mugnier, C. J. (2000) : http://www.asprs.org/resources.html

Rimawi O., Udluft, P. (1985) : Natural water groups and their origin of the shallow aquifers complex in Azraq depression. - Jordan. Geol. Jb.,C 38 : 17-38p.; Hannover.

Rimawi, O. (1985) : Hydrochemistry an isotope hydrology of groundwater and surface water in the north-east of Mafraq, Dhuleil Halabat, Azraq basin, - Ph.D. Thesis, 240 p.; TU-München.

Rimawi, O., Salameh, E. (1991) : Precipitation water quality in Jordan. - 191p. Water research and study center, University of Jordan (Amman).

Rozanski, K., Araguás-Araguás, L. & Gonfiantini, R. (1993) : Isotopic patterns in modern global precipitation. - Continental isotope indicators of climate, Geophysical Union Monograph.

Salameh, E. (1991) : The special features of the groundwater flow system in central Jordan. - Geol. of Jordan, p. 51 - 53, 2 fig., Amman, Jordan (Goethe-Institut).

Salameh, E. (1991) : Water quality degradation in Jordan (impacts on enviroment, economy and future generations recources base). - 179 p.; Amman, Jordan (Friedrich Ebert Stiftung).

Salameh, E., Udluft, P. (1985) : The hydrodynamic pattern of the central part of Jordan. - Geol. Jb., Reihe C; 38, : 39-55p.; Hannover.

US salinity laboratory staff (1954) : Diagnosis and improvement of saline and alkali soils. - USDA, Agricultural Handbook, Vol. 60; Washington.

Water Authority Jordan (WAJ) (1967-1995) : Rainfall in Jordan, borehole logging, water level records and water abstraction; Technical papers and reports, Water Authority of Jordan, Hashemite Kingdom of Jordan.

Wolf, K. (1998) : Die tektonische Struktur des Jordan Grabens. - Auslandspraktikum Israel / Jordanien 1998., 52-56.; TU Bergakademie Freiberg.

Zuhair, H. el-Isa (1991) : Seismicity and seismic risk in Jordan. - Geol. of Jordan, p. 21 – 27, 5fig.; Amman, Jordan (Goethe-Institut).

9 Appendix

Please note: with regard to their respective size, some of the appendices had to be left out in printing and have been saved onto a CD-ROM (to be found at the end of this book).

- App. 1 Tectonic measurements of the Ramla sandstone formation above the weir No2. in the Zerqa river (N3664453, E36753799).

cleavage	
dip	strike
80.1	207.9
81	36
88.2	17.1
76.5	192.6
84.6	57.6
81	55.8
77.4	215.1
81.9	11.7
76.5	210.6
86.4	232.2
77.4	214.2
85.5	221.4
88.2	22.5
81	27
73.8	7.2
81	29.7
85.5	30.6
81	22.5
88.2	38.7
86.4	24.3
88.2	292.5
85.5	117
66.6	116.1
88.2	328.5
68.4	321.3
81	308.7
75.6	103.5
73.8	118.8
82.8	118.8
88.2	121.5
89.1	121.5
82.8	150.3
88.2	265.5
90	324.9
90	315
89.1	116.1
89.1	126
81.9	125.1
84.6	116.1
85.5	107.1

bedding	
dip	strike
0.9	279
4.5	258.3
14.4	298.8
0.9	331.2
9.9	274.5
8.1	275.4
9	293.4
7.2	285.3
18	335.7
3.6	310.5
15.3	311.4
9	333.9
9.9	337.5
6.3	335.7
8.1	322.2
6.3	351
4.5	329.4
0	328.5
4.5	306
10.8	351.9

- App. 2 Tectonic measurements of the Hamam formation (N3564993, E36750852).

cleavage	
dip	strike
88.2	88.2
79.2	261.9
88.2	92.7
74.7	273.6
72	265.5
58.5	265.5
86.4	262.8
81	264.6
85.5	93.6
74.7	102.6
84.6	265.5
81	101.7
76.5	92.7
85.5	74.7
81	93.6
81	82.8
82.8	258.3
84.6	80.1
84.6	79.2
85.5	263.7
85.5	331.2
84.6	324
86.4	358.2
85.5	196.2
81	178.2
87.3	342
81	169.2
82.8	178.2
82.8	169.2
81	336.6
85.5	346.5
88.2	9.9
90	350.1
81	344.7
76.5	15.3
86.4	338.4
84.6	324
80.1	183.6
81	171
90	338.4

bedding	
dip	strike
0.9	8.1
4.5	2.7
8.1	36.9
22.5	20.7
15.3	358.2
27	358.2
23.4	4.5
21.6	8.1
10.8	357.3
9	27.9
9.9	47.7
9	50.4
9	13.5
9	50.4
13.5	9

- App. 3 Tectonic measurements of the Dhahab Limestone formation (N3564453, E36753193).

cleavage	
dip	strike
85.5	165.6
82.8	179.1
79.2	132.3
88.2	296.1
90	114.3
85.5	312.3
85.5	312.3
85.5	306
76.5	117.9
85.5	268.2
66.6	306.9
86.4	305.1
73.8	126
88.2	309.6
76.5	132.3
86.4	306.9
85.5	304.2
86.4	137.7
87.3	124.2
89.1	309.6
54	178.2
77.4	179.1
88.2	169.2
86.4	165.6
85.5	251.1
81	248.4
86.4	241.2
76.5	234.9
83.7	81
85.5	252.9
86.4	270
88.2	55.8
85.5	193.5
87.3	53.1
86.4	49.5
85.5	44.1
88.2	67.5
84.6	237.6
85.5	224.1
81.9	228.6
85.5	236.7
80.1	229.5
90	234.9
81	61.2

bedding	
dip	strike
4.5	17.1
0.9	340.2
10.8	337.5
4.5	355.5
0	342

- App. 4 Tectonic measurements of the Abu Ruweis gypsum formation, southern outcrop (N35643260, E36756190).

cleavage	
dip	strike
82.8	301.5
62.1	306.9
80.1	312.3
85.5	135.9
77.4	333.9
76.5	331.2
90	40.5
81.9	213.3
58.5	197.1
85.5	279.9
76.5	3.6
81.9	88.2
67.5	0
72.9	141.3
89.1	54.9
80.1	135
75.6	232.2
89.1	245.7
49.5	147.6
89.1	14.4
89.1	15.3
81	316.8
89.1	173.7
77.4	222.3
86.4	278.1
85.5	274.5
63	229.5
80.1	312.3
81	283.5
90	283.5
76.5	147.6
72	202.5
66.6	193.5
71.1	208.8
85.5	137.7
81	279

bedding	
dip	strike
8.1	324.9
17.1	354.6

- App. 5 Tectonic measurements of the Kurnub sandstone group (N3565209, E36757076).

cleavage	
dip	strike
85.5	63.9
83.7	1.8
90	58.5
90	154.8
81	346.5
74.7	144.9
81.9	49.5
85.5	224.1
81	133.2
90	40.5
68.4	131.4
85.5	9
78.3	22.5
72	326.7
88.2	238.5
85.5	220.5
89.1	238.5
90	108
67.5	170.1
86.4	45
81	178.2

• App. 6 Determination methods for the different elements.

element	method	measuring device	remarks	detection limit
location	GPS	Magellan 300	The position was measured about 20min. From the collected data the average was taken	
pH		WTW MulitLine P4 with SenTIX 97/T pH electrode	Measuring time: 20min	0.01 ± 1 digit
temp.		WTW MultiLine P4 with SenTIX 97/T pH electrode		0.1K ± 1 digit
conductivity		WTW MulitLine P4 with TetraCon 325 conductivity cell		±1% of measured value ± 1 digit
Eh	Ag/AgCl	WTW MulitLine P4	values had to be readjusted for hydrogen electrode, measuring time: 20min	1mV ± 1 digit
O_2		WTW MulitLine P4 with CellOx 325		± 0.5% of measured value ± 1 digit
Cl^-, NO_3^-, SO_4^{2-}, Li^+ Na^+, Ca^{2+}, Mg^{2+}	IC	Combination Merck / Hitachi, D 6000 A	Done at the TU-Freiberg	s. App. 7
HCO_3, CO_2	titrimetric	digital titrator Hach	Done at the TU-Freiberg	s. App. 7
F^-	selective electrode	Ionselective electrode and gauge from WTW (pMX 3000)	Done at the TU-Freiberg	s. App. 7
NO_2^-, PO_4^{3-}, SiO_2, NH_4^+	spetrophotometric	Hach DR 2000	Done at the TU-Freiberg	s. App. 7
Fe	spetrophotometric	Hach DR 2000	Done at the TU-Freiberg, see chapter 5.2.2.	s. App. 7
heavy metals and trace elements	ICP-MS		Tharandt	s. App. 7

• App. 7 Summarised results of all chemical determinations for the selected wells and springs.

ID		**000228S2**	**000305S1**	**000305W1**	**000305W2**	**000305S2**
name		spring Abu Sair	Ain Addasseih	well Rawda	irigation well Kafrain Dam	Ain Sara
date		28.02.00	05.03.00	05.03.00	05.03.00	05.03.00
northing	UTM	3551921	3528462	3525832	3526499	3498734
easting	UTM	36770370	36761167	36753336	36753181	36743617
aquifer		Kurnub	A1/2	Zerqua (2)	recent	Kurnub
EC	µs/cm	874.00	167.00	4930.00	1050.00	1625.00
T	°C	18.40	20.40	30.00	23.00	52.70
pH		6.17	7.80	6.30	7.17	6.03
O2	%	315.00	103.20	0.00	78.50	67.30
O2	mg/L	23.70	9.44	0.00	6.55	3.95
Eh	mV	220.00	433.00	-183.00	31.00	48.00
Ehcorret.	mV	431.28	647.80	24.65	243.86	238.76
c CO2	mmol/L		0.19	8.13	0.34	1.65
c HCO3 -	mmol/L		4.50	15.45	4.53	2.96
F-	mg/L		0.40	0.80	0.60	0.40
Cl-	mg/L		47.00	1080.00	135.00	360.00
NO3-	mg/L		21.20	6.70	19.60	< 0.5
SO42-	mg/L		23.00	340.00	111.00	132.00
NO2-	mg/L		0.02	0.04	0.04	0.03
PO43-	mg/L		0.04	0.07	0.02	0.04
SiO2	mg/L		22.00	18.20	14.20	25.90
Li+	mg/L		< 0.05	< 0.05	< 0.05	0.10
Na+	mg/L		23.40	690.00	69.00	194.00
K+	mg/L		4.50	160.00	13.70	47.00
Ca2+	mg/L		75.00	130.00	95.00	120.00
Mg2+	mg/L		28.00	90.00	43.00	22.00
NH4+	mg/L		0.13	1.58	0.05	0.52
Anion	mmol/L		7.40	53.75	11.47	16.75
Cation	mmol/L		7.19	48.08	11.63	17.48
DOC	mg/L		0.11	< 0.1	0.27	< 0.1
Fe ges.	mg/L		<0.03	2.67	0.04	0.12
Al 27	µg/L		6.13	47.58	16.19	10.06
V 51	µg/L		3.75	32.73	6.74	15.67
Cr 52	µg/L		2.57	5.95	4.62	3.32
Mn 55	µg/L		< 7.8	130.97	< 7.8	754.93
Co 59	µg/L		0.39	1.54	0.55	0.54
Ni 60	µg/L		< 7.25	9.95	< 7.25	< 7.25
Cu 65	µg/L		2.83	11.53	5.31	6.05
Zn 66	µg/L		14.30	24.17	13.47	14.67
As 75	µg/L		2.56	50.76	6.16	15.36
Cd 111	µg/L		< 0.18	< 0.18	< 0.18	< 0.18
Hg 200	µg/L		< 0.27	< 0.27	< 0.27	< 0.27
Tl 205	µg/L		0.07	0.05	0.05	0.09
Pb 208	µg/L		< 2.57	< 2.57	< 2.57	< 2.57
Th 232	µg/L		< 0.03	< 0.03	< 0.03	< 0.03
U 238	µg/L		1.18	1.19	1.73	< 0.06
Tritium	(T/T.E.)		2.70	0.00	2.70	0.00
±	(T/T.E.)		0.50	0.30	0.50	0.30

ID		**000306W1**	**000306W2**	**000306S1**	**000307W1**
name		well Rami Shami	well Alftah Wrikat	spring at the bridge to Jerash	well upst. Kafrain Dam
date		06.03.00	06.03.00	06.03.00	07.03.00
northing	UTM	3549486	3553098	3567971	3528619
easting	UTM	36768686	36769924	36772757	36753833
aquifer		Kurnub	Kurnub	Kurnub	Kurnub
EC	µs/cm	615.00	1836.00	3160.00	958.00
T	°C	11.50	20.70	28.60	36.70
pH		7.31	7.57	6.31	6.71
O2	%	53.20	106.00	22.00	9.80
O2	mg/L	5.32	8.67	1.88	0.69
Eh	mV	68.00	310.00	-173.00	-104.00
Ehcorrect.	mV	289.42	524.57	35.69	98.66
c CO2	mmol/L	0.39	0.20	4.75	1.54
c HCO3 -	mmol/L	4.45	4.04	7.82	4.22
F-	mg/L	0.40	1.00	1.30	0.50
Cl-	mg/L	44.00	330.00	488.00	106.00
NO3-	mg/L	6.70	150.00	5.60	< 0.5
SO42-	mg/L	35.00	122.00	680.00	120.00
NO2-	mg/L	0.04	0.05	0.62	0.10
PO43-	mg/L	0.05	0.02	0.03	0.04
SiO2	mg/L	16.20	14.40	13.40	16.60
Li+	mg/L	< 0.05	< 0.05	0.08	<0.05
Na+	mg/L	32.00	240.00	300.00	70.00
K+	mg/L	7.50	27.00	75.00	14.00
Ca2+	mg/L	88.00	92.00	290.00	107.00
Mg2+	mg/L	24.00	53.00	80.00	35.00
NH4+	mg/L	0.05	0.22	0.22	0.18
Anion	mmol/L	7.09	18.84	36.36	10.29
Cation	mmol/L	7.95	20.09	36.04	11.63
DOC	mg/L	< 0.1	0.39	< 0.1	0.12
Fe ges.	mg/L	<0.03	<0.03	0.11	0.76
Al 27	µg/L	5.42	5.42	6.96	10.34
V 51	µg/L	3.47	13.74	16.93	5.12
Cr 52	µg/L	2.44	10.15	4.09	2.34
Mn 55	µg/L	< 7.8	< 7.8	111.02	68.25
Co 59	µg/L	0.42	0.62	1.63	0.37
Ni 60	µg/L	< 7.25	< 7.25	12.35	< 7.25
Cu 65	µg/L	10.49	7.23	16.58	4.90
Zn 66	µg/L	794.92	19.08	19.18	14.92
As 75	µg/L	2.73	12.51	19.46	5.28
Cd 111	µg/L	< 0.18	< 0.18	< 0.18	< 0.18
Hg 200	µg/L	< 0.27	< 0.27	< 0.27	< 0.27
Tl 205	µg/L	0.15	0.08	0.06	0.06
Pb 208	µg/L	< 2.57	< 2.57	< 2.57	< 2.57
Th 232	µg/L	< 0.03	< 0.03	< 0.03	< 0.03
U 238	µg/L	0.93	2.74	< 0.06	< 0.06
Tritium	(T/T.E.)	0.00	1.10	0.00	-0.30
±	(T/T.E.)	0.30	0.50	0.30	0.30

ID		**000308S1**	**000308S2**	**000308S3**	**000309S1**	**000309S2**
name		spring near Baqua/Jerash	Ain Mubis	spring SE-Baqua	spring 1 Wadi Zerqa	spring Men
date		08.03.00	08.03.00	08.03.00	09.03.00	09.03.00
northing	UTM	3548867	3554456	3554009	3564692	3564586
easting	UTM	36767986	36772347	36772466	36749313	36749512
aquifer		Kurnub	Kurnub	A1/2	Zerqua (2)	Zerqua (2)
EC	µs/cm	753.00	917.00	880.00	12160.00	11220.00
T	°C	18.00	18.60	17.10	34.30	34.90
pH		7.86	7.97	6.38	5.90	5.96
O2	%	115.00	77.60	117.00	6.70	0.00
O2	mg/L	11.03	6.07	10.50	0.55	0.00
Eh	mV	112.00	104.00	141.00	79.00	86.00
Ehcorrect.	mV	328.58	320.14	358.25	283.45	290.00
c CO2	mmol/L	7.65		7.75	6.29	6.39
c HCO3 -	mmol/L	4.40	4.48	4.54	18.60	20.60
F-	mg/L	0.50	0.50	0.60	1.40	1.00
Cl-	mg/L	73.00	113.00	118.00	3170.00	2770.00
NO3-	mg/L	36.00	44.00	24.30	60.00	38.00
SO42-	mg/L	38.00	41.00	78.00	1850.00	1660.00
NO2-	mg/L	0.04	0.04	0.06	0.12	0.21
PO43-	mg/L	0.07	0.07	0.02	0.09	0.11
SiO2	mg/L	27.70	19.40	18.40	19.30	18.70
Li+	mg/L	< 0.05	< 0.05	< 0.05	0.16	0.13
Na+	mg/L	32.00	62.00	68.00	2050.00	1790.00
K+	mg/L	5.20	9.40	12.40	360.00	320.00
Ca2+	mg/L	87.00	88.00	84.00	800.00	670.00
Mg2+	mg/L	44.00	43.00	45.00	160.00	160.00
NH4+	mg/L	0.06	0.05	0.04	2.82	2.32
Anion	mmol/L	8.78	9.91	10.53	148.22	134.59
Cation	mmol/L	9.49	10.87	11.17	151.64	132.79
DOC	mg/L	0.36	0.43	0.36	< 0.1	< 0.1
Fe ges.	mg/L	<0.03	<0.03	<0.03	<0.03	0.49
Al 27	µg/L	3.07	10.50	8.25	8.31	9.66
V 51	µg/L	4.54	6.07	5.88	82.21	67.25
Cr 52	µg/L	3.55	3.72	5.97	27.65	16.74
Mn 55	µg/L	< 7.8	< 7.8	< 7.8	< 7.8	80.79
Co 59	µg/L	0.36	0.45	0.32	3.37	4.60
Ni 60	µg/L	< 7.25	< 7.25	< 7.25	22.06	29.72
Cu 65	µg/L	2.44	3.58	3.22	27.58	29.70
Zn 66	µg/L	13.75	18.01	20.27	20.45	28.02
As 75	µg/L	3.66	4.83	4.96	151.59	130.81
Cd 111	µg/L	< 0.18	< 0.18	< 0.18	< 0.18	< 0.18
Hg 200	µg/L	< 0.27	< 0.27	< 0.27	1.02	< 0.27
Tl 205	µg/L	0.05	0.05	0.06	0.06	0.06
Pb 208	µg/L	< 2.57	< 2.57	< 2.57	< 2.57	< 2.57
Th 232	µg/L	< 0.03	< 0.03	< 0.03	< 0.03	< 0.03
U 238	µg/L	1.60	1.63	1.86	0.68	0.73
Tritium	(T/T.E.)	3.40	3.10	1.00	0.20	
±	(T/T.E.)	0.40	0.40	0.20	0.30	

ID		**000312S1**	**000313S1**	**000313S2**	**000313S3**	**000314S1**	**000314S2**	**000314S3**
name		spring Women	Ain Rimon	Ain Ajlun	Ain Asabatha	Ain Wadi Sir	Ain Tarabil	Ain Mahis
date		12.03.00	13.03.00	13.03.00	13.03.00	14.03.00	14.03.00	14.03.00
northing	UTM	3564837	3575322	3579614	3576518	3538854	3535324	3542476
easting	UTM	36749875	36765746	36758113	36768376	36766231	36761801	36761498
aquifer		Zerqua (2)	A1/2	A7	A4/A7	A7	A4	A1/2
EC	µs/cm	5390.00	503.00	655.00	471.00	768.00	817.00	609.00
T	°C	34.80	16.90	17.30	19.30	18.40	18.90	18.60
pH		6.10	7.28	7.66		7.21	7.31	7.34
O2	%	1.00	107.10	75.10	106.90	107.70	82.10	101.80
O2	mg/L	0.07	9.28	6.14	8.92	9.24	7.32	7.67
Eh	mV	28.00	96.00	246.00	175.00	141.00	148.00	646.00
Ehcorrect.	mV	232.08	313.40	463.10	390.62	357.28	363.91	862.14
c CO2	mmol/L	6.74	7.71	7.45	7.71		7.58	7.67
c HCO3 -	mmol/L	15.95	4.36	5.10	3.97		4.70	4.80
F-	mg/L	1.60	0.10	0.10	0.20		0.30	0.20
Cl-	mg/L	920.00	17.00	27.80	19.00		76.00	35.00
NO3-	mg/L	< 5	12.60	35.00	19.30		48.00	29.40
SO42-	mg/L	1030.00	18.70	27.00	14.50		39.00	15.50
NO2-	mg/L	0.11	0.03	0.05	0.02		0.02	0.04
PO43-	mg/L	0.06	0.01	0.16	0.03		0.02	0.10
SiO2	mg/L	15.30	9.20	29.50	13.80		17.60	13.80
Li+	mg/L	< 0.05	< 0.05	< 0.05	< 0.05		< 0.05	< 0.05
Na+	mg/L	640.00	10.60	17.60	12.40		36.00	17.50
K+	mg/L	150.00	1.90	6.70	1.90		6.40	2.90
Ca2+	mg/L	470.00	110.00	130.00	91.00		120.00	110.00
Mg2+	mg/L	100.00	17.00	19.00	16.00		31.00	27.00
NH4+	mg/L	1.08	0.05	0.04	0.01		0.04	0.01
Anion	mmol/L	63.94	5.74	8.00	5.59		9.03	7.06
Cation	mmol/L	63.41	7.40	8.99	6.45		10.27	8.55
DOC	mg/L	< 0.1	0.30	0.38	0.14		0.41	0.19
Fe ges.	mg/L	0.18	<0.03	<0.03	<0.03	<0.03	<0.03	<0.03
Al 27	µg/L	76.43	14.94	11.67	3.00	4.55	2.37	24.95
V 51	µg/L	27.38	3.24	2.69	2.55	4.79	5.41	2.87
Cr 52	µg/L	6.57	1.88	1.79	3.61	4.93	5.65	2.41
Mn 55	µg/L	70.32	< 7.8	< 7.8	< 7.8	< 7.8	< 7.8	< 7.8
Co 59	µg/L	3.31	0.40	0.55	0.47	0.60	0.55	0.47
Ni 60	µg/L	21.67	< 7.25	41.94	< 7.25	< 7.25	< 7.25	< 7.25
Cu 65	µg/L	23.95	7.04	15.69	3.44	3.84	2.82	3.64
Zn 66	µg/L	23.69	17.91	20.65	12.34	14.09	12.36	219.90
As 75	µg/L	39.76	3.04	2.35	1.93	3.56	3.87	2.44
Cd 111	µg/L	< 0.18	< 0.18	< 0.18	< 0.18	< 0.18	< 0.18	< 0.18
Hg 200	µg/L	< 0.27	< 0.27	< 0.27	< 0.27	< 0.27	< 0.27	< 0.27
Tl 205	µg/L	0.05	0.06	0.04	0.05	0.08	0.05	0.04
Pb 208	µg/L	< 2.57	< 2.57	< 2.57	< 2.57	< 2.57	< 2.57	83.05
Th 232	µg/L	< 0.03	< 0.03	< 0.03	0.55	0.15	0.10	0.05
U 238	µg/L	0.26	0.78	0.67	0.86	0.99	1.33	0.87
Tritium	(T/T.E.)	0.40	5.80	5.80	6.60		4.60	
±	(T/T.E.)	0.30	0.60	0.60	0.70		0.50	

ID		**000320S1**	**000320S2**
name		Ain Rumainin	Ain Um Dananir
date		20.03.00	20.03.00
northing	UTM	3556364	3553515
easting	UTM	36764616	36765965
aquifer		A7	A7
EC	µs/cm	1077.00	440.00
T	°C	19.70	20.20
pH		7.29	7.52
O2	%	94.00	91.40
O2	mg/L	8.18	7.72
Eh	mV	56.00	78.00
Ehcorrect.	mV	271.32	292.95
c CO2	mmol/L	7.49	
c HCO3 -	mmol/L	6.18	3.33
F-	mg/L	0.40	0.40
Cl-	mg/L	117.00	24.30
NO3-	mg/L	38.00	21.50
SO42-	mg/L	57.00	10.00
NO2-	mg/L	0.04	0.02
PO43-	mg/L	0.06	0.05
SiO2	mg/L	24.90	14.30
Li+	mg/L	< 0.05	< 0.05
Na+	mg/L	56.00	14.00
K+	mg/L	8.70	3.10
Ca2+	mg/L	130.00	70.00
Mg2+	mg/L	47.00	17.80
NH4+	mg/L	0.04	0.04
Anion	mmol/L	12.13	5.07
Cation	mmol/L	13.01	5.65
DOC	mg/L	< 0.1	0.15
Fe ges.	mg/L		
Al 27	µg/L	25.13	32.61
V 51	µg/L	6.14	5.09
Cr 52	µg/L	3.58	3.82
Mn 55	µg/L	< 7.8	< 7.8
Co 59	µg/L	0.58	0.23
Ni 60	µg/L	< 7.25	< 7.25
Cu 65	µg/L	4.74	2.51
Zn 66	µg/L	14.06	11.70
As 75	µg/L	6.15	2.60
Cd 111	µg/L	< 0.18	< 0.18
Hg 200	µg/L	< 0.27	< 0.27
Tl 205	µg/L	0.05	0.05
Pb 208	µg/L	< 2.57	< 2.57
Th 232	µg/L	0.05	0.05
U 238	µg/L	1.69	1.80
Tritium	(T/T.E.)		2.87
±	(T/T.E.)		0.50

• App. 8 Limitations for the analyzed elements.

element	limitations	Jordanien standards	WHO Guidelines (1993)	remarks
cond.	2,000 µS/cm (TrinkwV 1990)		1,400µS/cm	
temp.	25°C (TrinkwV 1990)	8-25°C	12-25°C	
pH	6.5-9.5 (TrinkwV 1990)	6.5-9	6.5-8.5	
oxygen	5mg/L O2 (TrinkwV 1990)			
HCO_3		100-500mg/L	125-350mg/L	
F	1.5mg/L (TrinkwV 1990)			
Cl	250mg/L (TrinkwV 1990)		250mg/L	
NO_3		45-70mg/L	50mg/L	
SO_4	240mg/L (TrinkwV 1990)	200-500mg/L	acceptable: 200mg/L maximum: 400mg/L	
NO_2	0.1mg/L (TrinkwV 1990)			
PO_4	6.7mg/L PO_4^{3-} (TrinkwV 1990)			
Li				no limitations in Germany and USA
Na	150mg/L (TrinkwV 1990)	200-400mg/L	acceptable: 75mg/L maximum: 200mg/L	
K	12mg/L (TrinkwV 1990)	12mg/L	12mg/L	
Ca	400mg/L (TrinkwV 1990)	75-200mg/L	acceptable: 75mg/L maximum: 200mg/L	
Mg	50mg/L (TrinkwV 1990)	50-150mg/L	<125mg/L	
Fe	0.2mg/L (TrinkwV 1990)		acceptable: 0.3mg/L maximum: 1mg/L	
Al	0.2mg/L (TrinkwV 1990)			
Cr	0.05mg/L (TrinkwV 1990) 0.1mg/L (USA)			
Mn	0.05mg/L (TrinkwV 1990)		acceptable: 0.1mg/L maximum: 0.5mg/L	
Co				no limitations from WHO
Ni	0.02mg/L (European Community) 0.05mg/L (TrinkwV 1990)			
Cu	3mg/L (TrinkwV 1990)		acceptable: 1mg/L maximum: 2mg/L	
Zn	5mg/L (TrinkwV 1990)		3mg/L	
As	0.01mg/L (TrinkwV 1990)			
Cd	0.05mg/L (TrinkwV 1990)			
Ti				no limitations in Germany
Pb	0.04mg/L (TrinkwV 1990)		0.01mg/L	
Th				no limitations
U	20µg/L (USA)		α-activity: 0.1 Bq/L β-activity: 1.0 Bq/l	

• App. 9 Saturation indices calculated with PhreeqC2 all elements considered as far as they were determined.

soln	000305S1	000305W1	000305W2	000305S2	000306W1	000306W2	000306S1	000307W1	000308S1
si Magnesi	-1,93	-2,21	-2,01	-3,31	-2,30	-1,84	-2,58	-2,45	-1,84
si Dolomit	-3,17	-4,00	-3,41	-5,61	-3,77	-3,17	-4,33	-4,99	-3,12
si Calcite	-1,27	-1,82	-1,43	-2,34	-1,50	-1,36	-1,78	-2,57	-1,31
si Anhydri	-2,43	-1,42	-1,76	-1,63	-2,19	-1,83	-0,80	-2,16	-2,22
si Gypsum	-2,21	-1,21	-1,54	-1,41	-1,97	-1,61	-0,58	-1,94	-2,00
si Brucite	-4,55	-6,44	-4,82	-6,74	-5,22	-4,38	-6,52	-5,95	-4,48
si Chrysot	-2,20	-8,04	-3,40	-8,64	-4,48	-2,07	-8,55	-6,64	-1,79
si Aragoni	-1,42	-1,96	-1,58	-2,48	-1,64	-1,51	-1,92	-2,72	-1,45
si Forster	-7,16	-11,03	-7,90	-11,47	-8,63	-7,01	-11,32	-10,08	-6,92
si Diopsid	-1,97	-6,19	-2,98	-5,91	-3,44	-2,20	-6,21	-5,80	-1,76
si Clinoen	-2,49	-4,46	-2,95	-4,61	-3,29	-2,50	-4,67	-4,01	-2,32
si Tremoli	2,39	-12,04	-1,20	-11,76	-3,09	1,72	-12,83	-9,94	3,43
si Sepioli	-1,49	-5,51	-2,60	-5,66	-3,23	-1,70	-6,07	-4,65	-1,05
si Talc	1,73	-4,27	0,15	-4,56	-0,81	1,50	-5,04	-2,95	2,34
si Hydroma	-18,79	-21,79	-19,38	-26,49	-20,93	-18,24	-23,36	-22,26	-18,34
si Adulari	-0,41	1,31	-0,10	0,87	-0,65	-0,29	-0,55	-0,16	-0,36
si Albite	-2,04	-0,39	-1,73	-0,85	-2,36	-1,67	-2,29	-1,80	-1,91
si Anorthi	-3,44	-2,65	-2,95	-3,05	-3,76	-3,98	-4,88	-3,81	-3,81
si Analcim	-3,90	-2,18	-3,41	-2,79	-4,09	-3,36	-3,94	-3,55	-3,88
si Kmica	5,53	10,36	7,06	8,93	5,77	5,50	6,20	7,82	5,06
si Phlogop	-4,74	-8,71	-5,25	-10,04	-6,99	-4,12	-10,81	-8,70	-4,48
si Illite	0,44	3,51	1,28	2,59	0,32	0,12	0,20	1,78	0,22
si Kaolini	2,24	5,19	3,08	4,51	2,46	1,72	2,64	4,05	1,93
si Halloys	-2,82	0,13	-1,98	-0,55	-2,61	-3,34	-2,42	-1,01	-3,14
si Beidell	0,72	4,04	1,49	3,34	0,74	0,07	0,81	2,50	0,51
si Chlorit	-0,68	-7,28	-1,40	-9,31	-3,95	-0,55	-10,37	-6,00	-0,54
si Alunite	-8,65	2,76	-4,49	-0,08	-6,45	-6,88	-0,41	-1,07	-8,86
si Gibbsit	0,17	1,72	0,77	1,23	0,41	0,09	0,57	1,19	-0,09
si Boehmit	-0,31	1,25	0,30	0,75	-0,07	-0,39	0,10	0,72	-0,57
si Pyrophy	5,78	8,58	6,25	8,20	5,74	4,90	5,77	7,35	5,67
si Phillip	-0,64	1,04	-0,33	0,60	-0,91	-0,39	-0,83	-0,40	-0,55
si Nahcoli	-6,71	-4,77	-6,26	-5,99	-6,57	-5,80	-5,42	-6,26	-6,61
si Trona	-19,39	-15,18	-18,22	-18,04	-19,27	-16,57	-16,83	-18,92	-19,10
si Natron	-11,61	-9,35	-10,90	-10,99	-11,63	-9,71	-10,35	-11,59	-11,43
si Thermon	-13,05	-10,78	-12,33	-12,43	-13,07	-11,15	-11,78	-13,03	-12,86
si Fluorit	-1,79	-1,32	-1,43	-1,70	-1,72	-1,09	-0,52	-2,05	-1,59
si Montmor	0,94	3,92	1,61	3,38	0,93	0,09	0,83	2,53	0,70
si Halite	-7,53	-4,80	-6,63	-5,77	-7,43	-5,73	-5,49	-6,72	-7,22
si Thenard	-9,79	-5,96	-8,24	-7,29	-9,34	-7,19	-6,38	-8,19	-9,35
si Mirabil	-8,85	-5,03	-7,30	-6,36	-8,40	-6,26	-5,45	-7,26	-8,42
si Siderit		-1,27	-3,41	-3,10			-2,95	-2,01	
si Hydroxy	0,52	-4,38	-1,21	-3,88	-0,19	-0,79	-3,91	-5,89	1,05
si Fluorap	2,25	-1,33	0,88	-1,16	1,85	1,31	-0,62	-3,20	2,92
si Chalced	0,11	0,03	-0,08	0,19	-0,02	-0,07	-0,10	-0,01	0,21
si Magadii	-5,11	-5,33	-6,16	-4,68	-6,19	-5,39	-6,59	-6,37	-4,32
si Cristob	0,15	0,07	-0,04	0,22	0,02	-0,03	-0,06	0,03	0,25
si Silicag	-0,42	-0,50	-0,61	-0,35	-0,55	-0,60	-0,63	-0,54	-0,32

soln	000305S1	000305W1	000305W2	000305S2	000306W1	000306W2	000306S1	000307W1	000308S1
si Quartz	0,54	0,46	0,35	0,62	0,41	0,36	0,33	0,42	0,64
si Viviani		-2,93	-9,01	-6,63			-7,88	-3,90	
si Magneti		16,85	16,49	13,95			12,67	17,22	
si Hematit		16,12	16,48	14,25			13,33	16,50	
si Maghemi		5,73	6,08	3,86			2,94	6,10	
si Goethit		7,06	7,24	6,12			5,66	7,25	
si Greenal		-2,42	-4,80	-5,21			-6,86	-2,53	
si Fe(OH)3		1,16	1,34	0,23			-0,23	1,35	
si Annite		7,81	4,24	4,27			1,77	6,31	
si Montmor		6,23	4,81	5,67			3,50	5,28	
si Montmor		5,34	4,29	4,64			2,57	4,47	
si Huntite	-9,67	-11,04	-10,07	-14,86	-11,00	-9,48	-12,12	-12,52	-9,42
si Chlorit	-4,05	-10,65	-4,77	-12,68	-7,32	-3,92	-13,75	-9,37	-3,91
si Laumont	0,93	1,56	1,04	1,47	0,35	0,02	-0,92	0,32	0,76
si Jarosit		-2,76	-6,60	-6,84			-6,61	-4,27	
si Mn2(SO4		-58,15		-57,19			-57,40	-59,29	
si Al(OH)3	-2,52	-0,97	-1,92	-1,46	-2,28	-2,60	-2,12	-1,50	-2,78
si Prehnit	-2,39	-3,85	-2,45	-3,82	-3,38	-3,14	-5,88	-5,07	-2,73
si Strengi		0,28	-1,50	-0,95			-1,50	0,00	
si Leonhar	9,70	10,96	9,91	10,77	8,54	7,88	5,99	8,47	9,35
si Nesqueh	-4,34	-4,62	-4,42	-5,72	-4,71	-4,25	-4,99	-4,86	-4,25
si Artinit	-7,27	-9,44	-7,62	-10,84	-8,31	-7,01	-9,89	-9,19	-7,10
si Sepioli	-4,39	-8,41	-5,50	-8,56	-6,13	-4,60	-8,97	-7,55	-3,95
si Diaspor	1,40	2,95	2,01	2,46	1,64	1,32	1,80	2,42	1,14
si Wairaki	-3,32	-2,69	-3,21	-2,79	-3,90	-4,23	-5,18	-3,94	-3,50
si Fe(OH)2		6,63	6,28	5,54			5,14	6,47	
si MnSO4		-11,62		-11,01			-11,40	-12,04	
si Pyrolus		-13,01		-11,72			-13,08	-12,32	
si Birness		-15,23		-13,94			-15,30	-14,54	
si Nsutite		-14,19		-12,90			-14,27	-13,50	
si Bixbyit		-14,87		-12,48			-15,02	-13,88	
si Hausman		-18,32		-14,84			-18,54	-17,04	
si Pyrochr		-8,03		-6,94			-8,10	-7,74	
si Mangani		-7,57		-6,38			-7,64	-7,08	
si Rhodoch		-3,08		-2,78			-3,44	-3,52	
si MnCl2:4		-11,95		-11,95			-12,70	-14,00	
si Mn3(PO4		-19,02		-16,33			-20,01	-19,08	
si MnHPO4		0,29		1,08			-0,17	0,11	
si Jarosit		-3,81	-7,62	-8,00			-7,76	-5,42	
si Jarosit		-0,76	-4,62	-4,91			-4,67	-2,42	
si CuMetal	-5,61	-4,48	-4,97	-4,15	-4,49	-5,22	-3,87	-4,10	-5,58
si Nantoki	-6,53	-4,09	-5,44	-4,21	-5,44	-5,32	-3,81	-4,67	-6,32
si CuF	-22,20	-20,85	-21,40	-20,75	-21,07	-21,44	-20,00	-20,62	-22,09
si Cuprite	-3,80	-3,73	-2,91	-2,88	-2,15	-3,00	-2,51	-2,57	-3,84
si Cu2SO4	-22,70	-19,46	-20,78	-19,08	-20,27	-21,28	-17,94	-19,00	-22,46
si Cuprous		12,33	12,92	11,83			11,55	13,11	
si Melanot	-18,66	-14,90	-17,13	-15,47	-17,60	-16,63	-14,97	-16,46	-18,26
si CuCO3	-6,32	-5,77	-5,88	-6,04	-5,49	-5,99	-5,44	-5,72	-6,36
si CuF2	-17,96	-16,40	-17,00	-16,53	-16,84	-16,84	-15,32	-16,33	-17,77
si CuF2:2H	-14,03	-12,47	-13,07	-12,60	-12,91	-12,91	-11,39	-12,40	-13,84

soln	000305S1	000305W1	000305W2	000305S2	000306W1	000306W2	000306S1	000307W1	000308S1
si Cu(OH)2	-2,33	-3,40	-2,09	-2,88	-1,81	-1,94	-2,79	-2,62	-2,40
si Malachi	-4,46	-4,98	-3,78	-4,72	-3,11	-3,74	-4,05	-4,15	-4,58
si Azurite	-8,69	-8,65	-7,57	-8,66	-6,50	-7,63	-7,39	-7,77	-8,84
si Atacami	-5,35	-5,07	-4,22	-4,56	-4,03	-3,73	-4,19	-4,67	-5,25
si Cu2(OH)	-7,19	-8,77	-6,55		-6,34	-5,57	-7,62		-7,05
si Antleri	-8,67	-8,70	-6,91	-7,60	-6,32	-6,85	-6,57	-7,06	-8,60
si Brochan	-9,41	-10,52	-7,41	-8,88	-6,54	-7,20	-7,77	-8,09	-9,42
si Langite	-10,86	-11,97	-8,86	-10,33	-7,99	-8,65	-9,22	-9,54	-10,87
si Tenorit	-1,31	-2,38	-1,07	-1,85	-0,79	-0,92	-1,77	-1,60	-1,38
si CuOCuSO	-18,22	-17,18	-16,70	-16,60	-16,39	-16,80	-15,66	-16,32	-18,08
si Cu3(PO4	-12,54	-11,79	-11,78	-10,81	-9,65	-12,14	-10,73	-10,38	-12,19
si Cu3(PO4	-14,27	-13,52	-13,51	-12,54	-11,38	-13,87	-12,46	-12,11	-13,92
si CuSO4	-16,00	-13,90	-14,73	-13,85	-14,70	-14,98	-12,99	-13,82	-15,80
si Chalcan	-10,35	-8,25	-9,08	-8,20	-9,05	-9,33	-7,34	-8,17	-10,15
si CupricF		11,47	13,14	10,13			9,29	12,63	
si ZnMetal	-40,63	-40,60	-40,70	-40,69	-38,87	-40,62	-40,72	-40,64	-40,67
si ZnCl2	-19,74	-17,09	-18,92	-18,07	-18,04	-18,09	-17,88	-19,06	-19,41
si Smithso	-3,73	-4,28	-4,01	-4,96	-2,26	-3,79	-4,69	-4,65	-3,84
si ZnCO3:H	-3,47	-4,02	-3,75	-4,70	-2,00	-3,53	-4,43	-4,39	-3,58
si ZnF2	-14,84	-14,39	-14,60	-14,93	-13,08	-14,11	-14,03	-14,74	-14,72
si Zn(OH)2	-3,92	-6,10	-4,40	-5,98	-2,76	-3,91	-6,22	-5,73	-4,06
si Zn(OH)2	-3,67	-5,85	-4,15	-5,73	-2,51	-3,66	-5,97	-5,48	-3,81
si Zn(OH)2	-3,22	-5,40	-3,70	-5,28	-2,06	-3,21	-5,52	-5,03	-3,36
si Zn(OH)2	-3,18	-5,36	-3,66	-5,24	-2,02	-3,17	-5,48	-4,99	-3,32
si Zn(OH)2	-2,97	-5,15	-3,45	-5,03	-1,81	-2,96	-5,27	-4,78	-3,11
si Zn2(OH)	-8,76	-10,70	-9,06	-11,01	-6,17	-7,93	-11,28	-11,14	-8,81
si Zn5(OH)	-17,10	-23,15	-18,17	-23,66	-10,76	-15,42	-24,42	-23,67	-17,33
si Zn2(OH)	-9,74	-10,92	-9,66	-11,16	-6,65	-9,10	-10,86	-10,90	-9,75
si Zn4(OH)	-13,58	-19,12	-14,45	-19,13	-8,17	-12,93	-19,29	-18,37	-13,87
si Zn(NO3)	-16,03	-17,10	-16,20		-15,28	-14,38	-17,36		-15,63
si ZnO(a)	-2,78	-4,96	-3,26	-4,84	-1,62	-2,77	-5,08	-4,59	-2,92
si Zincite	-2,61	-4,79	-3,09	-4,67	-1,45	-2,60	-4,91	-4,42	-2,75
si Zn3O(SO	-32,03	-32,21	-31,39	-32,82	-27,00	-30,76	-31,97	-32,54	-31,90
si Zn3(PO4	-10,68	-13,26	-12,07	-13,50	-5,89	-11,46	-14,39	-13,10	-10,54
si ZnSiO3	2,16	-0,09	1,50	0,18	3,19	1,98	-0,34	0,23	2,12
si Willemi	-1,71	-6,14	-2,85	-5,75	0,47	-1,88	-6,51	-5,46	-1,89
si Zincosi	-13,78	-12,78	-13,22	-13,14	-11,84	-13,15	-12,60	-13,13	-13,64
si ZnSO4:H	-10,20	-9,20	-9,64	-9,56	-8,26	-9,57	-9,02	-9,55	-10,06
si Bianchi	-9,00	-8,01	-8,45	-8,37	-7,07	-8,37	-7,83	-8,35	-8,87
si Goslari	-8,81	-7,82	-8,25	-8,18	-6,87	-8,18	-7,64	-8,16	-8,68
si Jarosit		-8,70	-12,43	-12,45			-12,28	-9,54	
si AlumK	-21,43	-13,14	-18,49	-14,99	-19,72	-19,51	-14,01	-15,90	-21,13
si Melante		-5,44	-8,30	-6,95			-6,54	-6,16	
si Epsomit	-4,86	-3,59	-4,11	-4,37	-4,76	-4,08	-3,37	-3,80	-4,52
si SiO2(a)	-0,73	-0,80	-0,92	-0,65	-0,86	-0,91	-0,93	-0,85	-0,63
si FCO3Apa	12,83	7,20	10,78	6,39	11,96	11,90	8,48	2,79	13,99
si Dolomit	-2,62	-3,45	-2,86	-5,06	-3,22	-2,62	-3,78	-4,44	-2,57
si NiCO3		-7,82					-8,00		
si Ni(OH)2		-4,82					-4,71		
si Ni4(OH)		-24,21					-23,47		
si Bunseni		-6,47					-6,36		

soln	000305S1	000305W1	000305W2	000305S2	000306W1	000306W2	000306S1	000307W1	000308S1
si Ni3(PO4		-15,11					-15,56		
si Retgers		-8,11					-7,70		
si Morenos		-7,79					-7,38		
si Ni2SiO4		-6,10					-6,01		
si Fe3(OH)		0,36	0,00	-2,54			-3,82	0,73	
si Dioptas	-3,63	-4,78	-3,58	-4,10	-3,24	-3,42	-4,30	-4,04	-3,60
si Jurbani	-7,79	-3,06	-6,15	-4,04	-6,77	-7,25	-3,91	-4,31	-7,77
si Basalum	-8,90	0,49	-5,43	-1,96	-7,16	-8,58	-3,79	-2,34	-9,65
si As2O5	-34,83	-28,62	-33,38	-29,83	-33,64	-34,39	-29,43	-31,03	-34,38
si AlAsO4:	-10,55	-5,89	-9,22	-6,99	-9,72	-10,41	-7,44	-7,63	-10,58
si Ca3(AsO	-12,91	-13,20	-12,53	-13,57	-13,33	-12,54	-13,02	-15,67	-12,64
si Cu3(AsO	-15,29	-12,29	-13,11	-11,91	-12,53	-13,66	-11,25	-12,34	-15,04
si Scorodi		-5,26	-7,45	-6,79			-7,05	-6,27	
si Mn3(AsO		-12,91		-10,83			-13,93	-14,43	
si Ni3(AsO		-19,67					-20,15		
si Zn3(AsO	-16,19	-16,52	-16,17	-17,38	-11,53	-15,74	-17,67	-17,83	-16,16
si Arsenol	-71,48	-50,26	-66,98	-53,48	-66,70	-70,60	-51,86	-56,67	-70,16
si Claudet	-71,21	-50,00	-66,71	-53,22	-66,44	-70,34	-51,60	-56,41	-69,90
si Portlan	-10,30	-12,46	-10,65	-12,18	-10,83	-10,32	-12,13	-12,48	-10,36
si Rhodoch		-2,34		-2,04			-2,70	-2,78	
si Na4UO2(	-30,82	-26,58	-28,71		-31,37	-26,04			-30,78
si Uranini	-8,57	-8,29	-7,68		-8,78	-7,53			-8,82
si UO2(a)	-13,47	-13,19	-12,58		-13,68	-12,43			-13,72
si U4O9(c)	-26,69	-27,77	-23,54		-28,15	-22,52			-27,79
si U3O8(c)	-13,83	-17,39	-11,97		-15,68	-10,71			-14,79
si Coffini	-9,14	-8,93	-8,44		-9,48	-8,28			-9,29
si UF4(c)	-44,54	-39,00	-42,22		-43,55	-42,05			-44,27
si UF4:2,5	-35,58	-30,04	-33,26		-34,58	-33,09			-35,31
si U(OH)2S	-29,47	-26,01	-27,55		-28,90	-27,80			-29,44
si UO2HPO4	-8,97	-8,91	-8,46		-9,12	-8,32			-9,04
si U(HPO4)	-26,38	-22,15	-25,45		-25,28	-26,13			-26,06
si Ningyoi	-15,27	-13,20	-14,70		-14,70	-15,04			-15,02
si UO3(gam	-6,73	-8,65	-6,24		-7,54	-5,69			-7,08
si Gummite	-9,41	-11,33	-8,92		-10,23	-8,37			-9,76
si B-UO2(O	-4,55	-6,47	-4,06		-5,37	-3,51			-4,90
si Schoepi	-4,41	-6,33	-3,92		-5,23	-3,37			-4,76
si Rutherf	-6,81	-7,11	-6,13		-7,32	-5,84			-7,14
si (UO2)3(	-27,93	-29,74	-26,43		-29,06	-25,60			-28,42
si H-Autun	-18,39	-18,28	-17,38		-18,71	-17,10			-18,53
si Na-Autu	-9,58	-8,82	-8,05		-10,23	-6,32			-9,56
si K-Autun	-10,64	-9,73	-9,09		-11,12	-7,85			-10,77
si Saleeit	-10,38	-12,17	-9,65		-11,37	-8,93			-10,45
si Autunit	-9,89	-11,94	-9,24		-10,74	-8,63			-10,09
si Basseti		-13,25	-13,07						
si Torbern	-14,74	-15,69	-13,49		-14,53	-13,05			-14,95
si Uranoph	-9,88	-16,04	-9,64		-12,31	-8,18			-10,44
si CO2(g)	-4,11	-2,49	-3,91	-3,29	-3,80	-4,18	-2,78	-3,22	-4,08
si O2(g)	-36,32	-40,72	-37,12	-40,32	-37,52	-36,32	-40,72	-39,92	-36,52
si H2(g)	-23,40	-21,20	-23,00	-21,40	-22,80	-23,40	-21,20	-21,60	-23,30

soln	000308S2	000308S3	000309S1	000309S2	000312S1	000313S1	000313S2	000313S3	000314S2
si Magnesi	-1,58	-1,73	-2,43	-2,27	-2,13	-2,15	-2,34	-2,20	-2,02
si Dolomit	-2,59	-2,93	-3,90	-3,65	-3,31	-3,22	-3,57	-3,38	-3,18
si Calcite	-1,04	-1,23	-1,50	-1,41	-1,22	-1,10	-1,27	-1,21	-1,20
si Anhydri	-2,20	-1,95	-0,32	-0,40	-0,56	-2,36	-2,18	-2,53	-2,09
si Gypsum	-1,98	-1,73	-0,11	-0,19	-0,34	-2,14	-1,96	-2,31	-1,87
si Brucite	-3,90	-4,29	-7,00	-6,79	-6,21	-4,74	-5,23	-4,76	-4,78
si Chrysot	-0,36	-1,58	-9,63	-9,01	-7,48	-3,53	-3,99	-3,24	-3,08
si Aragoni	-1,18	-1,37	-1,65	-1,56	-1,36	-1,25	-1,41	-1,36	-1,34
si Forster	-5,91	-6,72	-12,10	-11,68	-10,63	-7,92	-8,40	-7,78	-7,71
si Diopsid	-0,91	-1,77	-6,68	-6,36	-5,34	-2,73	-2,68	-2,48	-2,46
si Clinoen	-1,89	-2,31	-4,97	-4,77	-4,30	-3,06	-3,04	-2,90	-2,81
si Tremoli	6,25	3,27	-14,50	-13,28	-9,92	-1,22	-0,55	-0,06	0,34
si Sepioli	-0,36	-1,20	-6,50	-6,12	-5,26	-3,01	-2,47	-2,52	-2,23
si Talc	3,45	2,19	-5,76	-5,18	-3,85	-0,37	0,19	0,28	0,66
si Hydroma	-16,74	-17,73	-23,25	-22,37	-21,23	-19,83	-21,09	-20,07	-19,36
si Adulari	-0,05	-0,10	-0,40	0,24	1,24	-1,54	0,41	-1,70	-0,98
si Albite	-1,57	-1,69	-1,96	-1,34	-0,46	-3,13	-1,51	-3,23	-2,57
si Anorthi	-3,07	-3,35	-6,24	-4,88	-1,95	-3,25	-2,41	-4,36	-4,30
si Analcim	-3,37	-3,48	-3,80	-3,16	-2,18	-4,61	-3,50	-4,89	-4,33
si Kmica	5,85	5,99	4,99	6,87	10,38	5,16	7,40	3,60	4,36
si Phlogop	-2,42	-3,65	-12,09	-10,81	-8,07	-6,44	-5,97	-6,66	-5,99
si Illite	0,69	0,69	-0,69	0,78	3,49	-0,29	1,87	-1,27	-0,63
si Kaolini	2,08	2,23	1,62	2,84	5,14	2,23	3,54	1,20	1,44
si Halloys	-2,98	-2,84	-3,45	-2,23	0,08	-2,83	-1,52	-3,87	-3,62
si Beidell	0,63	0,73	-0,08	1,34	3,92	0,12	2,32	-0,84	-0,34
si Chlorit	2,36	0,53	-13,60	-11,33	-6,24	-2,02	-2,67	-2,98	-2,71
si Alunite	-8,75	-7,19	-0,51	0,99	3,21	-8,12	-6,10	-10,39	-8,70
si Gibbsit	0,14	0,24	-0,11	0,51	1,76	0,54	0,69	-0,15	-0,14
si Boehmit	-0,33	-0,24	-0,59	0,04	1,29	0,07	0,21	-0,63	-0,61
si Pyrophy	5,51	5,61	5,10	6,29	8,39	5,02	7,34	4,33	4,79
si Phillip	-0,22	-0,31	-0,59	0,03	0,98	-1,75	0,04	-1,88	-1,19
si Nahcoli	-6,35	-6,27	-4,31	-4,32	-4,82	-7,07	-6,81	-7,03	-6,51
si Trona	-17,99	-17,99	-14,14	-14,10	-15,19	-20,43	-19,96	-20,29	-18,92
si Natron	-10,58	-10,66	-8,78	-8,74	-9,31	-12,30	-12,09	-12,19	-11,35
si Thermon	-12,02	-12,10	-10,20	-10,16	-10,74	-13,73	-13,52	-13,63	-12,79
si Fluorit	-1,60	-1,47	-0,33	-0,67	-0,28	-2,81	-2,77	-2,27	-1,89
si Montmor	0,77	0,84	-0,18	1,24	3,90	0,46	2,59	-0,52	-0,12
si Halite	-6,75	-6,69	-3,94	-4,05	-4,92	-8,32	-7,90	-8,20	-7,16
si Thenard	-8,75	-8,39	-4,60	-4,73	-5,66	-10,57	-10,01	-10,52	-9,25
si Mirabil	-7,82	-7,46	-3,68	-3,81	-4,73	-9,64	-9,07	-9,59	-8,32
si Siderit				-2,31	-2,40				
si Hydroxy	2,24	-0,35	-3,27	-2,68	-1,69	-0,46	2,23	0,71	-0,24
si Fluorap	3,80	1,50	0,29	0,63	1,51	0,67	3,61	2,14	1,47
si Chalced	0,06	0,04	0,08	0,06	-0,03	-0,27	0,24	-0,09	0,02
si Magadii	-4,84	-5,14	-4,88	-4,95	-5,71	-8,09	-4,58	-6,79	-5,72
si Cristob	0,09	0,07	0,12	0,10	0,00	-0,23	0,28	-0,05	0,05
si Silicag	-0,48	-0,50	-0,45	-0,47	-0,57	-0,80	-0,29	-0,62	-0,52
si Quartz	0,48	0,46	0,51	0,49	0,40	0,16	0,67	0,34	0,45
si Viviani				-6,17	-6,58				

soln	000308S2	000308S3	000309S1	000309S2	000312S1	000313S1	000313S2	000313S3	000314S2
si Magneti				12,46	14,20				
si Hematit				13,05	14,44				
si Maghemi				2,66	4,05				
si Goethit				5,52	6,22				
si Greenal				-6,33	-5,49				
si Fe(OH)3				-0,37	0,33				
si Annite				2,76	4,81				
si Montmor				4,01	5,91				
si Montmor				3,05	5,00				
si Huntite	-8,39	-9,02	-11,40	-10,81	-10,19	-10,14	-10,87	-10,41	-9,85
si Chlorit	-1,02	-2,85	-16,97	-14,70	-9,61	-5,39	-6,04	-6,35	-6,08
si Laumont	1,19	0,87	-1,94	-0,62	2,13	0,36	2,21	-0,40	-0,13
si Jarosit				-5,52	-4,97				
si Mn2(SO4				-57,48	-57,66				
si Al(OH)3	-2,55	-2,45	-2,80	-2,18	-0,93	-2,15	-2,00	-2,84	-2,83
si Prehnit	-1,54	-2,28	-7,42	-5,93	-2,46	-2,40	-1,52	-3,41	-3,42
si Strengi				-0,89	-0,92				
si Leonhar	10,21	9,57	3,95	6,60	12,09	8,55	12,26	7,03	7,58
si Nesqueh	-3,99	-4,14	-4,85	-4,68	-4,54	-4,55	-4,74	-4,61	-4,43
si Artinit	-6,27	-6,81	-10,23	-9,85	-9,13	-7,67	-8,36	-7,75	-7,58
si Sepioli	-3,26	-4,10	-9,40	-9,02	-8,16	-5,91	-5,37	-5,42	-5,13
si Diaspor	1,37	1,47	1,12	1,74	2,99	1,77	1,92	1,08	1,09
si Wairaki	-3,06	-3,39	-6,19	-4,87	-2,13	-3,89	-2,04	-4,65	-4,38
si Fe(OH)2				5,27	5,73				
si MnSO4				-11,54	-11,58				
si Pyrolus				-14,25	-12,80				
si Birness				-16,47	-15,02				
si Nsutite				-15,43	-13,98				
si Bixbyit				-16,92	-14,72				
si Hausman				-21,19	-18,24				
si Pyrochr				-8,85	-8,10				
si Mangani				-8,60	-7,50				
si Rhodoch				-3,60	-3,29				
si MnCl2:4				-11,61	-12,46				
si Mn3(PO4				-20,72	-19,93				
si MnHPO4				-0,16	-0,14				
si Jarosit				-6,45	-6,01				
si Jarosit				-3,51	-2,95				
si CuMetal	-6,00	-5,66	-4,96	-4,82	-4,07	-5,24	-4,41	-5,55	-5,39
si Nantoki	-6,55	-6,18	-4,15	-4,05	-3,76	-6,60	-5,56	-6,86	-6,11
si CuF	-22,50	-22,08	-21,14	-21,13	-20,16	-22,42	-21,59	-22,42	-22,11
si Cuprite	-4,07	-3,78	-5,32	-4,82	-2,64	-3,02	-1,88	-3,64	-3,59
si Cu2SO4	-23,26	-22,29	-19,92	-19,64	-18,25	-22,04	-20,24	-22,75	-22,07
si Cuprous				10,25	12,04				
si Melanot	-18,30	-17,92	-14,54	-14,50	-14,65	-19,17	-17,92	-19,38	-18,04
si CuCO3	-6,50	-6,32	-6,54	-6,24	-5,23	-5,94	-5,33	-6,29	-6,19
si CuF2	-18,19	-17,69	-16,49	-16,63	-15,42	-18,78	-17,96	-18,48	-18,01
si CuF2:2H	-14,26	-13,76	-12,56	-12,70	-11,49	-14,85	-14,03	-14,55	-14,08
si Cu(OH)2	-2,22	-2,28	-4,51	-4,16	-2,71	-1,94	-1,63	-2,25	-2,35

soln	000308S2	000308S3	000309S1	000309S2	000312S1	000313S1	000313S2	000313S3	000314S2
si Malachi	-4,53	-4,41	-6,86	-6,21	-3,76	-3,69	-2,77	-4,35	-4,35
si Azurite	-8,94	-8,62	-11,29	-10,34	-6,89	-7,53	-6,00	-8,54	-8,45
si Atacami	-4,99	-4,89	-6,55	-6,00	-3,91	-5,00	-3,91	-5,57	-5,06
si Cu2(OH)	-6,90	-7,07	-9,75	-9,35		-6,63	-5,31	-7,06	-6,75
si Antleri	-8,62	-8,11	-10,89	-10,07	-6,52	-7,60	-6,01	-8,62	-8,30
si Brochan	-9,25	-8,80	-13,81	-12,63	-7,65	-7,94	-6,05	-9,28	-9,06
si Langite	-10,70	-10,25	-15,26	-14,09	-9,10	-9,39	-7,50	-10,73	-10,51
si Tenorit	-1,20	-1,26	-3,49	-3,14	-1,69	-0,92	-0,61	-1,23	-1,33
si CuOCuSO	-18,28	-17,71	-18,26	-17,79	-15,69	-17,54	-16,26	-18,25	-17,83
si Cu3(PO4	-12,82	-13,28	-14,29	-13,32	-10,44	-12,63	-8,34	-12,54	-12,86
si Cu3(PO4	-14,55	-15,01	-16,02	-15,05	-12,17	-14,36	-10,07	-14,27	-14,59
si CuSO4	-16,18	-15,56	-13,88	-13,75	-13,10	-15,72	-14,76	-16,13	-15,60
si Chalcan	-10,53	-9,91	-8,24	-8,11	-7,45	-10,07	-9,11	-10,48	-9,95
si CupricF				7,64	10,48				
si ZnMetal	-40,60	-40,53	-40,89	-40,74	-40,71	-40,53	-40,47	-40,68	-40,72
si ZnCl2	-18,97	-18,86	-16,53	-16,48	-17,35	-20,52	-20,05	-20,58	-19,43
si Smithso	-3,50	-3,59	-4,86	-4,55	-4,26	-3,63	-3,79	-3,81	-3,91
si ZnCO3:H	-3,24	-3,33	-4,60	-4,29	-4,00	-3,37	-3,53	-3,55	-3,65
si ZnF2	-14,65	-14,43	-14,28	-14,41	-13,92	-15,93	-15,89	-15,48	-15,20
si Zn(OH)2	-3,39	-3,72	-7,01	-6,65	-5,92	-3,80	-4,26	-3,95	-4,25
si Zn(OH)2	-3,14	-3,47	-6,76	-6,40	-5,67	-3,55	-4,01	-3,70	-4,00
si Zn(OH)2	-2,69	-3,02	-6,31	-5,95	-5,22	-3,10	-3,56	-3,25	-3,55
si Zn(OH)2	-2,65	-2,98	-6,27	-5,91	-5,18	-3,06	-3,52	-3,21	-3,51
si Zn(OH)2	-2,44	-2,77	-6,06	-5,70	-4,97	-2,85	-3,31	-3,00	-3,30
si Zn2(OH)	-7,58	-8,02	-11,79	-11,23	-10,57	-8,97	-9,43	-9,23	-9,10
si Zn5(OH)	-14,20	-15,42	-26,23	-24,77	-22,70	-17,39	-18,77	-18,06	-18,09
si Zn2(OH)	-8,98	-8,96	-11,62	-11,13	-10,45	-9,62	-9,89	-10,02	-9,98
si Zn4(OH)	-11,76	-12,40	-21,63	-20,43	-18,29	-13,22	-14,42	-13,93	-14,48
si Zn(NO3)	-15,39	-15,83	-15,56	-15,79		-16,38	-15,45	-16,16	-15,43
si ZnO(a)	-2,25	-2,58	-5,87	-5,51	-4,78	-2,66	-3,12	-2,81	-3,11
si Zincite	-2,08	-2,41	-5,70	-5,34	-4,61	-2,49	-2,95	-2,64	-2,94
si Zn3O(SO	-31,04	-30,66	-32,69	-32,07	-31,45	-31,90	-31,99	-32,55	-32,18
si Zn3(PO4	-9,72	-11,00	-15,18	-14,19	-13,44	-11,60	-9,64	-11,04	-11,94
si ZnSiO3	2,63	2,28	-0,96	-0,62	0,01	1,90	1,95	1,92	1,74
si Willemi	-0,71	-1,39	-7,91	-7,22	-5,86	-1,85	-2,27	-1,98	-2,46
si Zincosi	-13,55	-13,20	-12,57	-12,43	-12,49	-13,78	-13,59	-14,02	-13,69
si ZnSO4:H	-9,97	-9,62	-8,99	-8,85	-8,91	-10,20	-10,01	-10,44	-10,11
si Bianchi	-8,77	-8,42	-7,80	-7,67	-7,72	-9,00	-8,81	-9,25	-8,91
si Goslari	-8,58	-8,23	-7,61	-7,47	-7,53	-8,81	-8,62	-9,05	-8,72
si Jarosit				-11,50	-10,98				
si AlumK	-21,49	-20,11	-12,75	-12,50	-12,77	-21,66	-19,92	-22,53	-20,88
si Melante				-5,87	-6,31				
si Epsomit	-4,51	-4,22	-3,03	-3,04	-3,25	-5,18	-5,02	-5,29	-4,68
si SiO2(a)	-0,78	-0,80	-0,76	-0,77	-0,87	-1,11	-0,60	-0,93	-0,82
si FCO3Apa	15,83	12,00	10,57	11,08	12,74	9,85	14,44	12,35	11,64
si Dolomit	-2,04	-2,38	-3,35	-3,10	-2,76	-2,67	-3,02	-2,83	-2,63
si NiCO3			-7,93	-7,64	-7,43		-6,72		
si Ni(OH)2			-5,27	-4,93	-4,29		-2,39		
si Ni4(OH)			-24,87	-23,73	-21,96		-17,11		

soln	000308S2	000308S3	000309S1	000309S2	000312S1	000313S1	000313S2	000313S3	000314S2
si Bunseni			-6,92	-6,58	-5,94		-4,04		
si Ni3(PO4			-15,64	-14,70	-14,23		-9,70		
si Retgers			-7,44	-7,32	-7,46		-8,31		
si Morenos			-7,12	-7,00	-7,14		-7,99		
si Ni2SiO4			-6,94	-6,28	-5,10		-1,02		
si Fe3(OH)				-4,04	-2,29				
si Dioptas	-3,57	-3,65	-5,84	-5,51	-4,16	-3,61	-2,80	-3,75	-3,74
si Jurbani	-8,11	-7,34	-3,77	-3,37	-2,91	-7,54	-6,74	-8,32	-7,68
si Basalum	-9,28	-8,23	-5,72	-3,43	0,78	-7,51	-6,27	-10,38	-9,69
si As2O5	-35,32	-34,52	-26,91	-27,32	-29,34	-34,72	-33,99	-35,10	-34,07
si AlAsO4:	-10,82	-10,32	-6,87	-6,45	-6,21	-10,12	-9,61	-11,00	-10,47
si Ca3(AsO	-11,80	-12,28	-11,56	-11,55	-11,66	-12,22	-12,90	-12,83	-12,36
si Cu3(AsO	-15,43	-14,79	-13,89	-13,25	-10,93	-13,98	-12,32	-15,29	-14,58
si Scorodi				-6,14	-6,45				
si Mn3(AsO				-14,06	-13,82				
si Ni3(AsO			-19,31	-18,70	-18,78		-17,73		
si Zn3(AsO	-15,09	-15,28	-17,54	-16,88	-16,70	-15,71	-16,38	-16,56	-16,42
si Arsenol	-74,45	-71,24	-44,36	-45,97	-52,81	-71,33	-67,79	-72,09	-69,00
si Portlan	-9,76	-10,19	-12,48	-12,34	-11,71	-10,11	-10,57	-10,18	-10,37
si Rhodoch				-2,86	-2,55				
si Na4UO2(	-28,83	-28,01	-25,66	-25,71	-26,92	-31,20	-33,31	-31,93	-29,62
si Uranini	-8,84	-7,71	-8,24	-8,52	-8,83	-7,57	-9,90	-8,48	-7,80
si UO2(a)	-13,74	-12,61	-13,14	-13,42	-13,73	-12,47	-14,80	-13,38	-12,70
si U4O9(c)	-27,27	-23,15	-28,20	-29,13	-29,66	-22,69	-32,50	-26,32	-23,86
si U3O8(c)	-13,64	-11,06	-18,50	-18,94	-18,46	-10,81	-18,82	-13,53	-12,01
si Coffini	-9,46	-8,36	-8,84	-9,14	-9,54	-8,52	-10,34	-9,25	-8,46
si UF4(c)	-45,49	-43,25	-36,92	-38,17	-38,96	-45,97	-47,28	-45,66	-43,84
si UF4:2,5	-36,53	-34,29	-27,96	-29,21	-29,99	-37,00	-38,31	-36,69	-34,87
si U(OH)2S	-30,03	-28,22	-24,84	-25,35	-26,44	-28,59	-30,26	-29,59	-28,28
si UO2HPO4	-9,05	-8,47	-9,09	-9,20	-9,53	-8,59	-9,76	-8,99	-8,58
si U(HPO4)	-27,27	-26,44	-21,29	-21,65	-23,40	-26,66	-25,63	-26,55	-25,88
si Ningyoi	-15,63	-15,22	-12,36	-12,58	-13,70	-15,36	-14,80	-15,32	-14,84
si UO3(gam	-6,50	-5,77	-9,22	-9,30	-8,91	-5,71	-8,55	-6,62	-6,20
si Gummite	-9,18	-8,45	-11,91	-11,99	-11,59	-8,40	-11,24	-9,30	-8,88
si B-UO2(O	-4,32	-3,59	-7,05	-7,13	-6,74	-3,54	-6,38	-4,44	-4,02
si Schoepi	-4,18	-3,45	-6,91	-6,99	-6,60	-3,40	-6,24	-4,30	-3,88
si Rutherf	-6,88	-5,91	-7,35	-7,48	-7,53	-5,82	-8,36	-6,76	-6,14
si (UO2)3(	-27,87	-25,98	-30,66	-30,98	-31,24	-26,17	-31,35	-27,87	-26,63
si H-Autun	-18,56	-17,39	-18,62	-18,86	-19,52	-17,64	-19,98	-18,44	-17,61
si Na-Autu	-8,42	-7,58	-8,91	-9,06	-9,87	-9,50	-11,92	-10,15	-8,68
si K-Autun	-9,69	-8,68	-10,09	-10,22	-10,78	-10,62	-12,39	-11,41	-9,81
si Saleeit	-9,90	-9,13	-13,06	-13,08	-13,17	-9,83	-12,65	-10,64	-9,83
si Autunit	-9,53	-8,79	-12,30	-12,40	-12,43	-8,95	-11,76	-9,82	-9,18
si Basseti				-15,15	-15,47				
si Torbern	-14,79	-13,68	-17,13	-17,02	-16,25	-13,59	-15,62	-14,70	-13,98
si Uranoph	-9,00	-8,01	-17,12	-17,18	-15,95	-8,42	-13,55	-9,95	-9,08
si CO2(g)	-4,41	-4,16	-2,15	-2,20	-2,64	-4,13	-3,83	-4,16	-3,96
si O2(g)	-35,32	-36,12	-41,96	-41,56	-40,16	-36,28	-37,32	-36,28	-36,80
si H2(g)	-23,90	-23,50	-20,58	-20,78	-21,48	-23,42	-22,90	-23,42	-23,16

soln	000314S3	000320S1	000320S2
si Magnesi	-1,99	-1,85	-2,29
si Dolomit	-3,10	-2,99	-3,71
si Calcite	-1,15	-1,17	-1,46
si Anhydri	-2,48	-1,94	-2,78
si Gypsum	-2,26	-1,72	-2,56
si Brucite	-4,63	-4,79	-4,74
si Chrysot	-2,85	-2,83	-3,16
si Aragoni	-1,29	-1,32	-1,60
si Forster	-7,53	-7,60	-7,74
si Diopsid	-2,37	-2,34	-2,58
si Clinoen	-2,77	-2,68	-2,87
si Tremoli	0,55	1,14	-0,15
si Sepioli	-2,26	-1,82	-2,44
si Talc	0,67	1,21	0,39
si Hydroma	-19,10	-18,70	-20,40
si Adulari	-0,61	0,62	-0,40
si Albite	-2,17	-0,91	-2,09
si Anorthi	-2,48	-1,95	-2,36
si Analcim	-3,83	-2,82	-3,76
si Kmica	6,60	8,18	7,02
si Phlogop	-5,19	-4,44	-5,32
si Illite	1,04	2,47	1,34
si Kaolini	3,10	3,96	3,34
si Halloys	-1,96	-1,10	-1,72
si Beidell	1,41	2,82	1,70
si Chlorit	-0,43	-0,13	-0,74
si Alunite	-7,25	-4,71	-7,22
si Gibbsit	0,80	0,97	0,91
si Boehmit	0,33	0,50	0,43
si Pyrophy	6,24	7,62	6,51
si Phillip	-0,80	0,45	-0,66
si Nahcoli	-6,84	-6,22	-7,10
si Trona	-19,81	-18,26	-20,39
si Natron	-11,90	-10,97	-12,23
si Thermon	-13,34	-12,40	-13,66
si Fluorit	-2,24	-1,65	-1,77
si Montmor	1,70	2,99	1,97
si Halite	-7,80	-6,78	-8,04
si Thenard	-10,25	-8,74	-10,56
si Mirabil	-9,31	-7,81	-9,62
si Hydroxy	2,24	0,76	0,84
si Fluorap	3,70	2,68	2,59
si Chalced	-0,09	0,17	-0,07
si Magadii	-6,68	-4,56	-6,64
si Cristob	-0,05	0,20	-0,04
si Silicag	-0,62	-0,36	-0,61
si Quartz	0,34	0,60	0,35

soln	000314S3	000320S1	000320S2
si Huntite	-9,71	-9,32	-10,92
si Chlorit	-3,80	-3,50	-4,12
si Laumont	1,49	2,53	1,63
si Al(OH)3	-1,89	-1,72	-1,78
si Prehnit	-1,53	-1,08	-1,54
si Leonhar	10,81	12,90	11,10
si Nesqueh	-4,40	-4,26	-4,69
si Artinit	-7,41	-7,43	-7,82
si Sepioli	-5,16	-4,72	-5,34
si Diaspor	2,03	2,20	2,14
si Wairaki	-2,76	-1,72	-2,62
si CuMetal	-5,45	-5,00	-5,64
si Nantoki	-6,50	-5,54	-6,85
si CuF	-22,34	-21,61	-22,22
si Cuprite	-3,52	-3,00	-3,88
si Cu2SO4	-22,56	-21,17	-23,09
si Melanot	-18,76	-17,29	-19,26
si CuCO3	-6,19	-5,80	-6,53
si CuF2	-18,41	-17,40	-17,97
si CuF2:2H	-14,48	-13,47	-14,04
si Cu(OH)2	-2,23	-2,15	-2,38
si Malachi	-4,22	-3,76	-4,72
si Azurite	-8,31	-7,46	-9,15
si Atacami	-5,24	-4,38	-5,72
si Cu2(OH)	-6,81	-6,36	-7,27
si Antleri	-8,49	-7,37	-9,13
si Brochan	-9,13	-7,93	-9,93
si Langite	-10,58	-9,38	-11,38
si Tenorit	-1,21	-1,13	-1,36
si CuOCuSO	-18,14	-17,11	-18,63
si Cu3(PO4	-11,39	-11,03	-12,38
si Cu3(PO4	-13,12	-12,76	-14,11
si CuSO4	-16,04	-15,08	-16,37
si Chalcan	-10,39	-9,43	-10,72
si ZnMetal	-39,45	-40,68	-40,69
si ZnCl2	-18,82	-19,02	-20,37
si Smithso	-2,58	-3,87	-3,97
si ZnCO3:H	-2,32	-3,61	-3,71
si ZnF2	-14,27	-14,94	-14,88
si Zn(OH)2	-2,80	-4,39	-4,00
si Zn(OH)2	-2,55	-4,14	-3,75
si Zn(OH)2	-2,10	-3,69	-3,30
si Zn(OH)2	-2,06	-3,65	-3,26
si Zn(OH)2	-1,85	-3,44	-3,05
si Zn2(OH)	-6,62	-9,11	-9,20
si Zn5(OH)	-11,69	-18,25	-18,05
si Zn2(OH)	-7,64	-9,95	-10,22

soln	000314S3	000320S1	000320S2
si Zn4(OH)	-9,24	-14,73	-14,23
si Zn(NO3)	-14,57	-15,60	-16,08
si ZnO(a)	-1,66	-3,25	-2,86
si Zincite	-1,49	-3,08	-2,69
si Zn3O(SO	-28,95	-31,98	-32,90
si Zn3(PO4	-6,49	-11,15	-10,62
si ZnSiO3	3,08	1,75	1,89
si Willemi	0,33	-2,59	-2,06
si Zincosi	-12,80	-13,52	-14,18
si ZnSO4:H	-9,22	-9,94	-10,60
si Bianchi	-8,03	-8,74	-9,40
si Goslari	-7,83	-8,55	-9,21
si AlumK	-21,31	-19,10	-21,49
si Epsomit	-5,09	-4,38	-5,37
si PbMetal	-19,36		
si Cotunni	-8,42		
si Matlock	-5,76		
si Phosgen	-7,36		
si Cerrusi	-0,85		
si PbF2	-9,75		
si Massico	-4,66		
si Litharg	-4,47		
si PbO:0,3	-4,73		
si Pb2OCO3	-5,23		
si Larnaki	-2,66		
si Pb3O2SO	-5,10		
si Pb4O3SO	-8,55		
si PbHPO4	-1,69		
si Pb3(PO4	1,63		
si Clpyrom	13,73		
si Hxypyro	2,81		
si Pb3O2CO	-8,50		
si Plumbog	0,29		
si Hinsdal	-15,70		
si Tsumebi	-1,04		
si PbSiO3	-2,71		
si Pb2SiO4	-6,90		
si Anglesi	-3,40		
si Plattne	-17,71		
si Pb2O3	-21,20		
si Minium	-25,60		
si Pb(OH)2	0,10		
si Laurion	-3,10		
si Pb2(OH)	-3,02		
si Hydroce	-2,25		
si Pb2O(OH	-9,70		
si Pb4(OH)	-7,55		

soln	000314S3	000320S1	000320S2
si SiO2(a)	-0,93	-0,67	-0,91
si FCO3Apa	15,00	13,79	13,05
si Dolomit	-2,55	-2,44	-3,16
si Dioptas	-3,73	-3,39	-3,87
si Jurbani	-7,30	-6,25	-7,37
si Basalum	-6,50	-4,94	-6,25
si As2O5	-34,78	-33,36	-34,75
si AlAsO4:	-9,89	-9,01	-9,77
si Ca3(AsO	-12,57	-12,14	-12,92
si Cu3(AsO	-14,92	-13,25	-15,35
si Pb3(AsO	-9,13		
si Zn3(AsO	-12,78	-16,13	-16,36
si Arsenol	-71,14	-66,86	-71,23
si Claudet	-70,87	-66,59	-70,97
si Portlan	-10,20	-10,53	-10,33
si Na4UO2(	-32,28	-29,61	-32,29
si Uranini	-9,42	-8,56	-8,64
si UO2(a)	-14,32	-13,46	-13,54
si U4O9(c)	-30,14	-27,08	-26,99
si U3O8(c)	-16,50	-14,65	-14,09
si Coffini	-10,19	-9,07	-9,40
si UF4(c)	-46,49	-43,79	-44,53
si UF4:2,5	-37,52	-34,83	-35,56
si U(OH)2S	-30,46	-28,73	-29,85
si UO2HPO4	-9,46	-8,91	-8,90
si U(HPO4)	-26,40	-25,43	-26,13
si Ningyoi	-15,19	-14,55	-15,05
si UO3(gam	-7,63	-7,14	-6,82
si Gummite	-10,32	-9,82	-9,50
si B-UO2(O	-5,46	-4,96	-4,64
si Schoepi	-5,32	-4,82	-4,50
si Rutherf	-7,69	-6,90	-7,06
si (UO2)3(	-29,83	-28,23	-27,89
si H-Autun	-19,38	-18,27	-18,26
si Na-Autu	-10,89	-9,15	-9,91
si K-Autun	-12,08	-10,40	-10,85
si Saleeit	-11,46	-10,51	-10,45
si Autunit	-10,78	-10,01	-9,79
si Torbern	-15,62	-14,43	-14,66
si Przheva	-14,70		
si Uranoph	-12,00	-10,82	-10,47
si CO2(g)	-4,08	-3,78	-4,26
si O2(g)	-36,44	-37,16	-36,36
si H2(g)	-23,34	-22,98	-23,38

• App. 10 Contour base map of the B3 aquitard.

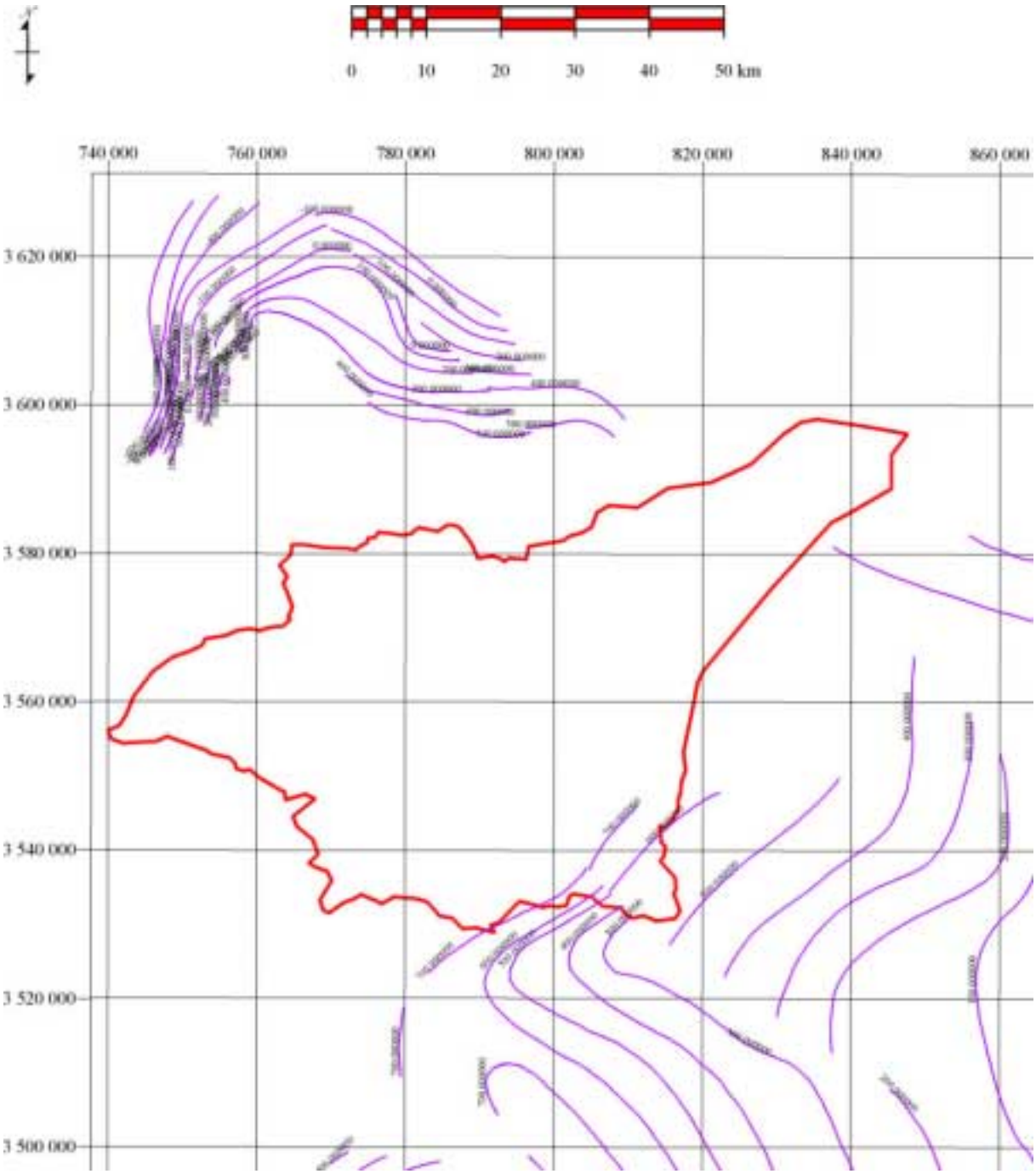

• App. 11 Contour base map of the A7/B2 aquifer.

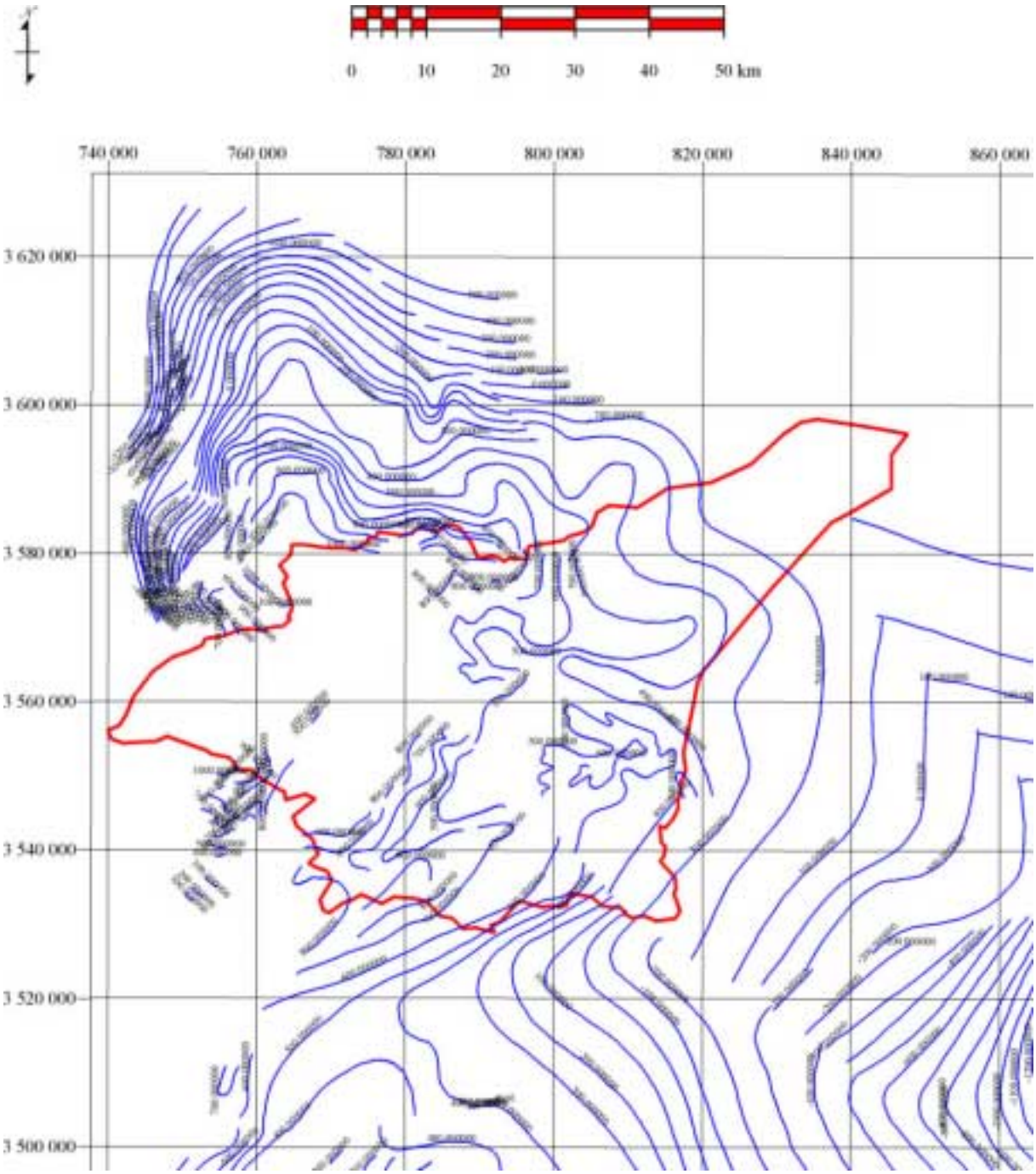

• App. 12 Contour base map of the A1/A6 aquitard.

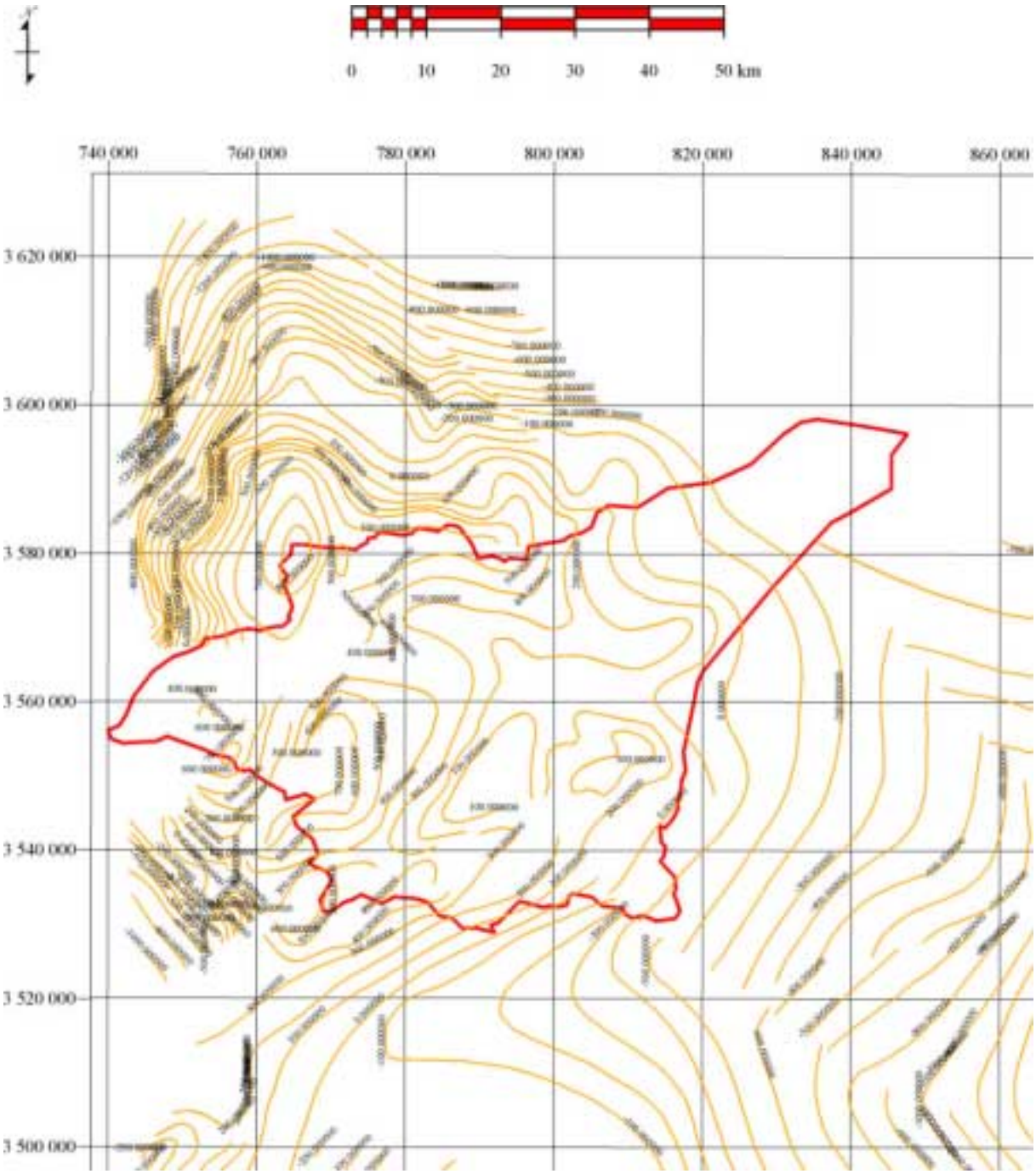

• App. 13 Contour base map of the Kurnub aquifer.

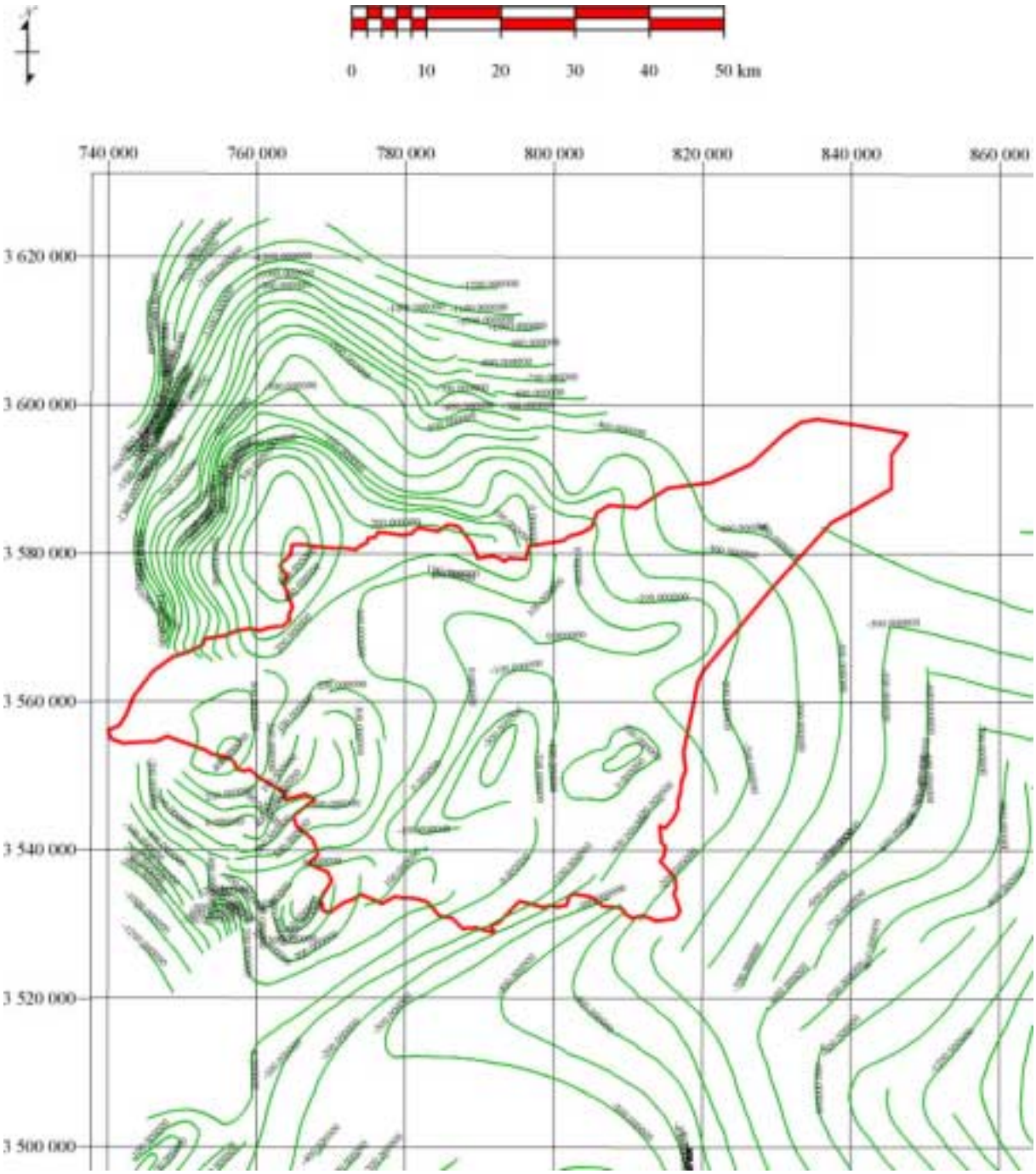

- App. 14 TNT-Mips script for offset calculation.

```
##########################################################################

# Z-Offset Vectorpoint
        clear();
        GetInputVector(K);
        GetOutputVector(V, "VectorToolkit, Network, 3DVector");
# Inout filenames
                strin$= GetObjectFileName(K)
                objNumIn = GetObjectNumber(K)
                strout$= GetObjectFileName(V)
                objNumOut = GetObjectNumber(V)
# copy subobjects
        print ("Iput: ", objNumIn, strin$)
        print ("Out: ", objNumOutm, strout$)
                CopySubobjects(K,V)

                offset = PopupNum("Please enter Offsetvalue: ",100
                                ,-10000 , 10000, 2)
# calculation
                for each point in K begin
                print ("nummer: ",zerq)
                        zahl=zahl+1
                x=K.point[zahl].Internal.x
                y=K.point[zahl].Internal.y
                z=K.point[zahl].Internal.z
                VectorAddPoint(V, x, y)
                zerq=z+(offset)

                VectorSetZValue(V, "point", zahl, zerq);

                end

##########################################################################
```

• App. 15 Points of the B3 aquitard used to created the geological model.

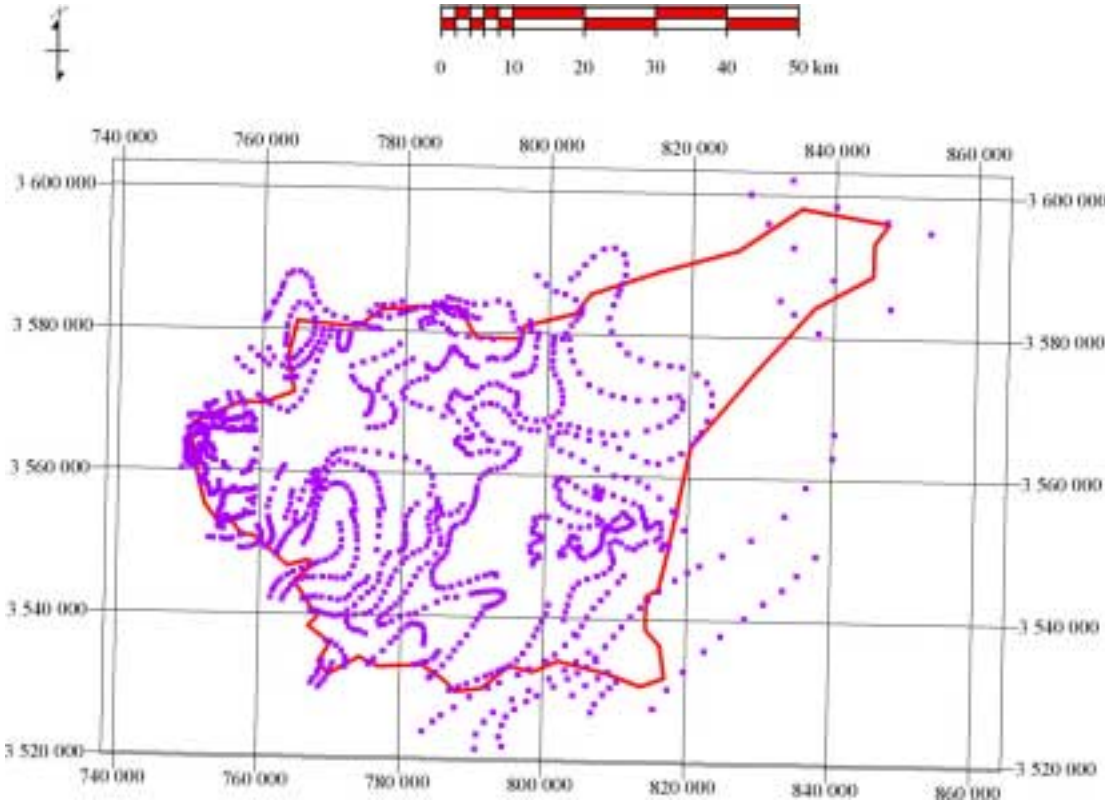

• App. 16 Points of the A7/B2 aquifer used to created the geological model.

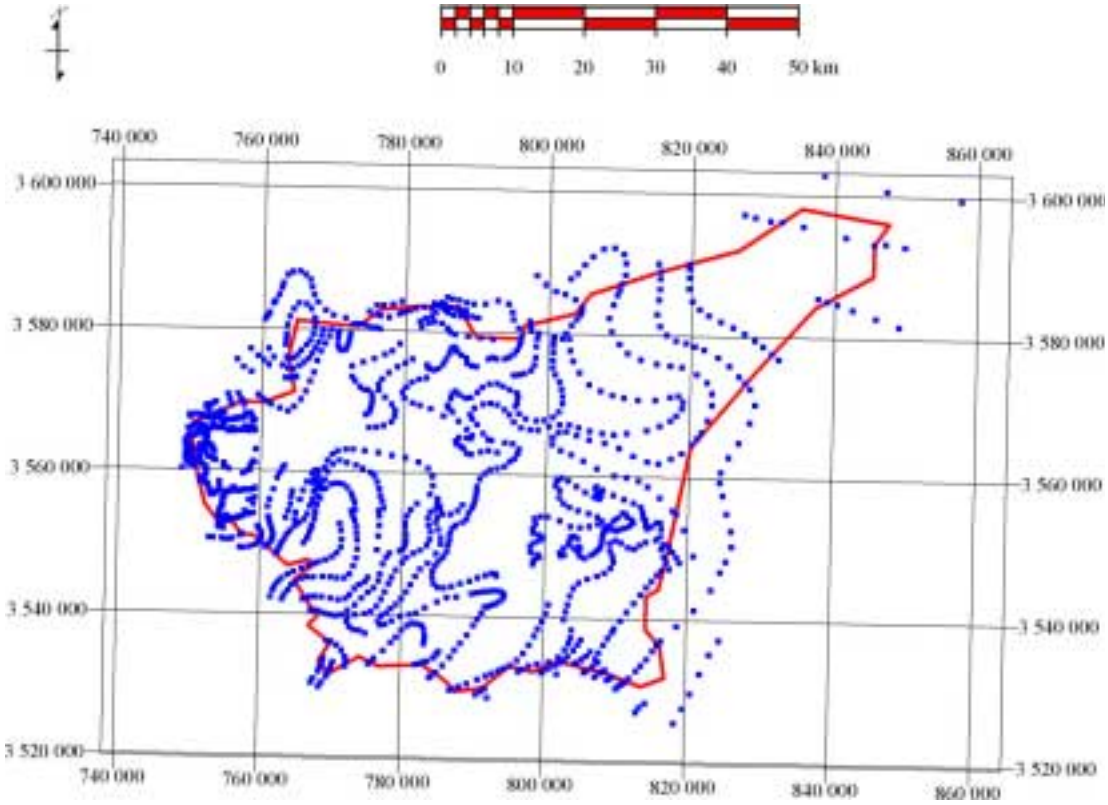

• App. 17 Points of the A1/A6 aquitard used to created the geological model.

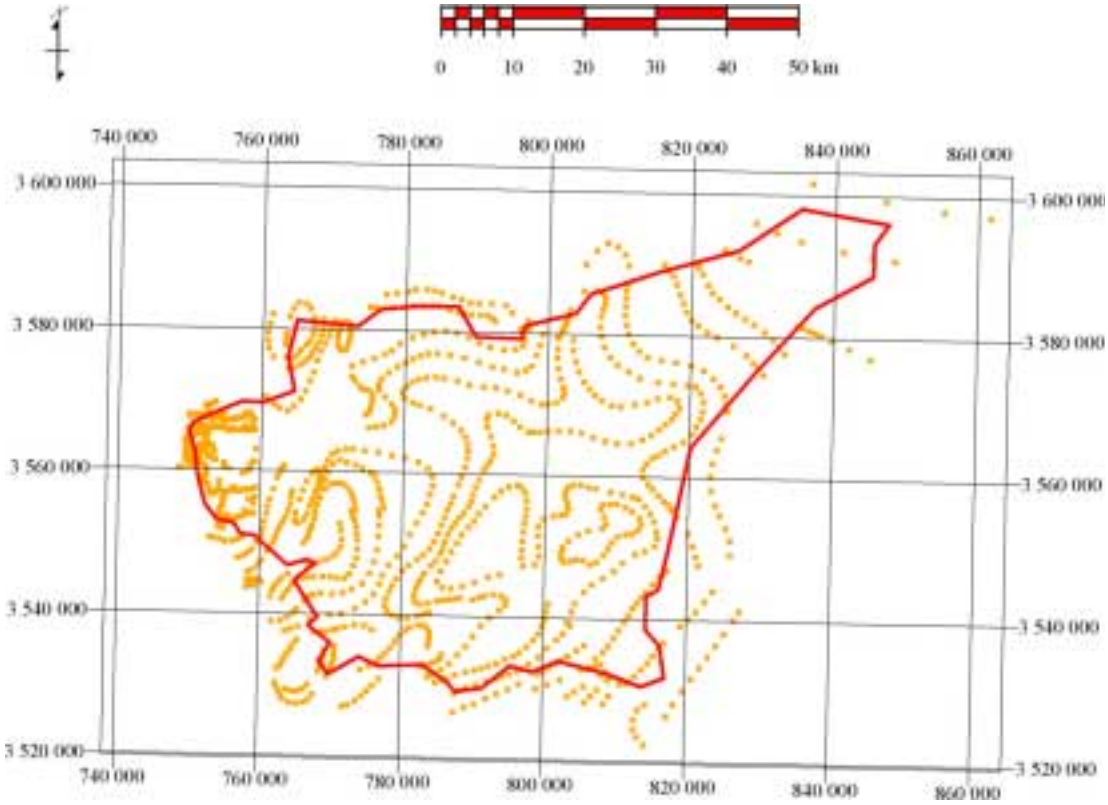

• App. 18 Points of the Kurnub aquifer used to created the geological model.

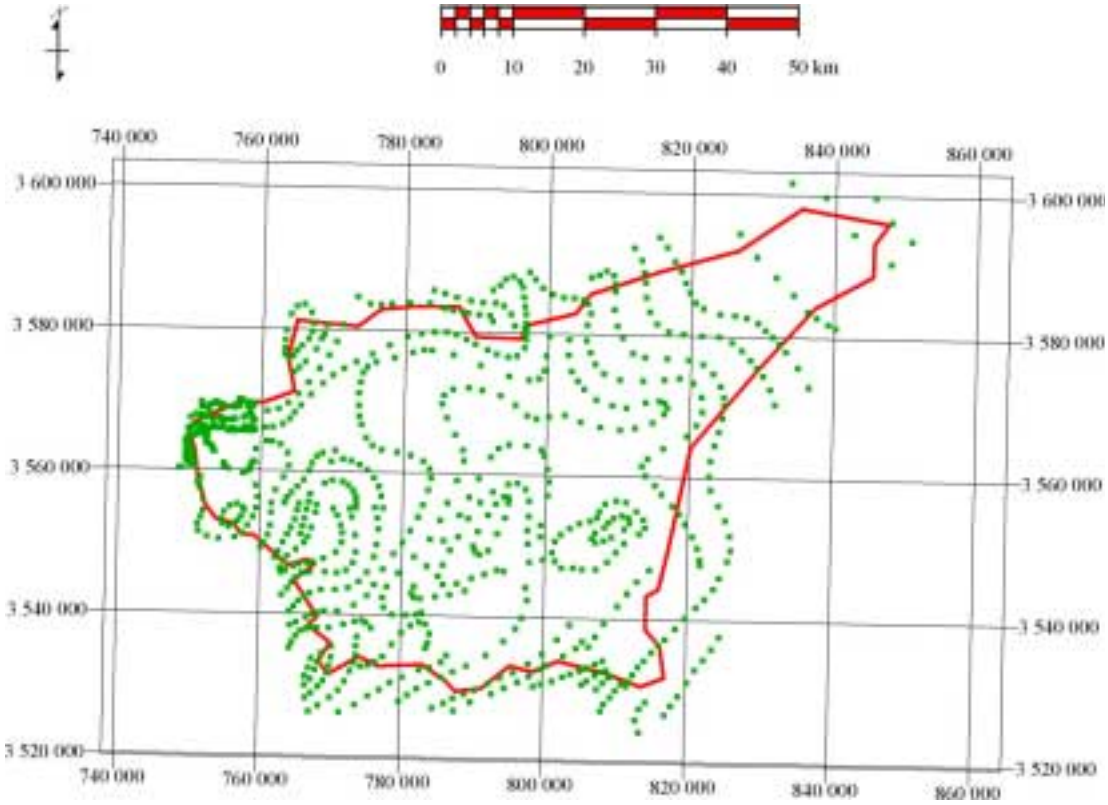

• App. 19 Calculated points of the Zerqa aquifer used to created the geological model.

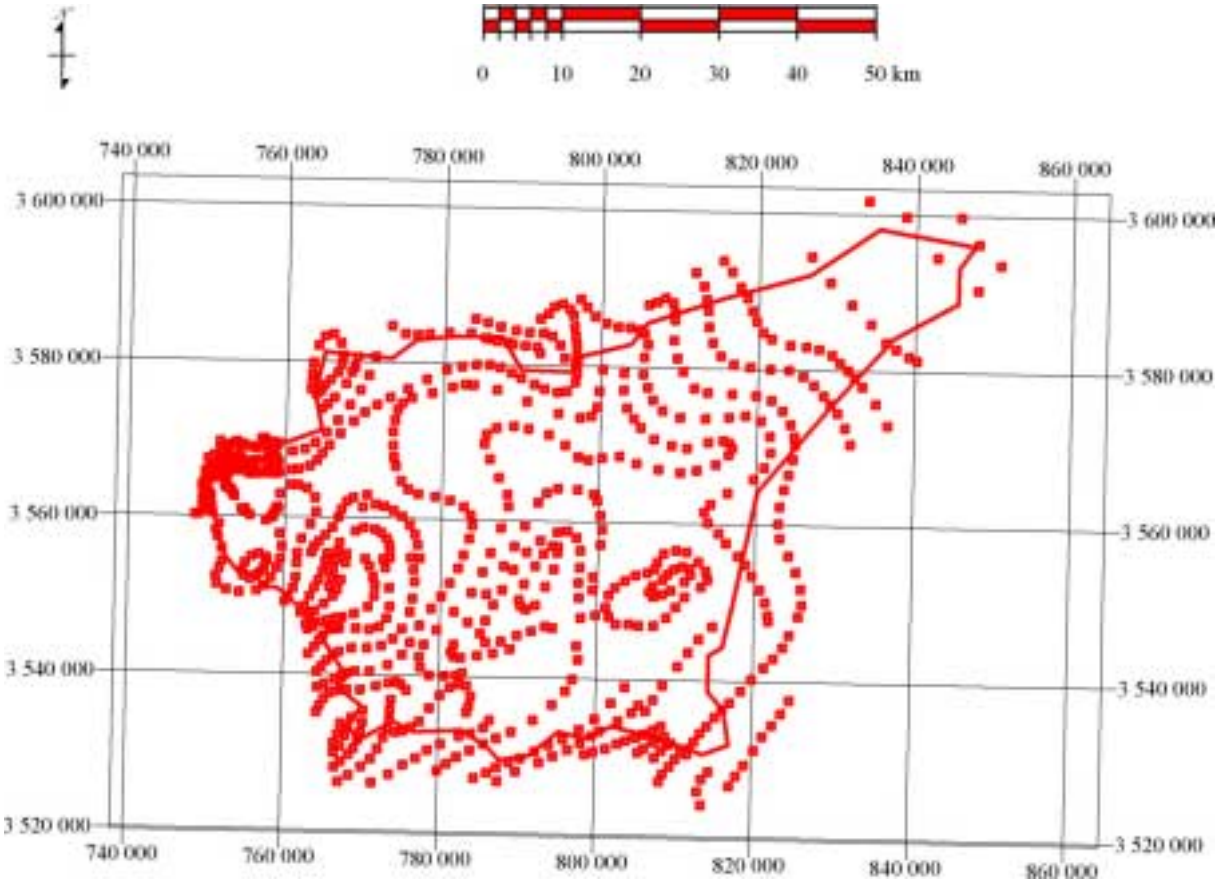

• App. 20 Groundwater levels of the A7/B2 aquifer.

station ID	altitude (mfsl)	easting (PG)	northing (PG)	water level (mfsl)
AD1001	620	259560	208860	449.02
AD1005	642	258895	208890	445.2
AD1012	590	264018	210565	476.4
AD1013	612	263740	205470	479.61
AD1015	603	264270	206800	476.5
AD1016	617	260980	207120	455.7
AD1017	633	260930	206850	457.78
AD1018	658	261060	205105	487
AD1019	618	260355	208190	454.6
AD1020	610	261040	208335	453.7
AD1021	596	261960	209340	458.7
AD1022	602	261645	208615	455.75
AD1024	605	261140	209440	456.52
AD1025	605	261810	207880	456.3
AD1027	589	266070	210260	493
AD1028	591	266355	211115	494.57
AD1031	589	265665	210020	485.5
AD1033	590	266335	210345	493
AD1035	600	267020	208020	492.5
AD1036	593	266360	208400	489.21
AD1039	609	266420	205365	485.23
AD1040	606	265820	205765	486.52
AD1041	596	265735	208180	482.45
AD1042	601	265335	207185	483.1
AD1046	620	264160	203700	480.86
AD1047	624	264980	204480	483
AD1049	613	265185	205185	481.7
AD1052	618	259725	211980	470
AD1053	616	260480	211540	472.35
AD1054	637	260625	210690	455.8
AD1056	606	260310	212485	471.5
AD1057	621	259550	212825	472.5
AD1058	597	261760	211700	472.59
AD1059	617	261395	210625	462.52
AD1062	654	270940	202540	495.5
AD1064	587	261915	212420	474.5
AD1070	661	273730	203640	504.4
AD1073	657	272020	206300	504
AD1074	653	272800	206460	503.7
AD1075	657	273900	206675	503.7
AD1076	680	275380	204930	504.4
AD1077	666	274460	205520	503.9

station ID	altitude (mfsl)	easting (PG)	northing (PG)	water level (mfsl)
AD1078	682	275840	204250	506
AD1079	682	275600	202530	505.85
AD1080	692	277420	202760	513.12
AD1081	672	275700	203700	504.6
AD1082	663	271900	201490	505
AD1083	660	272740	202550	505.4
AD1086	663	274200	202665	504.7
AD1088	656	270950	204200	499
AD1089	654	269930	202650	495.9
AD1090	665	269790	200180	508.05
AD1092	670	271000	200050	506.15
AD1093	655	269630	201380	505.05
AD1095	691	275710	200450	507.2
AD1096	696	276570	199900	506.6
AD1099	679	274860	201420	505.7
AD1101	683	274220	200270	505
AD1102	672	271340	199200	508.4
AD1103	660	267570	201160	512.7
AD1107	698	276575	201730	506
AD1109	658	270380	201940	498.1
AD1110	651	269150	200880	502.3
AD1116	691	275320	199530	507.5
AD1118	723	279305	200760	509
AD1121	598	266440	207265	484.4
AD1122	601	266790	207260	466
AD1123	596	266340	207715	485.2
AD1124	597	265980	207685	483.12
AD1126	605	267550	207660	491.04
AD1148	622	264360	203900	483.21
AD1149	596	264890	208590	4.706.843
AD1150	608	264865	206090	481.31
AD1159	514	240248	218401	221.3
AD1168	559	249300	215527	254.9
AD1169	558	249606	214231	257.5
AD1170	560	248433	211302	273.4
AD1174	661	274118	194520	507.7
AD1179	705	278430	204910	508.15
AD1184	609	260685	213465	475
AD1220	705	236128	203350	512.3
AD1233	783	235884	200679	645.4
AD1245	534	242092	218866	246.8
AD1248	580	275300	204960	405
AD1270	558	249100	214820	258.6
AD1327	575	263000	213000	459.3
AG1003	-20	208800	207600	-57.28

station ID	altitude (mfsl)	easting (PG)	northing (PG)	water level (mfsl)
AL1175	519	255085	171190	489.17
AL1300	595	252728	160010	5.653.627
AL1906	550	255670	170070	504
AL2689	790	298000	182700	512.8
AL2695	718.5	279750	199820	494.93
AL2697	652	275200	189940	514
AL2704	620	295000	180000	428.21
CD1074	740	240150	130100	588.25
CD1075	745	238225	131150	570
F 1308	710	320920	165870	522.8
AL1040	596	271278	177834	511.5
AL1041	567	272484	171392	517
F 1125	804	323920	173870	528.42
deir abu said		214600	211500	340
abu zaid		211300	212800	70
al jadideh		212800	212300	90
el beida		209200	212400	-75
abu thableh		208600	208000	50
tabqat fahil		208000	206250	-65
sbeirah		207600	196600	-75
el tina		207500	196300	-90
el-beida		208300	195400	120
abu falah		208000	194800	30
manhaleh		209500	193600	200
el huneideh		207400	193600	-10
qama soun		214100	161300	550
sakhne at		208150	222060	-80
el aqdeh		215100	187900	680
ras el ain		237000	150500	760
ruseifa		246600	158610	600
zerqa seil		252600	162700	560
el khandaq		218700	160600	850
jadour tahta		219200	160000	750
farkha		219500	159400	682
shoreal		221050	157750	595
Al azraq		222050	158810	750
wadi es sir		227200	151400	715
el roudhah		227700	139200	850

• App. 21 Groundwater levels of the A1/B6 aquitard.

station ID	altitude (mfsl)	easting (PG)	northing (PG)	water level (mfsl)	aquifer 1	aquifer 2
A11(S8)	636	242520	155610	705	A4?	
A13(PP278)	749	240960	154570	739.5	A4?	
A14(PP469)	732	239870	151375	760.5	A4?	
A17	628	247250	158610	628	A4?	
A181	758	237780	152405	741	A4?	
A185	817	236383	151844	727	A4?	
A186(S17)	787	237234	149433	765	A4?	
A187	787	237518	149433	751	A4?	
A188	733	247943	150851	698.8	A4?	
A190(PP468)	689	247801	156099	651	A4?	
A191	694	246454	157376	636.3	A4?	
A193	676	243830	158653	676	A4?	
A194	719	241560	159290	690.5	A4?	
A195	762	240050	159300	732.2	A4?	
A196	774	239433	158936	761.9	A4?	
A197	1012	231986	158511	1004.2	A4?	
A198	596	250709	158936	596	A4?	
A200(S14)	563	254960	167000	493.9	A4?	
A203	502	250300	168085	488	A4?	
A204	497	250150	169362	490.5	A4?	
A205	548	251702	171135	496.8	A4?	
A206	505	250800	171915	473.7	A4?	
A208	475	251631	173404	458	A4?	
A209	472	252128	173575	468	A4?	
A210	506	253262	174284	464.5	A4?	
A214(PP111)		250700	158900	637	A4?	
A215(PP180)		254700	171600	490	A4?	
A216(PP221)		243000	159800	832	A4?	
A217(PP308)		231700	158600	1008	A4?	
A218(PP313)		230200	141600	389	A4?	
A219(PP458)		244500	155200	744	A4?	
A23	735.5	245190	156275	674.5	A4?	
A24	749	241201	151577	697.5	A4?	
A26	860	234950	152150	810.6	A4?	
AB1364	360.03	215300	201380	220.03	A4	A1/2
AL1782	790	243750	152500	682	A4	
A182(S10)a		240350	150600	667	A1/2	
A220(PP463)		227090	158690	861.2	A1/2	
AL1043	557	267100	171506	504.95	A7	A4

station ID	easting (PG)	northing (PG)	water level (mfsl)
um jatta	208500	193300	50
el suleikat	207800	193000	-10
musa north	220200	131550	450
jammala	219100	133100	410
rasun	222000	202000	730
tannur	220500	201500	675
urjan fouqa	220400	200500	690
et teis	222000	194750	910
el rijal	219000	199100	620
urajan tahta	219300	200500	590
barrraneyyah	222550	193550	870
sharqeyya	223000	193600	870
el fawwar	222600	193300	890
um sarab	222300	193300	835
el balad	220900	193400	771
basset el haddadeh	220300	192400	725
el qantara	220100	192100	680
yajuz	236000	160300	860
ain zarbi	243400	158800	700
sukhneh	250500	171000	440
seil husayyah	251600	173400	450
nimar	248000	172800	440
birein	240500	167600	763
el khalla	245800	172600	540
al kook at yajouz	238730	158880	796
deir el fouqa	225000	149200	540
deir el tahta	224300	148800	570
el khour	223400	149300	580
tarabil	222800	148100	500
el manakhir	222100	147700	480
um zweiteeneh	222800	141800	500
faria	225600	138400	675
ain wadi hisban	225400	138300	670
kdeeshan	225300	138200	665
fodeileh	224700	136000	560
mbeirdeh	223200	136300	500
sumiya	223200	136200	490

• App. 22 Groundwater levels of the Kurnub aquifer.

station ID	altitude (mfsl)	easting (PG)	northing (PG)	water level (mfsl)
A182(S10)	777	240350	150600	377
A199(S13)	563	254965	166809	381
AL1430	631	229021	165035	488
AL1433	683	230140	163010	638.7
AL1539	710	230260	162550	552
AL1541	678.58	230940	164465	520.48
AL1892	683	230135	163020	601
TEST-WELL3	-183.5	206753	157174	-187.5
Al Hammam		240100	180100	275
S-90		250000	210400	418
Ain el azab		219300	173800	300
Ain Hajjaj		215450	173450	420
Ain h Sara		225200	173600	435
Ain el Husan		219600	171400	425
Ain ed Daffali		218550	170800	475
Ain Zamma		215200	178900	120
Es Sahn		213700	167500	310
Ain Jebarat		233500	184600	480
Bisas el neil		234200	182600	385
el majthoub		236300	182700	440
um quseir		232400	185250	510
amama east		232950	182650	415
deek		229850	186050	600
basset el ghul		230200	185750	500
el ramel		230000	183650	540
el majdal		229500	181600	550
sharqia		230000	182000	440
basset hammed		231200	180600	325
el balad		227650	182100	550
sfar		227800	181800	515
bissas		227300	181900	525
hamta		227650	181150	500
udeis		226400	180250	490
jalad		223700	169500	580
um jurn		224200	180700	570
re shouni		221800	171150	575
el balad		221700	171700	500
esh shati		222900	175100	350
el azab		219250	174000	310
ed dafali		218650	170900	480
el beida		219550	180150	450
el arqetain		219600	179600	375
subeihi		216350	172800	475
hafayer		215800	172900	450
hammeedi		221100	135800	175

• App. 23 Groundwater levels of the Zerqa aquifer.

station ID	easting (PG)	northing (PG)	water level (mfsl)
Test well 1	209056	175082	-249.6
kuhuneizir	212400	171400	300
um esh shananeer	211700	166500	258
ain wadi el muhtariqa	215600	133600	20
dafali	223200	175000	350

• App. 24 Simulated equipotential lines of the A7/B2 aquifer.

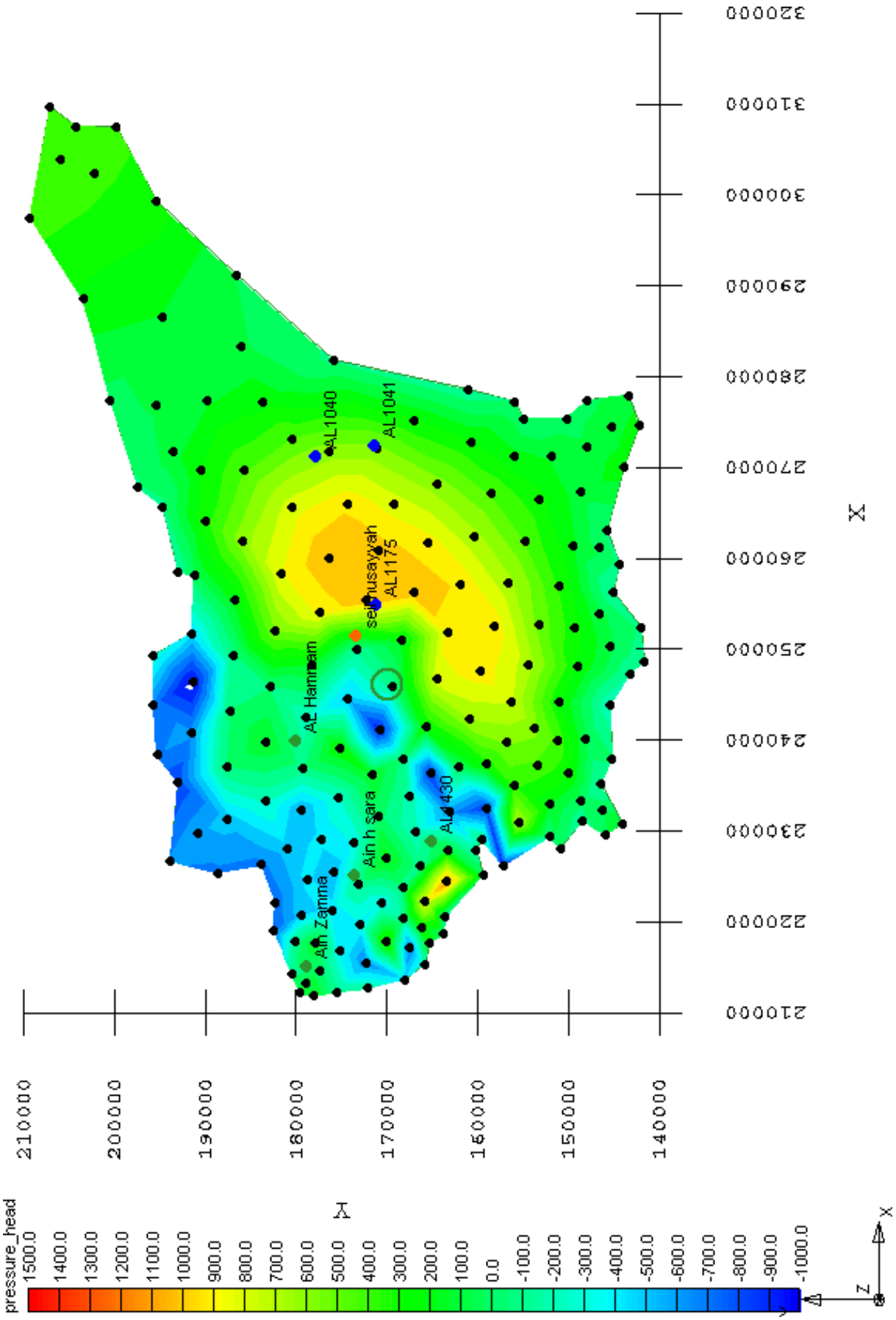

• App. 25 Simulated equipotential lines of the A1/A6 aquitard.

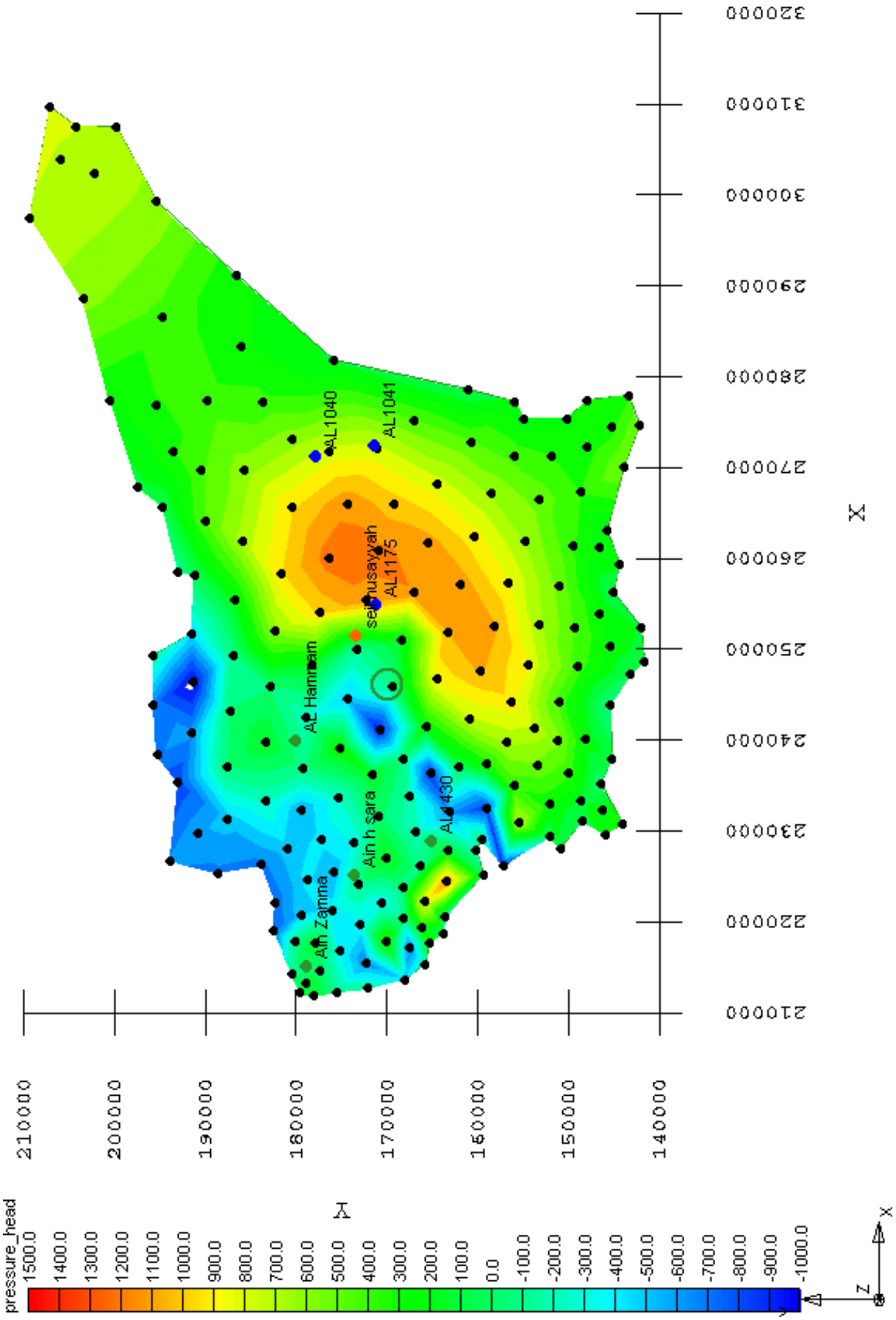

• App. 26 Simulated equipotential lines of the Kurnub aquifer.

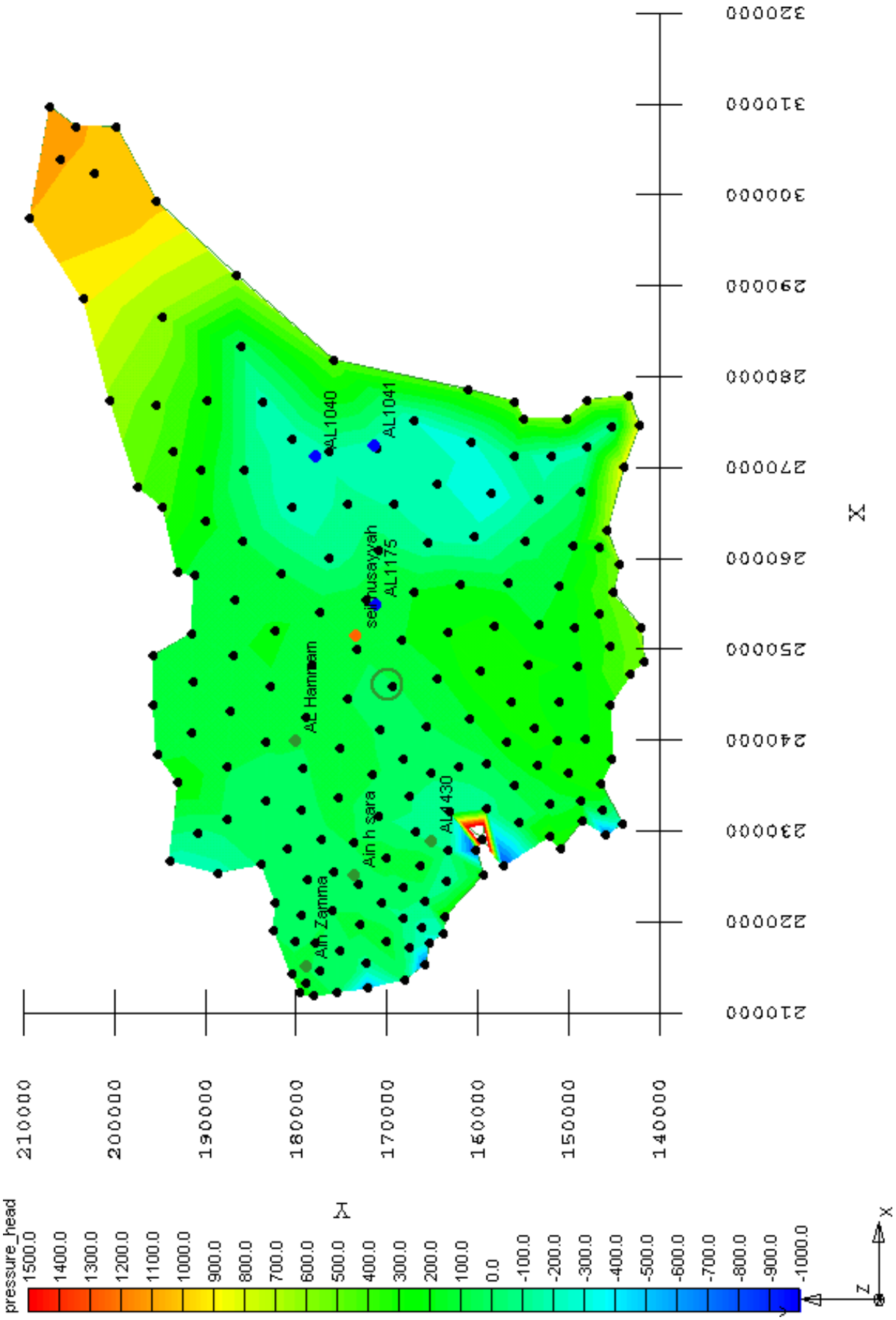

• App. 27 Simulated equipotential lines of the Zerqa aquifer.